Bending of a polyurethane based shape memory polymer: modeling and experiment

by

Xiaoang Ma

A thesis submitted in partial fulfillment of the requirements for the degree of

Master of Science

Department of Mechanical Engineering
University of Alberta

Abstract

Shape memory polymers (SMPs) can be used in many critical applications, including biomedical and aerospace fields, due to their ability to recover their original/permanent shape from a deformed/temporary shape upon application of a stimulus. SMPs are subjected to bending in a large number of these applications, e.g. morphing aircraft components or biomedical stents; however, predictive models used for bending are very limited in the literature. Consequently, there is a need to build a bending model for SMPs, and this thesis addresses this gap in the literature. A rheological model previously developed by Tobushi for uniaxial loading was extended to bending and implemented numerically to calculate the time-dependent deflection of a thin beam. Corresponding experiments for a polyurethane based shape memory polymer were conducted to verify the model. Creep tests were conducted to extract the values of parameters required for the rheological model. Extrusion based additive manufacturing (EBAM) technique was used to produce the specimens used in experimental tests. Results indicate that the rheological model is able to describe the material behavior well over a certain range of temperature while the discrepancy between experiment and model becomes significant if the temperature deviates from this range. Through this study, the manufacturing, modeling and related mechanical characterization of the shape memory polyurethane were investigated and these findings can be used for further studies and design of SMPs.

Acknowledgements

First and foremost, I would like to express my sincere gratitude to my supervisor Dr. Tian Tang for providing numerous creative ideas and valuable guidance towards my graduate research. I would have fallen down several times but she is the person who consistently encourages me and helps me which paves the way for my success. Her modest and prudent attitudes toward research have great influence on my future career. I would like to thank my supervisor Dr. Cagri Ayranci for providing excellent experimental guidance and great effort during the course of my study. He keeps encouraging me and talking with me patiently when I meet difficulties or suffer from frustration.

I also wish to express my thanks to my group members, Irina Garces, Daniel Aldrich and Elisa Aznarte Garcia, for their generous help during my graduate study. They make my course of the study an enjoyable journey.

Finally, I would like to express my gratitude to my parents for their forever love and consistent encouragement.

Table of Contents

List of Tables

List of Figures

List of Symbols

a	Location in a beam cross section separating regime 1 and regime 2
α	Coefficient of thermal expansion
b	Width of beam
β	Bending angle between two neighboring bonds in a polymer chain
C	Coefficient relating creep strain and irrecoverable strain
δ	Deflection at mid of beam
Δe	Torsional energy barrier
Δt	Time interval
Δx	Interval along x axis
Δy	Interval along y axis
E	Elastic modulus
E'	Storage modulus
E''	Loss modulus
$E_r(t)$	Relaxation modulus
η	Viscosity of a dashpot
ϵ	Strain
$\dot{\epsilon}$	Strain rate
ϵ_c	Creep strain
ϵ_L	Threshold strain
ϵ_s	Irrecoverable strain
$\epsilon_{s,eff}$	Effective irrecoverable strain
h	Height of beam
I	Moment of Inertia
$J(t)$	Compliance modulus
κ	Curvature
L	Distance between two supports of the beam

λ	Retardation time
λ_{eff}	Effective retardation time
M	Bending moment
μ	Viscosity
μ_{eff}	Effective viscosity
P	Load applied at the mid span of the beam
Rr	Recoverable strain ratio
R^2	Coefficient of determination
σ	Stress
$\dot{\sigma}$	Stress rate
T	Temperature
T_g	Glass transition temperature
T_m	Melting temperature
t	Time
$tan\delta$	Tangent delta (Ratio between loss modulus and storage modulus)
θ	Torsional angle between two neighboring bonds in a polymer chain
w	Deflection
x	Longitudinal axis
y	Vertical axis

List of Abbreviations

1D	One-dimensional
2D	Two-dimensional
3D	Three-dimensional
DMA	Dynamic mechanical analysis
DSC	Differential scanning calorimetry
EBAM	Extrusion based additive manufacturing
FDM	Fused deposition modeling
MEMS	Microelectromechanical system
MM3520	The raw shape memory polymer pellet with $T_g = 35$
MM4520	The raw shape memory polymer pellet with $T_g = 45$
MM6520	The raw shape memory polymer pellet with $T_g = 65$
MM7520	The raw shape memory polymer pellet with $T_g = 75$
MS5510	The raw shape memory polymer solution with $T_g = 55$
SLS	Standard Linear Solid
SMAs	Shape memory alloys
SMGs	Shape memory gels
SMMs	Shape memory materials
SMPs	Shape memory polymers
SMPCs	Shape memory polymer composites
UV	Ultraviolet

Chapter 1 : Introduction

Shape memory materials (SMMs) are materials that have the ability to recover to its original (permanent) shape from a deformed (temporary) shape. The shape change can be achieved using different stimuli, such as heat and UV light [1], depending on the specific material. Most commonly utilized SMMs are shape memory alloys (SMAs), gels (SMGs) and polymers (SMPs). SMPs offer significant advantages over other types of SMMs, such as low density, low cost, and easier manufacturability [2]. Generally, SMPs can be categorized under two main types [2], namely thermoset and thermoplastic SMPs. Thermoset SMPs have chemical crosslinks which connect adjacent molecular chains covalently. These chemical crosslinks are formed during the curing of the polymer [3] [4], which is an irreversible process. Thermoplastic SMPs, on the other hand, do not have the chemical crosslinks. Consequently, they can be melted and reprocessed/reshaped by various techniques such as injection molding, extrusion or additive manufacturing [5]. These SMPs are easier and less costly to process, and more affordable; therefore, a vast majority of the SMP work presented in the open literature is currently concentrated on thermoplastic SMPs. The SMP used in this thesis is also a polyurethane based thermoplastic SMP (SMP Technologies Inc., Japan) which is thermo-responsive.

The focus of this thesis is on the mechanical behavior of shape memory polyurethane at different temperatures via a viscoelastic model and experimental study. The study is part of a larger program that investigates multifunctional shape memory polymer composites (SMPCs).

1.1 Network structure in shape memory polyurethanes

The shape memory polyurethane investigated in this thesis is a semi-crystalline thermoplastic polymer [2] which consists of crystalline regions and amorphous regions. The crystalline regions have orderly arranged structures where the chains are folded and aligned in a periodic form with strong intermolecular forces [3]. Such regions have relatively high melting temperatures, T_m, below which the crystalline regions are in solid state and have hard and brittle mechanical properties. In contrast, the amorphous regions have entangled chain molecules that are randomly oriented [6]. They can gradually transform from hard and glassy state into viscous and rubbery state over a certain range of temperature [7] which is characterized as glass transition. Even

though glass transition occurs over a temperature range, a single value is typically specified as the glass transition temperature (T_g). Many techniques such as differential scanning calorimetry (DSC) and dynamic mechanical analysis (DMA) can be used to obtain T_g, but it should be noted that different methods may generate slightly different values of T_g [3]. For a semi-crystalline polymer, the glass transition temperature of the amorphous regions is always lower than the melting point of the crystalline regions [3]. T_g of a semi-crystalline polymer therefore refers to T_g of its amorphous regions while its T_m refers to T_m of its crystalline regions [8]. During the solidification of the semi-crystalline polymer, the chain-end segments from many adjacent chains aggregate together to form the crystalline regions through hydrogen bonding due to the high polarity of the chain-end segments [4] [8]. As a result, the crystalline regions act as physical crosslinks that connect the amorphous regions together [4]. This specific network structure leads to the shape memory effect which will be discussed below.

1.2 Shape memory effect

The shape memory effect of polyurethane is due to the existence of coiled chains and physical crosslinks in the network structure [8]. Since the crystalline regions always have higher stiffness than the amorphous regions, they are regarded as hard segments while the amorphous regions are regarded as soft segments [2]. The soft segments have randomly coiled chain molecules with high flexibility [5]. The hard segments act as physical crosslinks which restrict the motion of the soft segments [5]. As a result, the chains in the amorphous regions between those physical crosslinks can only move locally instead of globally [9].

In semi-crystalline thermoplastic polymers, each chain molecule in the amorphous regions can be regarded as a collection of skeletal bonds covalently connected in sequence to form a coiled configuration. External energy (from applied force or thermal loading) can cause the torsion, bending, and/or stretching of the bonds [10]. As can be seen from Figure 1.1 (a), rotation of a bond (also referred as torsion) with respect to its neighbor corresponds to the change of angle θ, bending of two bonds corresponds to the change of angle β and stretching of a bond corresponds to the change of a bond length. Among the three modes of deformation, torsion is typically much easier than bending and stretching. Different torsional angles θ can lead to different chain

conformations. For example, Figure 1.1 (b) and (c) shows two possible conformations of a segment on the chain due to the different torsional angles.

The potential energy associated with torsion is dependent on θ, as demonstrated in Figure 1.2. The transition between different torsional angles therefore requires the application of external loading (mechanical or thermal) to overcome certain energy barriers. For example, in Figure 1.2, A, B and C represent three different torsional angles. In order to change the torsional angle from A to C, the external loading has to surmount the energy barrier Δe. This energy barrier could explain the shape fixity and shape recovery in SMPs as detailed below.

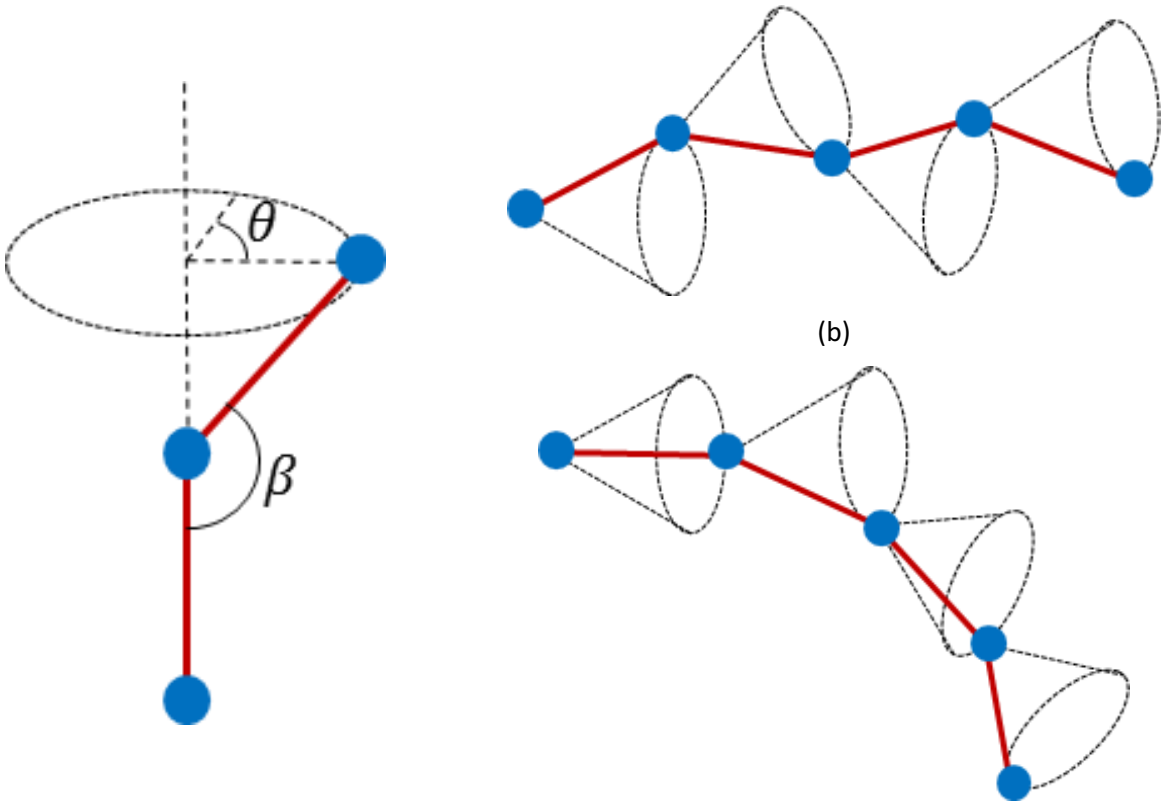

Figure 1.1 Schematic representations of how torsional angle affect the conformation of a chain molecule. (a) Rotation of a bond with respect to its neighbor, (b) and (c) Two possible conformations of a segment of a chain molecule due to different torsional angles. (adopted from [4])

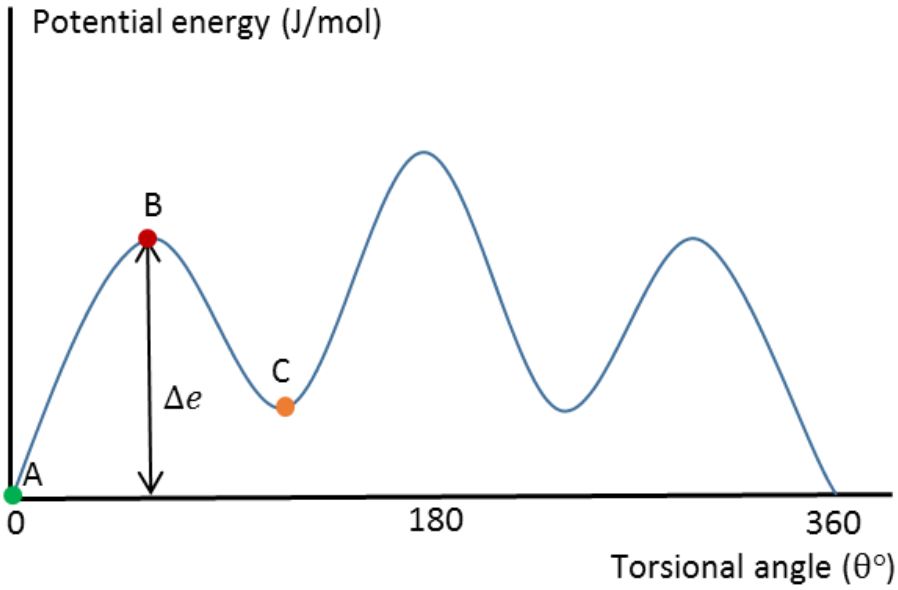

Figure 1.2 Potential energy landscape as a function of torsional angles (adopted from [3])

A schematic representation of the shape memory mechanism for a thermoplastic SMP is given in Figure 1.3. The permanent shape is determined by heating up the polymer above the melting point T_m, shaping via a manufacturing technique, and then cooling down below the glass transition temperature (T_g) [1]. The chain molecules in the soft segments maintain their random coiled state in the permanent shape [8].

The shape memory effect starts by heating the material above T_g at which the flexibility and mobility of the soft segments increase dramatically [8]. Then, external force/constraint is applied to change the permanent shape to a temporary shape at this temperature. If the material is cooled below the T_g, while maintaining the force/constraint, the temporary shape is obtained. This temporary shape can be maintained at this temperature, even when the constraint is removed, because the thermal energy below T_g is insufficient to surmount the energy barriers for bond rotation. In addition, intermolecular forces such as hydrogen bonding and van der Waals forces can also prevent the extended chains from going back to their most random coiled state [3]. Once the SMP with the temporary shape is heated above T_g, the thermal energy surmounts the energy barrier allowing the chains in the soft segments to return to their most coiled state [8]; as a result the permanent shape is recovered.

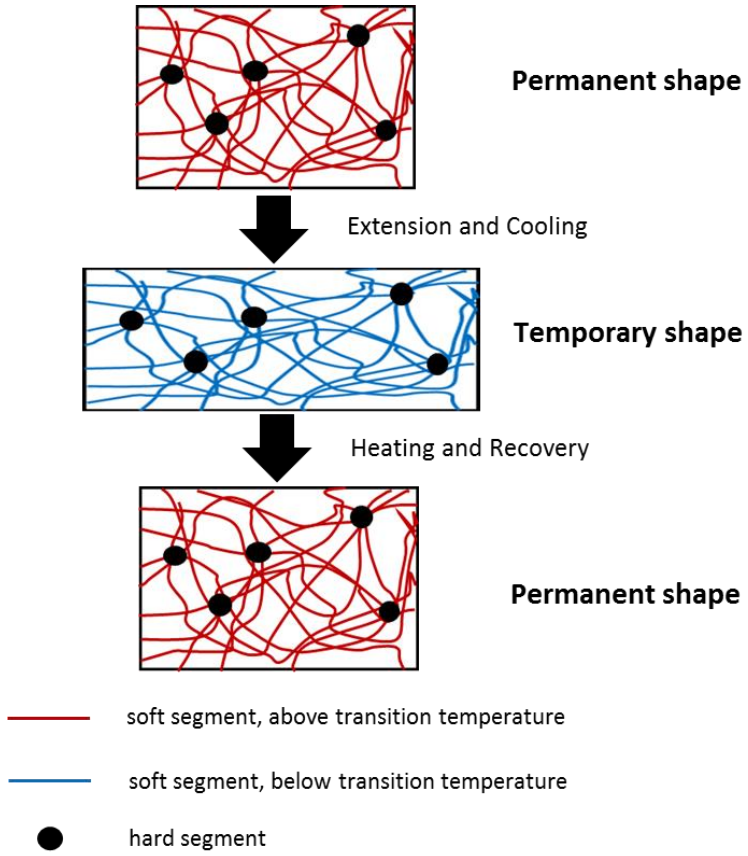

Figure 1.3 Shape memory mechanism of thermally induced SMPs (adopted from [5]).

1.3 Application of shape memory polymers

SMPs have the potential to be used in a variety of areas. Their biomedical and aerospace applications have drawn special attention and were investigated by a number of researchers [2] [11]. SMPs can offer excellent chemical stability, and some SMPs can even offer biocompatibility and biodegradability for use in biomedical field [2]. Yakacki *et al.* [12] proposed the potential application of SMP cardiovascular stents which can be implanted into body through minimally invasive surgery. The transition temperature of this SMP was tailored to be around the human body temperature. The stent was heated up and then deformed into a compact temporary shape. This compact temporary stent was implanted into blood vessels. Stimulated by the body temperature, the stent was expanded into its original shape which can support blood-carrying vessels. Lendlein *et al.* [13] explored the application of SMPs to a surgical suture. A shape memory fiber was stretched at high temperature to form a thinner fiber and was subsequently cooled down to fix a temporary shape. A knot was tied using the thinner

fiber to suture the wound lips of the tissue or muscle. Once the suture reached human body temperature, it was contracted and therefore tightened the knot. It was mentioned by the authors that the shape recovery force could be tailored to provide the suitable force for the suture of the wound. Additionally, since the SMP used was biodegradable, it was able to gradually degrade with time eliminating the need for a secondary operation for removal.

Another promising application was demonstrated in SMP reflectors developed for satellite structures [14]. They can be compacted and stored in the launch vehicle with minimal volume. Once it is sent into the orbit of a planet, the reflector can be deployed and recover its original shape by the application of a stimulus. Compared with traditional deployable structures which involve mechanical parts and motors, and the like, shape memory deployable structures significantly reduces the weight of the structure [11]. One strategically important example of aerospace applications is the potential use of SMP in the morphing wings of Unmanned Air Vehicles, and military planes [11]. By using SMPs, the wing is able to deform to different shape via shape memory effect upon appropriate stimulation. This shape can be tailored to meet the flight mission of the airplane, thus improving the performance and efficiency of the flight vehicle. In addition, SMPs are also promising to be used in Microelectromechanical system (MEMS) [11] and smart textiles [8].

1.4 Investigations on mechanical properties of SMPs

Based on the various aforementioned applications of SMPs, it is clear that SMPs are used in strategically critical structural and biomedical applications. As such, it is necessary to investigate their mechanical properties through fundamental research. This can be done by development of predictive models and verification of these models via methodological experimental studies.

Many researchers have investigated the mechanical properties of SMPs. In 1996, Tobushi *et al.* [15] conducted a variety of experiments such as dynamic mechanical analysis, thermomechanical, creep and stress relaxation tests to investigate the mechanical properties of shape memory polyurethane (MS5510) produced by Misubishi Heavy Industries Ltd. They then [16] developed a rheological model to capture the irrecoverable strain of SMPs by modifying the standard linear solid model. This is a 1D model that contains springs, dashpots and other elements to describe

the viscoelastic properties of SMPs. The rheological model was verified by thermomechanical tests, which showed good agreement. Later, Bhattacharyya and Tobushi [17] used the rheological model to solve, analytically, the response of the SMP in creep, stress relaxation, tensile and dynamic mechanical tests. However, no corresponding experiments were conducted to verify the model or the analytical solutions. Huang *et al.* [2] conducted tensile test for the SMP MM3520 (SMP Technologies Inc.) at different strain rates and different temperatures. Specifically, they did tensile tests at room temperature (around 22 ℃) with three different strain rates (0.01/s, 0.001/s and 0.0001/s) and at 50 ℃ with four different strain rates (0.1/s, 0.01/s, 0.001/s and 0.0005/s). The influence of strain rate and temperature on its mechanical properties are specified. It is found that the stress-strain response were highly strain rate dependent especially at high temperature and higher strain rate resulted in higher ultimate stress. Liu *et al.* [18] developed a "3D small-strain internal state variable constitutive model", where the polymer was considered as a mixture of two extreme phases (frozen phase and active phase). The volume fraction of two phases was assumed to vary when the temperature was changed. Although the model was intended to model general 3D deformation, it was only applied to 1D thermomechanical tests with uniaxial deformation. Corresponding thermomechanical experiments were conducted for a commercial thermoset epoxy produced by Composite Technology Development, Inc. It was reported that the model was able to describe the experimental results well. The modeling or experiments discussed above only focused on uniaxial tests, and little research has been conducted so far for more complicated loading conditions for SMPs.

Considering the loading conditions of a stent or the wing of a morphing aircraft, bending is one of the important loading types. Tobushi *et al.* [19] conducted 3-point bending thermomechanical test for the SMP MM6520 produced by Mitsubishi Heavy Industries, Ltd., but there was no corresponding model to describe the response of deformation of the beam. Ghosh *et al.* [20] implemented a small strain continuum model for the bending of a beam based on finite element method but it lacked the experiments to validate the accuracy of the model.

1.5 Overview of this research

Based on the knowledge gap described above, there is a need to develop a model for the bending of SMP and verify its accuracy via experiments. Consequently, the objectives of this thesis are:

1. Building a model, as an extension of the rheological model, which is capable of describing deformation of a thin beam under bending.
2. Developing numerical algorithm to implement the model and calculate time-dependent deflection of the beam at different temperatures.
3. Conducting creep experiments on a polyurethane based thermoplastic SMP (MM7520) to extract materials parameters and bending tests to verify the accuracy of the model.
4. By comparing the modeling and experimental results, addressing the applicability of the model to MM7520 and limitation of the model.

The organization of this thesis is as follows: In Chapter 2, the rheological model is introduced in detail and its numerical implementation to 1D uniaxial deformation is developed and validated. In Chapter 3, the model is extended to the bending of a thin beam and numerically implemented. In Chapter 4, the experimental methodology is introduced which includes specimen preparation via extrusion based additive manufacturing and experimental testing (creep, 3-point bending). In Chapter 5, experimental and modeling results are compared and discussed. In Chapter 6, conclusion and possible future work built upon this work is discussed.

Chapter 2 : Rheological viscoelastic model and its numerical implementation

In this chapter, several classical viscoelastic models are presented. Then, the rheological viscoelastic model developed by Tobushi is described in detail. Finally, a numerical scheme is implemented to solve for stress-strain relationship from the rheological model and the accuracy is validated against analytical solution.

2.1 Introduction to linear viscoelastic models

2.1.1 Basic element

The mechanical behavior of linearly elastic materials can be simply represented by a Hookean spring. However, polymers exhibit viscoelastic behavior that resembles a combination of elastic solid and viscous liquid [4]. Therefore, the mechanical behaviors of polymers are usually represented by the so-called "mechanical analogs" [7]. A mechanical analog system is usually a combination of several elements, such as springs and dashpots, which can represent the viscoelastic behavior of real polymers both qualitatively and quantitatively.

A Hookean spring can be used to represent the linearly elastic behavior of materials as shown in Figure 2.1. The mechanical response of Hookean spring follows Hook's law [7] as shown in Eqn. (2.1).

$$\sigma = E\epsilon \tag{2.1}$$

where σ is the applied stress, ϵ is corresponding strain and E is elastic modulus.

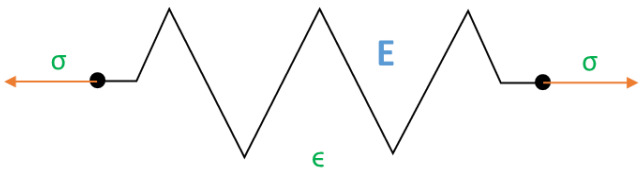

Figure 2.1 Schematic of Hookean spring

A dashpot can be used to represent the viscous behavior of Newtonian liquid as shown in Figure 2.2. The Newtonian liquid moves at a strain rate proportional to the applied stress and there is no strain recovery when the stress is removed. The mechanical response of a dashpot follows Newton's law [7] as shown in Eqn. (2.2).

$$\sigma = \eta \frac{d\epsilon}{dt} \tag{2.2}$$

where η represents the viscosity of the dashpot.

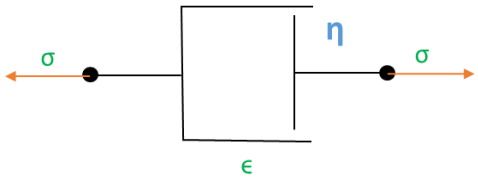

Figure 2.2 Schematic of Dashpot

2.1.2 Maxwell model

The Maxwell model [7] is a series combination of the spring and dashpot elements as shown in Figure 2.3. ϵ_1 represents the strain of the dashpot and ϵ_2 represents that of the spring. Therefore, the overall strain of Maxwell element is $\epsilon = \epsilon_1 + \epsilon_2$. Based on the mechanical properties of spring and dashpot given by Eqns. (2.1) and (2.2), the total strain rate $\dot{\epsilon} = \dot{\epsilon_1} + \dot{\epsilon_2}$ is therefore

$$\dot{\epsilon} = \frac{\sigma}{\eta} + \frac{\dot{\sigma}}{E} \tag{2.3}$$

where the dot above the symbols (eg. $\dot{\epsilon}$) represent the derivative with respect to time. Stress-strain relationships can be obtained by solving the ordinary differential equation, Eqn. (2.3).

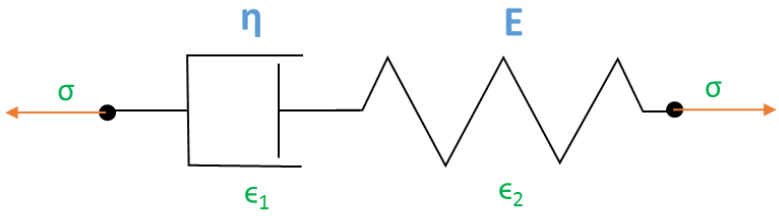

Figure 2.3 Schematic of Maxwell model

Consider the special case of stress relaxation where the model is subjected to an instantaneous constant strain ϵ_0. Initially, the dashpot cannot sustain a sudden deformation so the initial strain is all undertaken by the spring which gives the initial condition as $\sigma(0) = E\epsilon_0$. The stress response can hence be calculated as $\sigma(t) = E\epsilon_0 e^{-\frac{E}{\eta}t}$ by solving Eqn. (2.3) with the initial condition. This response is reasonable when compared to the result observed experimentally [15].

For a creep test where the model is subjected to an instantaneous constant stress σ_0, the spring responds to the stress instantaneously but the dashpot remains undeformed at beginning so that the initial condition is $\epsilon(0) = \frac{\sigma_0}{E}$. The strain response is obtained as $\epsilon(t) = \frac{\sigma_0}{E} + \frac{\sigma_0}{\eta}t$ by solving Eqn. (2.3) with the initial condition. The strain versus time is a straight line which is unrealistic when compared with the creep response observed experimentally [15]. Therefore, the Maxwell model cannot properly capture creep behavior.

2.1.3 Kelvin-Voigt model

The Kelvin-Voigt model [7] is a parallel combination of spring and dashpot (schematic shown in Figure 2.4) so the strain of the spring is equal to the strain of the dashpot. Based on the mechanical properties of spring and dashpot (Eqns. (2.1) and (2.2)), the total stress of the element $\sigma = \sigma_1 + \sigma_2$ is given by

$$\sigma = E\epsilon + \eta\dot{\epsilon} \tag{2.4}$$

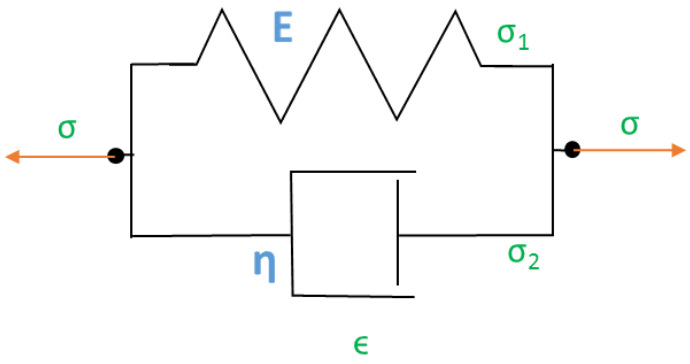

Figure 2.4 Schematic of Kelvin-Voigt model

Strain response during a creep test can be obtained by solving Eqn. (2.4) with appropriate initial condition. In this case, when the initial stress is suddenly applied the dashpot prevents the element from sudden deformation which lead to $\epsilon(0) = 0$. Thus, the strain response is $\epsilon(t) = \frac{\sigma_0}{E}\left(1 - e^{-\frac{E}{\eta}t}\right)$. It can describe the overall trend of creep response but the initial elastic strain response cannot be captured [15]. As for stress relaxation, the dashpot would develop an infinitely high value of stress when an initial strain is suddenly applied. Therefore, the Kelvin-Voigt model is not able to describe the stress relaxation response.

2.1.4 Standard linear solid model

Due to the limitation of Maxwell and Kelvin-Voigt models, standard linear solid model was introduced [21]. It is able to describe both creep and stress relaxation behavior of a typical viscoelastic material. The standard linear solid model contains three elements by paralleling a Maxwell model with a spring as shown in Figure 2.5.

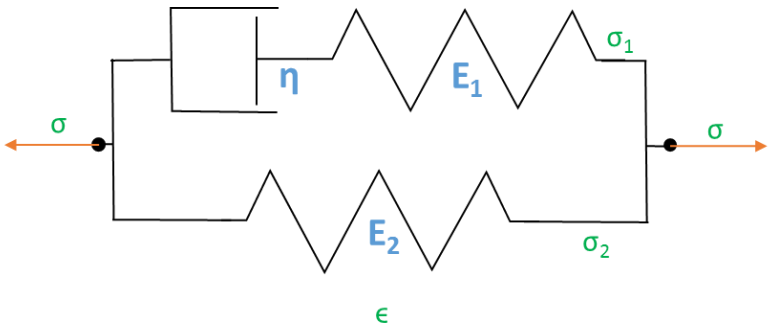

Figure 2.5 Schematic of Standard linear solid model

The strain on the upper side is equal to the strain on the lower side. The upper side of the model is a Maxwell model for which $\dot{\epsilon} = \frac{\sigma_1}{\eta} + \frac{\dot{\sigma_1}}{E_1}$. For the lower side of the model, $\sigma_2 = E_2\epsilon$ so $\dot{\epsilon} = \frac{\dot{\sigma_2}}{E_2}$. The total stress is the sum of the stresses on the upper and the lower sides. Substituting $\sigma = \sigma_1 + \sigma_2$ and $\dot{\epsilon} = \frac{\dot{\sigma_2}}{E_2}$ into $\dot{\epsilon} = \frac{\sigma_1}{\eta} + \frac{\dot{\sigma_1}}{E_1}$ results in $\dot{\epsilon} = \frac{\sigma - E_2\epsilon}{\eta} + \frac{\dot{\sigma} - E_2\dot{\epsilon}}{E_1}$ which can be rearranged into

$$\dot{\epsilon} = \frac{\dot{\sigma}}{E_1 + E_2} + \frac{\sigma}{\frac{\eta(E_1 + E_2)}{E_1}} - \frac{\epsilon}{\frac{\eta(E_1 + E_2)}{E_1 E_2}} \tag{2.5}$$

Define E, μ and λ as

$$E = E_1 + E_2 \tag{2.6}$$

$$\mu = \frac{\eta(E_1 + E_2)}{E_1} \tag{2.7}$$

$$\lambda = \frac{\eta(E_1 + E_2)}{E_1 E_2} \tag{2.8}$$

The equation that represents the standard linear solid model can be written as

$$\dot{\epsilon} = \frac{\dot{\sigma}}{E} + \frac{\sigma}{\mu} - \frac{\epsilon}{\lambda} \tag{2.9}$$

While able to describe the mechanical response of many viscoelastic polymers, it was found by Tobushi that the standard linear solid model cannot capture the so-called "irrecoverable strain" during creep tests for SMP [16] [15]. It was observed experimentally that a residual strain usually exists in the polymer even if it is unloaded for a long time. This residual strain is called irrecoverable strain. For the standard linear solid system in Figure 2.5, immediately after unloading, the strain of the spring on the upper side will vanish instantaneously but there is remaining strain on the spring on the lower side due to the resistance of the dashpot. However, after a long time, the overall strain of the system will tend to zero as the dashpot is completely relaxed. Therefore, there is a need to add a new element to capture the long term irrecoverable strain.

2.2 Rheological viscoelastic model

The rheological viscoelastic model, or simply called rheological model, was proposed by Tobushi *et al.* [16] and was explained in detail later by Bhattacharyya and Tobushi [17]. It is a modified standard linear solid model in order to capture the irrecoverable strain, as shown in Figure 2.6. It is believed [16] that the irrecoverable strain is caused by the irreversible slip and

realignment of the chain molecules. Thus, the slip mechanism of polymer [16] due to internal friction of molecule was considered by adding the friction element (ϵ_s). Also, thermal expansion [16] due to temperature change was considered in the rheological model. The relationship between stress and strain is shown in Eqn. (2.10).

$$\dot{\epsilon} = \frac{\dot{\sigma}}{E} + \frac{\sigma}{\mu} - \frac{\epsilon - \epsilon_s}{\lambda} + \alpha\dot{T} \tag{2.10}$$

where E, μ, λ and ϵ_s are called elastic modulus, viscosity, retardation time and irrecoverable strain respectively and they are all functions of temperature (T). α represents coefficient of thermal expansion and $\dot{T}$ is the rate of temperature change. E, μ, λ are related to E_1, E_2, η in Figure 2.6 and their relations will be explained later. In this thesis, only isothermal conditions were considered so that $\dot{T}$ is zero. Therefore, the equation is reduced into the format below:

$$\dot{\epsilon} = \frac{\dot{\sigma}}{E} + \frac{\sigma}{\mu} - \frac{\epsilon}{\lambda} + \frac{\epsilon_s}{\lambda} \tag{2.11}$$

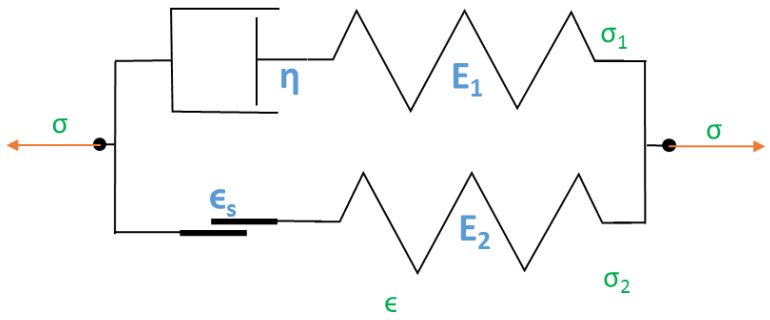

Figure 2.6 Schematic of rheological viscoelastic model

The term ϵ_s is expressed as Eqn. (2.12) and is divided into three different regimes based on the loading condition.

$$\epsilon_s(t > \tau) = \begin{cases} 0 & if\ \ \epsilon_c(\tau) < \epsilon_L \\ C[\epsilon_c(t) - \epsilon_L] & if\ \ \epsilon_c(\tau) \geq \epsilon_L\ and\ \dot{\epsilon}_c(\tau) > 0 \\ \epsilon_s(\tau) & if\ \ \epsilon_c(\tau) \geq \epsilon_L\ and\ \ \dot{\epsilon}_c(\tau) \leq 0 \end{cases} \tag{2.12}$$

ϵ_c in Eqn. (2.12) is called creep strain which is the difference between total strain and elastic strain as shown in Eqn. (2.13).

$$\epsilon_c(t) = \epsilon(t) - \frac{\sigma(t)}{E} \tag{2.13}$$

The irrecoverable strain ϵ_s (Eqn. (2.12)) is proposed based on the experimental observation by Tobushi [16]. It only appears when the creep strain ϵ_c during loading is beyond a certain threshold value ϵ_L; otherwise, $\epsilon_s = 0$ [17]. Thus, regimes 1 is defined as the situation where the ϵ_c does not exceed ϵ_L and $\epsilon_s = 0$. Once ϵ_c exceeds the threshold value, ϵ_s increases proportionally to ϵ_c which is defined as regimes 2. Also, it is proposed that ϵ_s will "stay" in the material and remain a constant value once the creep strain rate becomes zero or negative and this is defined as regime 3. It should be noted that Eqn. (2.12) is not restricted to creep test but can be used under any one dimensional loading conditions. If the strains are negative (e.g. during a compression test), all the quantities in Eqn. (2.12) refer to their absolute value. Because ϵ_s has different expressions in the 3 difference regimes, Eqn. (2.11) will have 3 different expressions and these are presented below.

In the first regime, $\epsilon_s(t) = 0$ so Eqn. (2.11) reduces into Eqn. (2.14) which is simply a standard linear solid model. Therefore, the relationships between E, μ, λ and E_1, E_2, η in the schematic of Figure 2.6 are identical to Eqns. (2.6), (2.7) and (2.8).

$$\dot{\epsilon}(t > \tau) = \frac{\dot{\sigma}(t)}{E} + \frac{\sigma(t)}{\mu} - \frac{\epsilon(t)}{\lambda} \qquad if\ \ \epsilon_c(\tau) < \epsilon_L \tag{2.14}$$

In the second regime, ϵ_s can be expressed as $\epsilon_s(t) = C\left[\epsilon(t) - \frac{\sigma(t)}{E} - \epsilon_L\right]$. Substituting this expression into Eqn. (2.11) results in

$$\dot{\epsilon}(t > \tau) = \frac{\dot{\sigma}(t)}{E} + \left(\frac{1}{\mu} - \frac{C}{\lambda E}\right)\sigma(t) - \left(\frac{1-C}{\lambda}\right)\epsilon(t) + \left(-\frac{C}{\lambda}\right)\epsilon_L \tag{2.15}$$

Introducing μ_{eff}, λ_{eff} and $\epsilon_{s,eff}$ as effective viscosity, effective retardation time and effective irrecoverable strain defined as follows

$$\mu_{eff} = \mu\left(1 - \frac{\mu C}{\lambda E}\right)^{-1} \tag{2.16}$$

$$\lambda_{eff} = \lambda(1 - C)^{-1} \tag{2.17}$$

$$\epsilon_{s,eff} = -\frac{C\epsilon_L}{1-C} \tag{2.18}$$

Eqn. (2.15) can be expressed as:

$$\dot{\epsilon}(t > \tau) = \frac{\dot{\sigma}(t)}{E} + \frac{\sigma(t)}{\mu_{eff}} - \frac{\epsilon(t)}{\lambda_{eff}} + \frac{\epsilon_{s,eff}}{\lambda_{eff}} \qquad if\ \ \epsilon_c(\tau) \geq \epsilon_L\ and\ \dot{\epsilon}_c(\tau) > 0 \tag{2.19}$$

In the third regime, the irrecoverable strain ϵ_s will maintain its value at τ once the strain rate become non-positive $\epsilon_s(t) = \epsilon_s(\tau)$. Substituting this into Eqn. (2.11) results in

$$\dot{\epsilon}(t > \tau) = \frac{\dot{\sigma}(t)}{E} + \frac{\sigma(t)}{\mu} - \frac{\epsilon(t)}{\lambda} + \frac{\epsilon_s(\tau)}{\lambda} \qquad if\ \ \epsilon_c(\tau) \geq \epsilon_L\ and\ \ \dot{\epsilon}_c(\tau) \leq 0 \tag{2.20}$$

In summary, stress-strain relationship for the rheological model is given by Eqns. (2.14), (2.19) and (2.20), respectively for the three regimes.

2.3 Selected analytical solutions to the rheological model

The analytical solution to the rheological model is only possible for simple loading histories such as creep, stress relaxation and uniaxial tension at constant stress or strain rate. These analytical solutions are provided in this section.

In general, if an ordinary differential equation has the form below:

$$\frac{dy}{dt} + P(t)y = Q(t), \tag{2.21}$$

the general solution can be expressed as:

$$y = e^{-\int P(t)dt}\left\{\int \left[Q(t)e^{\int P(t)dt}\right]dt + c\right\} \tag{2.22}$$

where c is an integration constant which depends on the initial condition. If P and Q are constants independent of t, then Eqn. (2.22) is simplified to

$$y = \frac{Q}{P} + ce^{-Pt} \tag{2.23}$$

This result will be used in the calculations below.

2.3.1 Creep

Eqn. (2.24) shows the loading history for a typical creep test and an illustration is given in Figure 2.7. Denote t_a as the time when creep strain exceeds the threshold strain ϵ_L and t_b as the unloading time. Therefore, the time from 0 to t_a corresponds to regime 1, the time between t_a and t_b is regime 2 and the time after t_b is regime 3.

$$\sigma(t) = \begin{cases} \sigma_0 & 0 \le t \le t_b \\ 0 & t > t_b \end{cases} \tag{2.24}$$

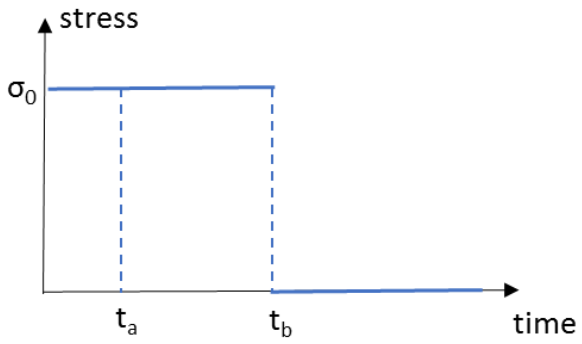

Figure 2.7 Stress history for creep test

In regime 1 ($t < t_a$), Eqn. (2.14) becomes $\dot{\epsilon}(t) + \frac{\epsilon(t)}{\lambda} = \frac{\sigma_0}{\mu}$, which is in the same form as Eqn. (2.21). By using Eqn. (2.23), we obtain the following solution for the strain

$$\epsilon(t) = \sigma_0 \frac{\lambda}{\mu} + c_1 e^{-\frac{t}{\lambda}} \tag{2.25}$$

where c_1 is a constant to be determined by the initial condition. When the stress is applied initially as shown in Figure 2.6, the element ϵ_s has not yet been triggered and the dashpot cannot produce an instantaneous strain so the whole system acts as two parallel springs. Therefore, the initial condition is $\epsilon(0) = \frac{\sigma_0}{E}$. Substituting this condition into Eqn. (2.25), c_1 can be obtained as $c_1 = \sigma_0 \left(\frac{1}{E} - \frac{\lambda}{\mu}\right)$, which leads to

$$\epsilon(t) = \sigma_0 \left(\frac{\lambda}{\mu} - \frac{1}{E}\right)\left(1 - e^{-\frac{t}{\lambda}}\right) + \frac{\sigma_0}{E} \qquad (0 \le t \le t_a) \tag{2.26}$$

In regime 2 ($t_a < t \le t_b$), Eqn. (2.19) becomes $\dot{\epsilon}(t) + \frac{\epsilon(t)}{\lambda_{eff}} = \frac{\sigma_0}{\mu_{eff}} + \frac{\epsilon_{s,eff}}{\lambda_{eff}}$, which is also in the same form as Eqn. (2.21). Using the Eqn. (2.23), we get:

$$\epsilon(t) = \left(\sigma_0 \frac{\lambda_{eff}}{\mu_{eff}} + \epsilon_{s,eff}\right) + c_2 e^{-\frac{t}{\lambda_{eff}}} \tag{2.27}$$

where c_2 is a constant and it can be obtained by using continuity condition at t_a when the strain at the end of regime 1 is equal to the strain at the beginning of regime 2. Since the creep strain at t_a is ϵ_L, the strain at this time is $\epsilon_L + \frac{\sigma_0}{E}$. Using Eqn. (2.27), c_2 can be solved and the final expression for strain is

$$\epsilon(t) = \left(\epsilon_L + \frac{\sigma_0}{E}\right) e^{-\frac{t-t_a}{\lambda_{eff}}} + \sigma_0 \left(\frac{\epsilon_{s,eff}}{\sigma_0} + \frac{\lambda_{eff}}{\mu_{eff}}\right)\left(1 - e^{-\frac{t-t_a}{\lambda_{eff}}}\right) \qquad (t_a < t \le t_b) \tag{2.28}$$

In regime 3 ($t > t_b$), when unloading happens, Eqn. (2.21) becomes $\dot{\epsilon}(t) + \frac{\epsilon(t)}{\lambda} = \frac{\epsilon_s(t_b)}{\lambda}$. By using Eqn. (2.23), we get:

$$\epsilon(t) = \epsilon_s(t_b) + c_3 e^{-\frac{t}{\lambda}} \tag{2.29}$$

When unloading just happens at t_b, only the two parallel springs can react to this loading change instantaneously because ϵ_s maintains its value and the dashpot cannot react instantaneously. Thus, the overall strain drops $\frac{\sigma_0}{E}$ from $\epsilon(t_b^-)$ to $\epsilon(t_b^+)$. Using Eqn. (2.29) for the moment when unloading just happens, $\epsilon(t_b^+) = \epsilon_s(t_b) + c_3 e^{-\frac{t_b}{\lambda}}$. Therefore, c_3 is solved and the final expression is given as

$$\epsilon(t) = \epsilon_s(t_b) + [\epsilon(t_b^+) - \epsilon_s(t_b)] e^{-\frac{t-t_b}{\lambda}} \qquad (t > t_b) \tag{2.30}$$

After t_b, the stress goes to zero so the creep strain is equal to the total strain. Thus, $\epsilon_s(t_b) = C(\epsilon(t_b^+) - \epsilon_L)$. In summary, the strain response for creep test is given by Eqns. (2.26), (2.28) and (2.30). Figure 2.8 shows a typical plot of strain response with respect to time for creep test.

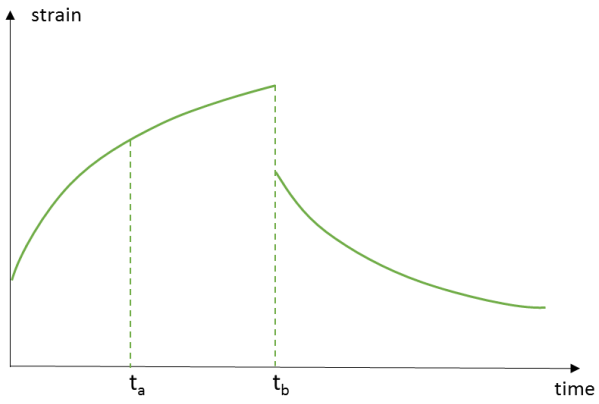

Figure 2.8 Strain response for creep test

2.3.2 Stress Relaxation

Eqn. (2.31) shows the strain history for stress relaxation test and a typical plot is illustrated in Figure 2.9. Denoting t_a as the time when the creep strain exceeds the threshold strain ϵ_L, the time from 0 to t_a corresponds to regime 1 and the time after t_a is regime 2.

$$\epsilon(\mathrm{t}) = \epsilon_0 \tag{2.31}$$

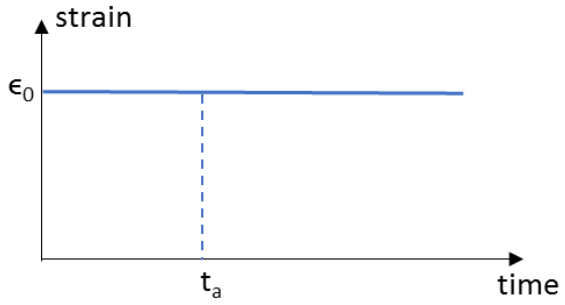

Figure 2.9 Strain history for stress relaxation test

In regime 1 $(t < t_a)$, Eqn. (2.14) becomes $\dot{\sigma}(t) + \frac{E}{\mu}\sigma(t) = \frac{E}{\lambda}\epsilon_0$. By using Eqn. (2.23), we obtain the following solution for the stress

$$\sigma(t) = \frac{\mu}{\lambda}\epsilon_0 + c_4 e^{-\frac{E}{\mu}t} \tag{2.32}$$

where c_4 is a constant which depends on the initial condition. When the strain is applied initially, the element ϵ_s in Figure 2.6 has not yet been triggered and the dashpot cannot produce an

instantaneous strain so the two parallel springs undertakes the initial strain. Therefore, the initial condition is $\sigma(0) = E\epsilon_0$. Substituting this condition into Eqn. (2.32), c_4 is obtained as $c_4 = \epsilon_0\left(E - \frac{\mu}{\lambda}\right)$, and the expression of stress response is given as

$$\sigma(t) = \frac{\mu}{\lambda}\epsilon_0 + \epsilon_0\left(E - \frac{\mu}{\lambda}\right)e^{-\frac{E}{\mu}t} \qquad (0 \le t \le t_a) \tag{2.33}$$

In regime 2 ($t > t_a$), Eqn (2.19) becomes $\dot{\sigma}(t) + \frac{E}{\mu_{eff}}\sigma(t) = \frac{E}{\lambda_{eff}}\epsilon_0 - \frac{E}{\lambda_{eff}}\epsilon_{s,eff}$, which can be solved using Eqn. (2.23)

$$\sigma(t) = \frac{\mu_{eff}}{\lambda_{eff}}\left(\epsilon_0 - \epsilon_{s,eff}\right) + c_5 e^{-\frac{E}{\mu_{eff}}t} \tag{2.34}$$

where c_5 is a constant and can be obtained by using continuity condition at time t_a when the stress at the end of regime 1 is equal to the stress at the beginning of regime 2. At t_a, $\epsilon_c(t_a) = \epsilon_0 - \frac{\sigma(t_a)}{E} = \epsilon_L$ so that $\sigma(t_a) = E(\epsilon_0 - \epsilon_L)$. Using Eqn. (2.34), c_5 can be solved and the final expression for the stress is

$$\sigma(t) = \frac{\mu_{eff}}{\lambda_{eff}}\left(\epsilon_0 - \epsilon_{s,eff}\right) + \left[E(\epsilon_0 - \epsilon_L) - \frac{\mu_{eff}}{\lambda_{eff}}\left(\epsilon_0 - \epsilon_{s,eff}\right)\right]e^{-\frac{E}{\mu_{eff}}(t-t_a)} \quad (t > t_b) \tag{2.35}$$

In summary, the stress response for stress relaxation is given by Eqns. (2.33) and (2.35). Figure 2.10 shows a typical plot of stress with respect to time for stress relaxation.

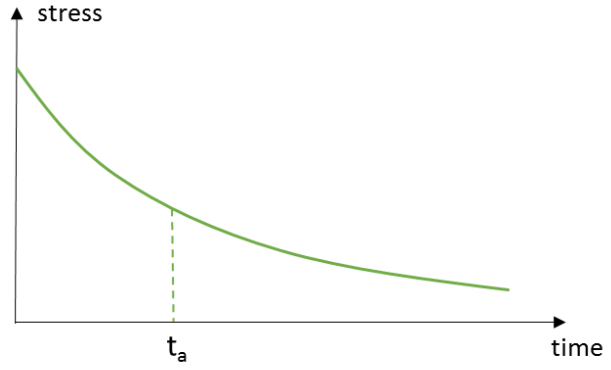

Figure 2.10 Stress response for stress relaxation test

2.3.3 Tensile test at fixed stress rate

The tensile test is conducted by applying an increasing stress at a fixed stress rate $\dot{\sigma_0}$. Eqn. (2.36) shows the loading history and a corresponding plot is shown in Figure 2.11. Denote t_a as the time when the creep strain exceeds the threshold strain ϵ_L. Therefore, the time from 0 to t_a corresponds to regime 1 and the time after t_a is regime 2.

$$\sigma(t) = \dot{\sigma_0} t \tag{2.36}$$

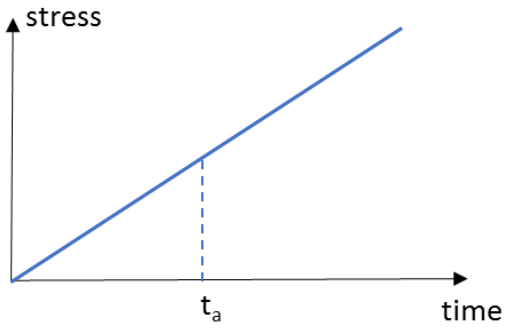

Figure 2.11 Stress history for tensile test

In regime 1 ($t < t_a$), Eqn. (2.14) becomes $\dot{\epsilon}(t) + \frac{\epsilon(t)}{\lambda} = \frac{\dot{\sigma_0}}{\mu} t + \frac{\dot{\sigma_0}}{E}$. By using Eqn. (2.22) and considering $\dot{\sigma_0}$ being constant, this solution can be obtained as

$$\epsilon(t) = e^{-\frac{1}{\lambda}t}\left[\dot{\sigma_0}\lambda\left(\frac{1}{E} - \frac{\lambda}{\mu}\right)e^{\frac{1}{\lambda}t} + \dot{\sigma_0}\frac{\lambda}{\mu}\, te^{\frac{1}{\lambda}t} + c_6\right] \tag{2.37}$$

Initially, the applied stress is zero so that the initial strain is also zero. Using the initial condition $\epsilon(0) = 0$ in Eqn. (2.37) allows us to determine c_6 and thus the expression for $\epsilon(t)$ is given as

$$\epsilon(t) = \dot{\sigma_0}\frac{\lambda}{\mu}\, t - \dot{\sigma_0}\lambda\left(\frac{\lambda}{\mu} - \frac{1}{E}\right)\left(1 - e^{-\frac{1}{\lambda}t}\right) \qquad (0 \le t \le t_a) \tag{2.38}$$

In regime 2 ($t > t_a$), Eqn. (2.19) becomes $\dot{\epsilon}(t) + \frac{\epsilon(t)}{\lambda_{eff}} = \frac{\dot{\sigma_0}}{\mu_{eff}} t + \frac{\dot{\sigma_0}}{E} + \frac{\epsilon_{s,eff}}{\lambda_{eff}}$. Similarly, the solution can be obtained by using Eqn. (2.22)

$$\epsilon(t) = e^{-\frac{1}{\lambda_{eff}}t}\left[\dot{\sigma_0}\lambda_{eff}\left(\frac{1}{E} - \frac{\lambda_{eff}}{\mu_{eff}}\right)e^{\frac{1}{\lambda_{eff}}t} + \epsilon_{s,eff}e^{\frac{1}{\lambda_{eff}}t} + \dot{\sigma_0}\frac{\lambda_{eff}}{\mu_{eff}}\, te^{\frac{1}{\lambda_{eff}}t} + c_7\right] \tag{2.39}$$

Using continuity condition at time t_a when the strain at the end of regime 1 is equal to the strain at the beginning of regime 2, c_7 can be obtained and the strain response in regime 2 is obtained as below:

$$\epsilon(t) = \epsilon(t_a)e^{-\frac{(t-t_a)}{\lambda_{eff}}} + \left[\dot{\sigma}_0\lambda_{eff}\left(\frac{1}{E} - \frac{\lambda_{eff}}{\mu_{eff}}\right) + \epsilon_{s,eff}\right]\left(1 - e^{-\frac{(t-t_a)}{\lambda_{eff}}}\right) + \dot{\sigma}_0\frac{\lambda_{eff}}{\mu_{eff}}\,t - \dot{\sigma}_0\frac{\lambda_{eff}}{\mu_{eff}}\,t_a e^{-\frac{(t-t_a)}{\lambda_{eff}}} \qquad (t > t_a) \tag{2.40}$$

In summary, the strain response for tensile test is given by Eqns. (2.38) and (2.40). Figure 2.12 shows a typical plot of stress-strain curve for the tensile test at fixed stress rate.

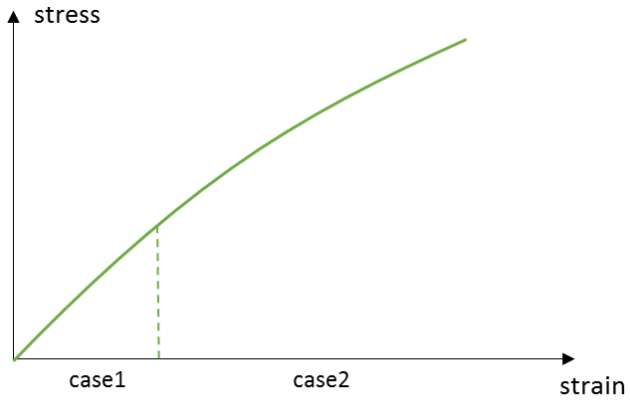

Figure 2.12 Stress-strain curve for tensile test at fixed stress rate

2.4 General numerical scheme to implement the model

Analytical solution to the rheological model might not exist for more complicated loading conditions. Therefore, numerical method is necessary to solve stress-strain relationships under general loading conditions. The Euler method [22] is a first order explicit numerical method for solving ordinary differential equations that can be readily implemented.

2.4.1 Implementation with Euler explicit method

Eqns. (2.14), (2.19) and (2.20) represent the stress-strain relationship for the rheological model in the three different regimes. Rewrite these expressions in a unified format as Eqn. (2.41)

$$\dot{\epsilon} = \frac{\dot{\sigma}}{E} + \frac{\sigma}{\mu_{EFF}} - \frac{\epsilon}{\lambda_{EFF}} + \frac{\epsilon_{s,EFF}}{\lambda_{EFF}} \tag{2.41}$$

where μ_{EFF}, λ_{EFF} and $\epsilon_{s,EFF}$ are defined as

$$\mu_{EFF} = \begin{cases} \mu & if\ \ \epsilon_c < \epsilon_L \\ \mu_{eff} = \mu\left(1 - \frac{\mu C}{\lambda E}\right)^{-1} & if\ \ \epsilon_c \geq \epsilon_L\ and\ \dot{\epsilon_c} > 0 \\ \mu & if\ \ \epsilon_c \geq \epsilon_L\ and\ \ \dot{\epsilon_c} \leq 0 \end{cases} \tag{2.42}$$

$$\lambda_{EFF} = \begin{cases} \lambda & if\ \ \epsilon_c < \epsilon_L \\ \lambda_{eff} = \lambda(1 - C)^{-1} & if\ \ \epsilon_c \geq \epsilon_L\ and\ \dot{\epsilon_c} > 0 \\ \lambda & if\ \ \epsilon_c \geq \epsilon_L\ and\ \ \dot{\epsilon_c} \leq 0 \end{cases} \tag{2.43}$$

$$\epsilon_{s,EFF} = \begin{cases} 0 & if\ \ \epsilon_c < \epsilon_L \\ \epsilon_{s,eff} = -\frac{C\epsilon_L}{1 - C} & if\ \ \epsilon_c \geq \epsilon_L\ and\ \dot{\epsilon_c} > 0 \\ \epsilon_s(\tau) = C[\epsilon_c(\tau) - \epsilon_L] & if\ \ \epsilon_c \geq \epsilon_L\ and\ \ \dot{\epsilon_c} \leq 0 \end{cases} \tag{2.44}$$

To numerically integrate (2.41), we discretize time (t) into N equal intervals $t_0\,(= 0), t_1, t_2, \ldots\ t_n, t_{n+1}, \ldots t_N$. The corresponding stress and strain are $\sigma_n = \sigma(t_n)$ and $\epsilon_n = \epsilon(t_n)$. Denote Δt as the time step, i.e., $\Delta t = t_{n+1} - t_n$. Based on the Euler method, strain rate $\dot{\epsilon}$ and stress rate $\dot{\sigma}$ can be approximate by $\frac{\epsilon_{n+1} - \epsilon_n}{\Delta t}$ and $\frac{\sigma_{n+1} - \sigma_n}{\Delta t}$ respectively. Thus, Eqn. (2.41) can be discretized as

$$\frac{\epsilon_{n+1} - \epsilon_n}{\Delta t} = \frac{\sigma_{n+1} - \sigma_n}{E\Delta t} + \frac{\sigma_n}{\mu_{EFF}} - \frac{\epsilon_n}{\lambda_{EFF}} + \frac{\epsilon_{s,EFF}}{\lambda_{EFF}} \tag{2.45}$$

If the stress history is given, i.e. we know $\sigma_n (n = 0,1,2, \ldots N)$, Eqn. (2.45) can be rewritten as

$$\epsilon_{n+1} = \frac{1}{E}\sigma_{n+1} + \epsilon_n\left(1 - \frac{\Delta t}{\lambda_{EFF}}\right) + \sigma_n\left(\frac{\Delta t}{\mu_{EFF}} - \frac{1}{E}\right) + \frac{\epsilon_{s,EFF}\Delta t}{\lambda_{EFF}} \tag{2.46}$$

With an given initial condition for strain ϵ_0, Eqn. (2.46) can be used to obtain the complete strain history. Specifically at each step, the values of σ_n, σ_{n+1}, ϵ_n are known. Next, the relationship between $\epsilon_c(t_n) = \epsilon_n - \frac{\sigma_n}{E}$ and ϵ_L is checked to see which expression among Eqns. (2.42)-(2.44) should be used for μ_{EFF}, λ_{EFF} and $\epsilon_{s,EFF}$. Then, ϵ_{n+1} can be calculated from Eqn. (2.46). The same procedure is followed to obtain the complete strain history $\epsilon_n (n = 1,2, \ldots N)$.

Similarly, if the strain history is given, i.e. we know $\epsilon_n (n = 0,1,2, \dots N)$, Eqn. (2.45) can be rewritten as Eqn. (2.47). The same procedure can be applied to solve for stress history $\sigma(t)$.

$$\sigma_{n+1} = E\epsilon_{n+1} + \sigma_n \left(1 - \frac{E\Delta t}{\mu_{EFF}}\right) + \epsilon_n \left(\frac{E\Delta t}{\lambda_{EFF}} - E\right) - \frac{\epsilon_{s,EFF} E\Delta t}{\lambda_{EFF}} \tag{2.47}$$

2.4.2 Validation against analytical solution

Euler method is an approximate method so its accuracy should be validated. Now that the analytical solutions exist for simple loading conditions, the results of analytical solutions and Euler solutions can be compared. In this section, the analytical solutions and Euler solutions for creep test, stress relaxation test and tensile test at fixed stress rate are compared.

To solve Eqn. (2.41) analytically or Eqn. (2.45) numerically, the values of E, μ ,λ ,C and ϵ_L need to be known. In this section, the values of these parameters are selected based on [16] at glass transition temperature T_g which are shown in Table 2.1. Also, the accuracy of Euler method depends on the time step (Δt). In this section, 1 second, 0.1 second, 0.01 second and 0.001 second will be used for Δt to test its effect on the results. The accuracy of Euler solutions are tested quantitatively by using the coefficient of determination R^2 [23] defined as

$$R^2 = 1 - \frac{\sum_i (y_i - f_i)^2}{\sum_i (y_i - \bar{y})^2} \tag{2.48}$$

where y_i represents analytical solution at time t_i, f_i represents Euler solution at t_i and $\bar{y}$ is the average value of the analytical solution. R^2 ranges from 0 to 1. The better the two group of data fit, the closer the value of R^2 is to 1.

Table 2.1 Values of parameters used for validation

Parameters	E(MPa)	μ(GPa·s)	λ(s)	C	ϵ_L(%)
Value	146	14	521	0.112	0.3

Figure 2.13 compares the creep results between analytical solution and Euler solution with different time steps. The R^2 value is equal to 0.99999967, 0.9999999967, 0.999999999967 and

0.99999999999967 respectively with the decrease of time step. Therefore, for creep the Euler solution is accurate as long as the time step is no more than 1 second.

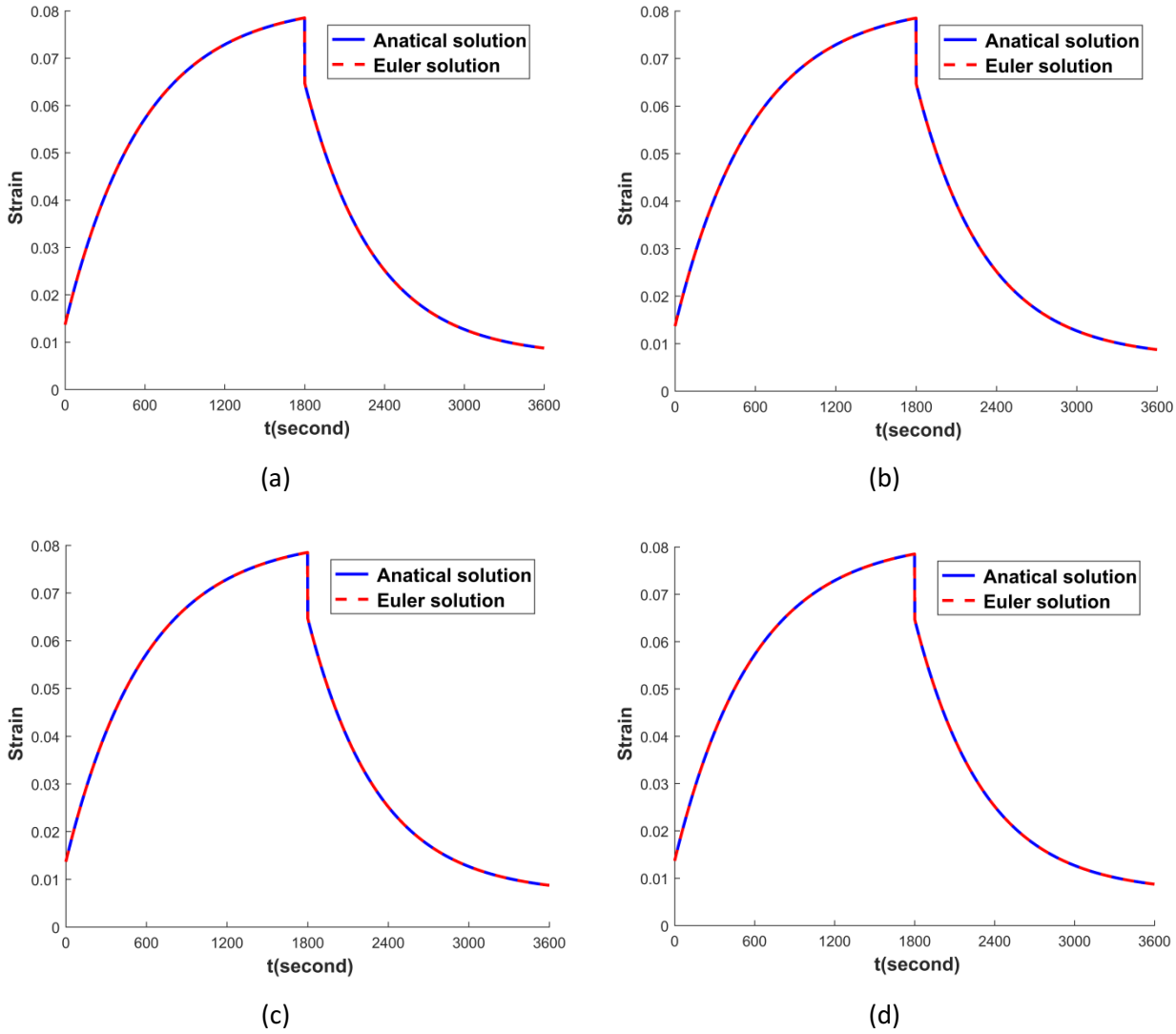

Figure 2.13 Creep results compare between analytical and Euler numerical solution with different times step. (a) $\Delta t = 1$ s, (b) $\Delta t = 0.1$ s, (c) $\Delta t = 0.01$ s, (d) $\Delta t = 0.001$ s.

Figure 2.14 compares the stress relaxation results between analytical solution and Euler solution with different time steps. The R^2 value is equal to 0.999985, 0.99999985, 0.9999999985 and 0.999999999985 respectively with the decrease of time step. Therefore, for stress relaxation the Euler solution is again accurate if the time step is no more than 1 second.

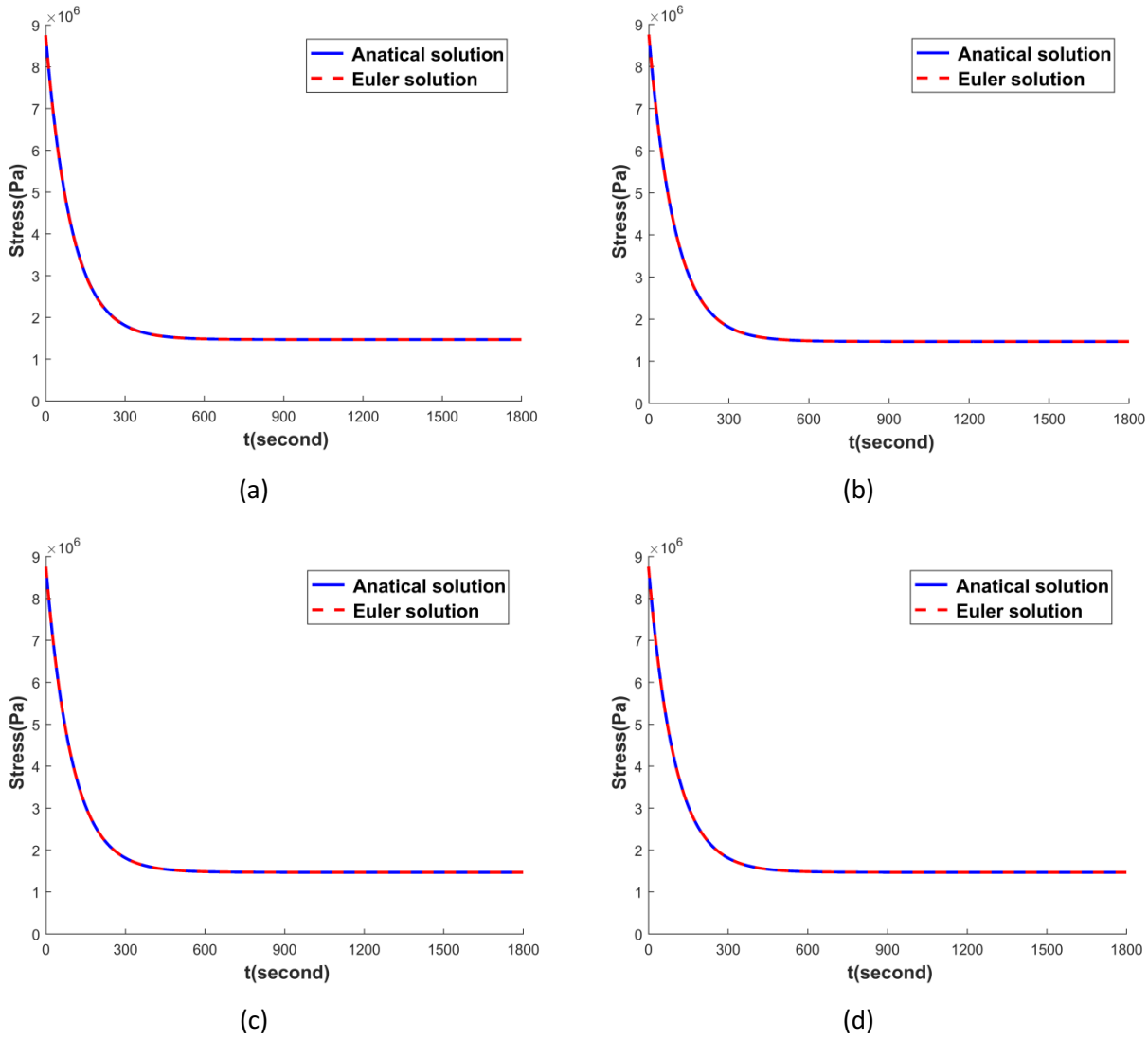

Figure 2.14 Stress relaxation compare between analytical and Euler solution with different time steps. (a) $\Delta t = 1$ s, (b) $\Delta t = 0.1$ s, (c) $\Delta t = 0.01$ s, (d) $\Delta t = 0.001$ s.

Figure 2.15 compares the results of uniaxial tension at constant loading rate (0.05 MPa/s) between analytical solution and Euler solution with different time steps. The R^2 value is equal to 0.999976, 0.99999976, 0.9999999976 and 0.999999999976 respectively with the decrease of time step. Again the Euler solution is accurate if the time step is no more than 1 second in this case.

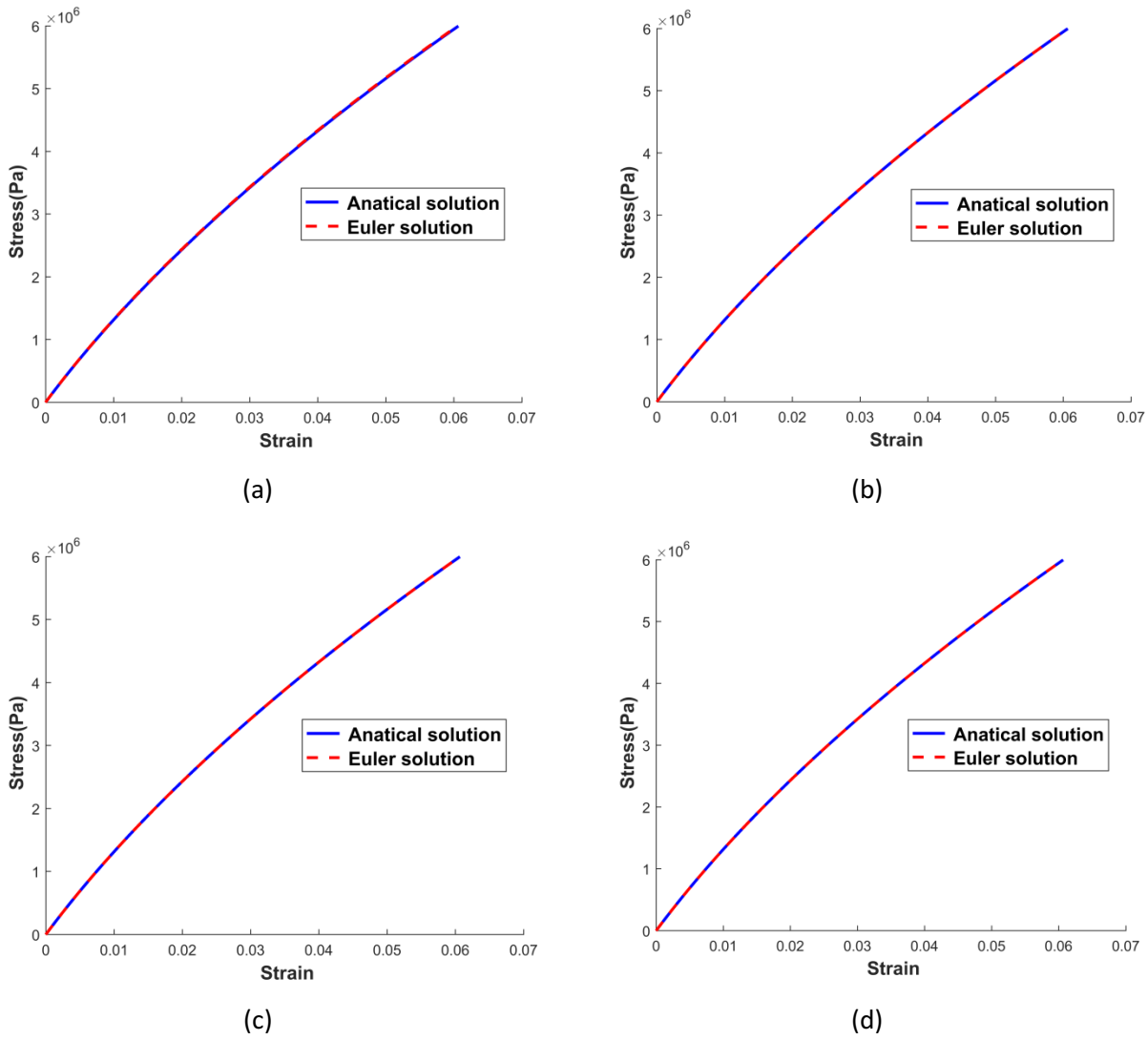

Figure 2.15 Tensile test compare between analytical and Euler solution with different time step. (a) $\Delta t = 1$ s, (b) $\Delta t = 0.1$ s, (c) $\Delta t = 0.01$ s, (d) $\Delta t = 0.001$ s.

In summary, when the time step is no more than 1 second, no obvious improvement was observed with finer discretization; therefore, any time step no more than 1 second can be used when numerically implementing the rheological model. Based on the investigation here, 0.1 second is chosen for numerical integration later in this thesis.

Chapter 3 : Application of the model to bending

Shape memory polymers have the potential to be used in different applications to achieve desired shape memory functions. For many of the applications, e.g., when they are used for polymeric cardiovascular stents [12] or morphing wings of aircrafts [11], they are inevitable subjected to bending load. For example, when the morphing wings of an airplane is unfolded, the two wings are hanged in their fuselage and can be regarded as two cantilever beams. In order to evaluate the bending response of structures made of SMP, there is a need to develop a model that can be used to predict the bending behavior of SMPs.

In the past, several researchers investigated the bending behavior of SMPs. Tobushi *et al.* [19] conducted thermomechanical bending tests consisting of the following steps. First, a displacement was applied on the beam at a high temperature above T_g. With the constant holding deformation, the specimen was cooled down to a low temperature below T_g. Then it was heated to a prescribed holding temperature and the deformation was maintained for a prescribed holding time. Finally, the specimen was unloaded and heated up to the same high temperature. The influence of different factors (e.g. holding temperature and holding time) on the shape recovery ratio (defined as the ratio of the difference between maximum strain in the beam and final residual strain in the beam to the maximum strain in the beam) was investigated. However, no corresponding predictive model was developed to compare with the experiments. Wang *et al.* [24] applied the Maxwell-Weichert model (two Maxwell models and one spring in parallel) to the 3-point bending of SMP. The relationship between stress and deformation on thermomechanical test is obtained. Baghani *et al.* integrated a viscoelastic model with Euler-Bernoulli beam theory to model the thermomechanical behavior of 3-point bending beam and cantilever beam respectively [25]. This viscoelastic model [26] regards the polymer as two phases, the active phase and frozen phase, which can be transformed into each other through heat stimuli. The curvature and deflection is obtained at some steps of the thermomechanical test. Ghosh *et al.* applied a thermodynamically based state evolution model to 3-point bending in a finite element framework [20]. The relationship between displacement and force at the middle of the beam in a thermomechanical cycle is obtained. However, in these works no corresponding experiments were performed to validate the feasibility and limitation of those models.

Since the rheological model discussed in Chapter 2 has not been applied under bending condition, this chapter will extend the rheological model to 3-point bending of a thin beam and corresponding experiments will be conducted to validate the model in the later chapters. Analytical solution based on the rheological model is not feasible for bending problems, so numerical implementation is necessary. Euler method is validated for uniaxial loading conditions in the last chapter and given that bending of a thin beam is also one dimensional loading, it will be used for the numerical implementation.

3.1 Assumptions

A schematic of 3-point bending is shown in Figure 3.1. A force P is applied at the mid span of the beam and there are two supports on the two end of the beam with hinge joints. The goal is to calculate the time-dependent deflection of the beam given a loading history $P(t)$.

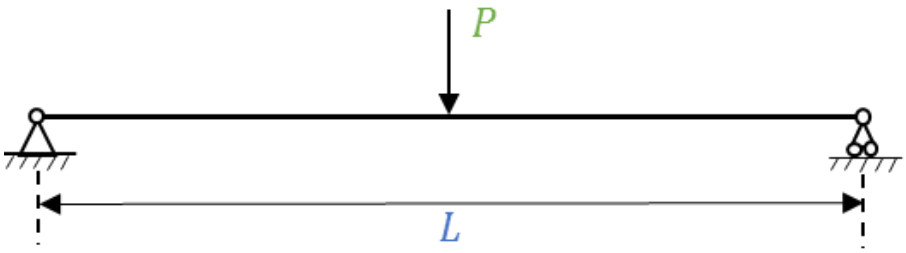

Figure 3.1 Schematic for 3-point bending of a thin beam

The beam considered in this analysis is a thin beam with rectangular constant cross sections. Figure 3.2 shows the side view of the beam with the establishment of the coordinate system. L, h and b represent the distance between the two supports, height and width of the beam respectively. The longitudinal axis x lies along the neutral axis of the beam while the vertical axis y passes through the left support of the beam. The applied load is symmetric about $x = L/2$ so the stress and strain distribution is symmetric about $x = L/2$. Therefore, for the calculations hereafter, only the left half of the beam will be investigated.

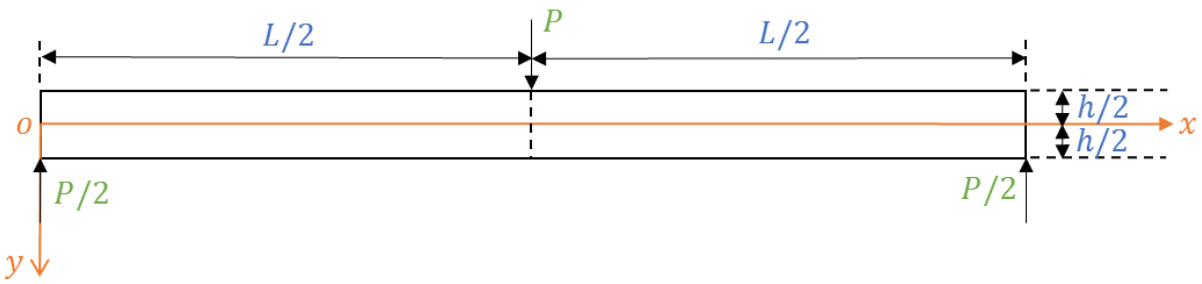

Figure 3.2 Front view of the beam

Since the beam is thin and only small deformation is considered in this thesis, the assumptions in the classical Euler-Bernoulli beam theory for elastic material [27] will be adopted. First, the length of the neutral axis is assumed to be constant during deformation. Second, all cross sections of the beam remain plane and perpendicular to the longitudinal axis x when the beam is deformed. Third, the deformation of the cross section within its own plane will not be considered. Based on these assumptions, the strain and curvature have the relation below

$$\epsilon(t,x,y) = \kappa(t,x)y \tag{3.1}$$

where κ represents curvature. In addition, all the quantities (E, μ, λ, C and ϵ_L) in Eqn. (2.41)-(2.44) are assumed to be the same for both tension and compression so that $\sigma(t,x,-y) = -\sigma(t,x,y)$ and $\epsilon(t,x,-y) = -\epsilon(t,x,y)$. The moment $M(t,x)$ at any cross section can be then calculated as

$$M(t,x) = \int \sigma(t,x,y)ydA = \int_{-h/2}^{h/2} \sigma(t,x,y)bydy = 2\int_{0}^{h/2} \sigma(t,x,y)bydy \tag{3.2}$$

where dA represents an area element in the cross section and dy represents a length element along y direction so that $dA = bdy$.

3.2 Formulation and numerical scheme

The numerical scheme developed in Chapter 2 for the rheological model is used in this chapter. For uniaxial loading, the stress and strain are uniformly distributed so each of them is only a function of time. For the bending of a beam, however, the stress and strain also depend on location besides their time dependence. As a result, moment $M(t,x)$ is a function of t and x;

curvature $\kappa(t,x)$ is a function of t and x; stress $\sigma(t,x,y)$ is a function of t, x and y; and strain $\epsilon(t,x,y)$ is a function of t, x and y. In order to solve for the deformation history of the entire beam, stress and strain need to be evaluated at any time and at any point of the beam. This requires the discretization along x and y axis besides the discretization of time.

First of all, as in Chapter 2, time (t) is discretized into N equal intervals which results in $t_0(=0), t_1, t_2, \dots t_n, t_{n+1}, \dots t_N$. At any cross section (i.e., given x), the bottom half of the cross section (from $y=0$ to $y=h/2$) is discretized into R equal intervals with size Δy leading to $y_0(=0), y_1, y_2, \dots y_r, y_{r+1}, \dots y_R(=h/2)$. In addition, the left half of the beam (from $x=0$ to $x=L/2$) is discretized into Q equal intervals with size Δx which results in $x_0(=0), x_1, x_2, \dots x_q, x_{q+1}, \dots x_Q(=L/2)$. σ_n and ϵ_n in Eqn. (2.47) will be written as $\sigma(t_n)$ and $\epsilon(t_n)$, for any given x and y, to indicate their time dependence.

At one particular cross section (given x) if the moment history $M(t_n)$ $(n=0,1,2,\dots N)$ is known (considering that the loading history at mid-span is given), the curvature history $\kappa(t_n)$ $(n=0,1,2,\dots N)$ can be obtained as follows. Eqn. (2.47) gives the relation between stress and strain at one particular point. Eqn. (3.1) gives the relation between strain and curvature. Substituting Eqns. (2.47) and (3.1) into Eqn. (3.2), the relation between moment and curvature can be obtained as

$$\begin{aligned} M(t_{n+1}) &= 2\int_0^{h/2} \sigma(t_{n+1},y)by\,dy \\ &= 2\int_0^{h/2} E\kappa(t_{n+1})by^2dy + 2\int_0^{h/2}\left(1-\frac{E\Delta t}{\mu_{EFF}}\right)\sigma(t_n,y)by\,dy \\ &\quad + 2\int_0^{h/2}\left(\frac{E\Delta t}{\lambda_{EFF}}-E\right)\kappa(t_n)by^2dy - 2\int_0^{h/2}\frac{\epsilon_{s,EFF}E\Delta t}{\lambda_{EFF}}by\,dy \end{aligned} \tag{3.3}$$

Using the definition of moment of inertia $I=\int y^2dA = 2\int_0^{h/2} by^2dy$ and rearranging Eqn. (3.3) result in

$$\kappa(t_{n+1}) = \kappa(t_n) + \frac{1}{EI}[M(t_{n+1}) - M(t_n)] + \frac{b\Delta t}{I}(\Phi - \Psi + \Omega) \tag{3.4}$$

where Φ, Ψ and Ω are defined as $2\int_0^{h/2}\frac{\epsilon_{s,EFF}}{\lambda_{EFF}}ydy$, $2\int_0^{h/2}\frac{1}{\lambda_{EFF}}\kappa_n y^2 dy$ and $2\int_0^{h/2}\frac{1}{\mu_{EFF}}\sigma_n ydy$ respectively.

In Section 2.2, it was described that the constitutive relation of the material can lie in 3 different regimes depending on the loading conditions as shown in Eqn. (2.12). Without unloading, the constitutive relation at any point of the beam is either in regime 1 or regime 2. Before any point reaches regime 2, there is a linear relationship between the creep strain ϵ_c and y so that ϵ_c will be greater at larger y. With the increase of external loading, beyond certain y at one particular cross section, creep strain might reach the threshold strain ϵ_L where the irrecoverable strain will be triggered. As a result, materials beyond that point will be in regime 2 while the rest still remain in regime 1. The value of μ_{EFF}, λ_{EFF} and $\epsilon_{s,EFF}$ in regimes 1 and the 2 have different expressions as shown in Eqns. (2.42)-(2.44) so in order to evaluate Φ, Ψ and Ω in Eqn. (3.4) there is a need to introduce a critical point $y = a$ where $\epsilon_c = \epsilon_L$. Regime 1 lies within $y < a$ where $\epsilon_c < \epsilon_L$ and μ_{EFF}, λ_{EFF} and $\epsilon_{s,EFF}$ are equal to μ, λ and 0 respectively. Regime 2 lies within $a < y \leq h/2$ where $\epsilon_c > \epsilon_L$ and μ_{EFF}, λ_{EFF} and $\epsilon_{s,EFF}$ are equal to μ_{eff}, λ_{eff} and $\epsilon_{s,eff}$ respectively. Φ, Ψ and Ω can then be calculated as

$$\Phi = \frac{\epsilon_{s,eff}}{\lambda_{eff}}\left(\frac{1}{4}h^2 - a^2\right) \tag{3.5}$$

$$\Psi = \kappa(t_n)\left[\frac{1}{\lambda}\frac{2}{3}a^3 + \frac{1}{\lambda_{eff}}\left(\frac{1}{12}h^3 - \frac{2}{3}a^3\right)\right] \tag{3.6}$$

$$\Omega = \frac{2}{\mu}\int_0^a \sigma_n ydy + \frac{2}{\mu_{eff}}\int_a^{\frac{h}{2}} \sigma_n ydy \tag{3.7}$$

In summary, if the loading history is given, the curvature history at one particular cross section can be calculated by using Eqns. (2.47), (3.1) and (3.4)-(3.7) with given initial conditions. Specifically, at each time step t_{n+1}, the values of $M(t_n)$ $M(t_{n+1})$, $\kappa(t_n)$, $\epsilon(t_n, y)$ and $\sigma(t_n, y)$ are known. Since y has been discretized, $\sigma(t_n, y)$ and $\epsilon(t_n, y)$ are also discretized along y direction. a can be obtained by using the condition $\epsilon_c(t_n, y) = \epsilon(t_n, y) - \frac{\sigma(t_n, y)}{E} = \epsilon_L$. Now that a is known, Φ can be calculated directly by using Eqn. (3.5). Given a and $\kappa(t_n)$, Ψ is obtained by using Eqn. (3.6). Given a and $\sigma(t_n, y)$, Ω is obtained by using Eqn. (3.7). Next, $\kappa(t_{n+1})$ can

be calculated by using Eqn. (3.4), followed by the calculation of $\epsilon(t_{n+1}, y)$ from Eqn. (3.1). Finally, $\sigma(t_{n+1}, y)$ is obtained by using Eqn (2.47). The same procedure is followed to obtain the complete curvature history $\kappa(t_n)(n = 1,2, \dots N)$. These procedures can be illustrated by a flowchart as shown in Figure 3.3.

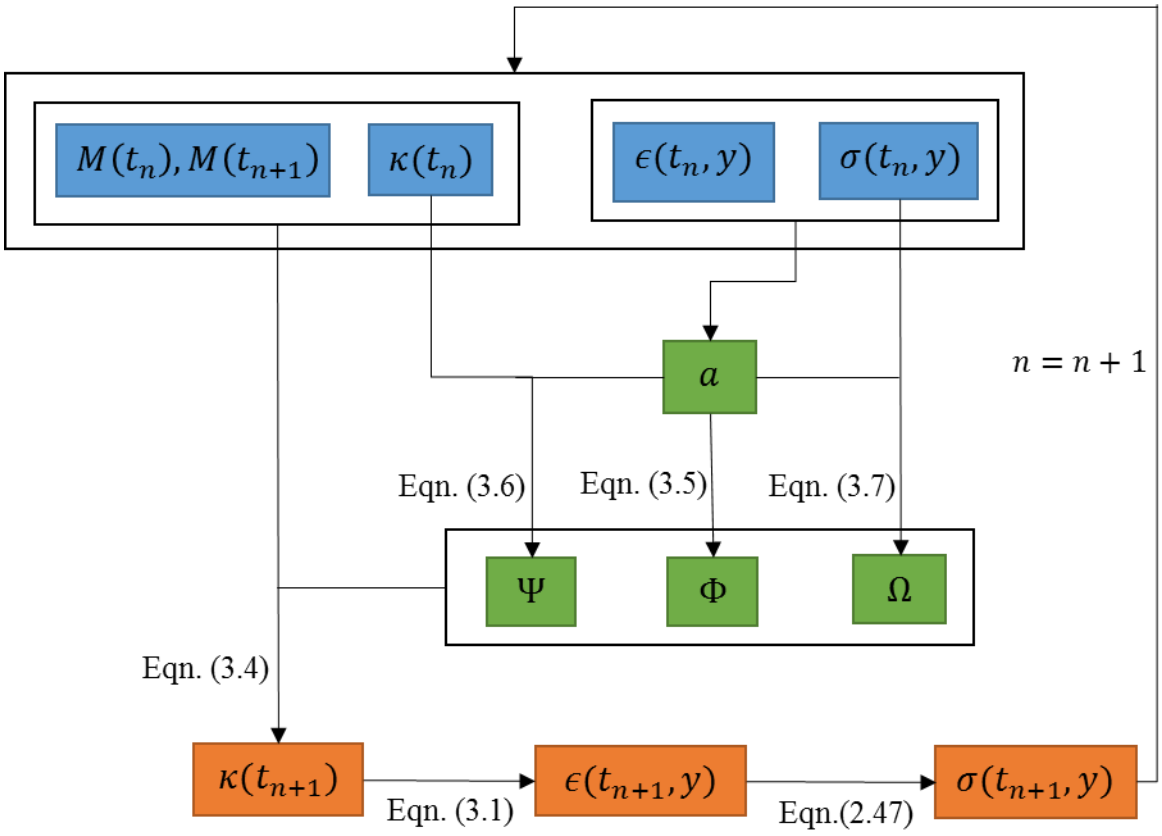

Figure 3.3 Flowchart of the calculation for curvature at one particular cross section

Since x axis (from $x = 0$ to $x = L/2$) is discretized as $x_0(= 0), x_1, x_2, \dots x_q, x_{q+1}, \dots x_Q(= L/2)$, the curvature at any time and any cross section can be obtained as $\kappa(t_n, x_q)$. Denote $\kappa(t_n, x_q)$ as κ_{nq} and the discretization of the curvature with respect to time and location of cross section is shown in Figure 3.4. At each time t_n, the expression for $\kappa(t_n, x)$ can be obtained by polynomial fitting of discretized values of $\kappa_{n0}, \kappa_{n1}, \dots \kappa_{n2}, \kappa_{nq}, \kappa_{n(q+1)}, \dots \kappa_{nQ}$. The order of polynomial that provides good fit will depend on the material parameters and dimension of the beam. Details about fitting of $\kappa(t, x)$ for the materials studied in this work will be discussed in Section 5.3.1.

Once the expression for curvature is known, the deflection can be obtained by integrating curvature in Eqn. (3.8)

$$\frac{\partial^2 w(t,x)}{\partial x^2} = -\kappa(t,x) \tag{3.8}$$

where w represents the deflection of the beam. For the 3-point bending, the deflection at $x = 0$ is zero due to the restriction of the support. Also, the rotation angle at $x = L/2$ is zero because of the symmetric condition. Thus, the boundary conditions (B.C.) can be specified as

$$w(x = 0) = 0, \qquad \frac{\partial w}{\partial x}(x = L/2) = 0 \tag{3.9}$$

$w(t,x)$ can be determined by integrating Eqn. (3.8) with Eqn. (3.9) which is illustrated in Figure 3.4.

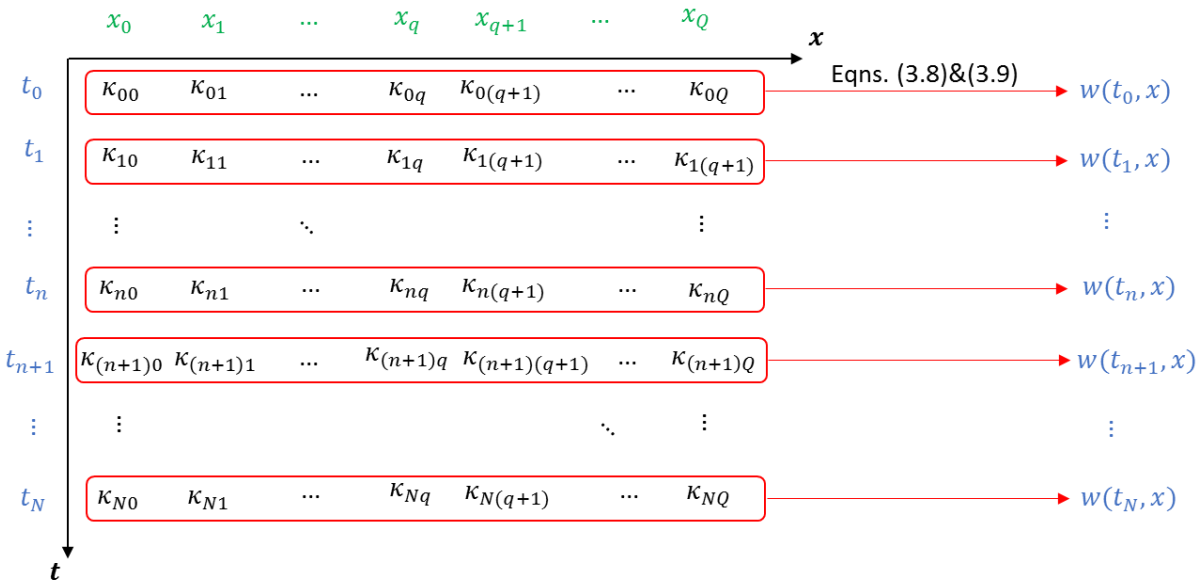

Figure 3.4 Illustration for discretization of curvature and the calculation of beam deflection

3.3 Accuracy of discretization along y axis

Since y is discretized and is a multiple of Δy, $\sigma(t_n, y)$ and $\epsilon(t_n, y)$ along y axis are also discretized. Theoretically, a is determined from solving $\epsilon_c(t_n, y) = \epsilon_L$. However, it is almost impossible to find a $\epsilon_c(t_n, a)$ which is exactly equal to ϵ_L considering that a is a multiple of Δy. Numerically, a is obtained by finding the minimum value of $|\epsilon_c(t_n, y) - \epsilon_L|$ along the y axis. a

obtained this way is an approximation with an error $\leq \Delta y/2$. This error can be reduced by finer discretization of y. In addition to a, numerical integration is used to calculate Ω as shown in Eqn. (3.7) because $\sigma(t_n, y)$ is discretized along y axis. Again, more accurate evaluation of Ω can be obtained by finer discretization of y. In this section, the effect of Δy on the a value and deformation of the beam is examined. The values of material parameters are selected from Table 2.1, and the dimension of the beam is given in Table 3.1. The loading history is taken to be $P(t) = 0.1t\ N$ which leads to the initial conditions $M(t_0) = 0$, $\epsilon(t_0, y) = 0$ and $\sigma(t_0, y) = 0$. y from 0 to $h/2$ is discretized into 100, 1000 and 10000 intervals respectively and the resulting curvature and a histories at $x = L/2$ are compared in Figure 3.5 and Figure 3.6 respectively. As can be seen, both curvature and a histories tend to be convergent with the increase of intervals along y axis. Therefore, the accuracy of the numerical results can be guaranteed as long as y is discretized sufficiently.

Table 3.1 Dimension of beam

Beam dimension	Width(mm)	Height(mm)	Distance between two support(mm)
Value	12	3	40

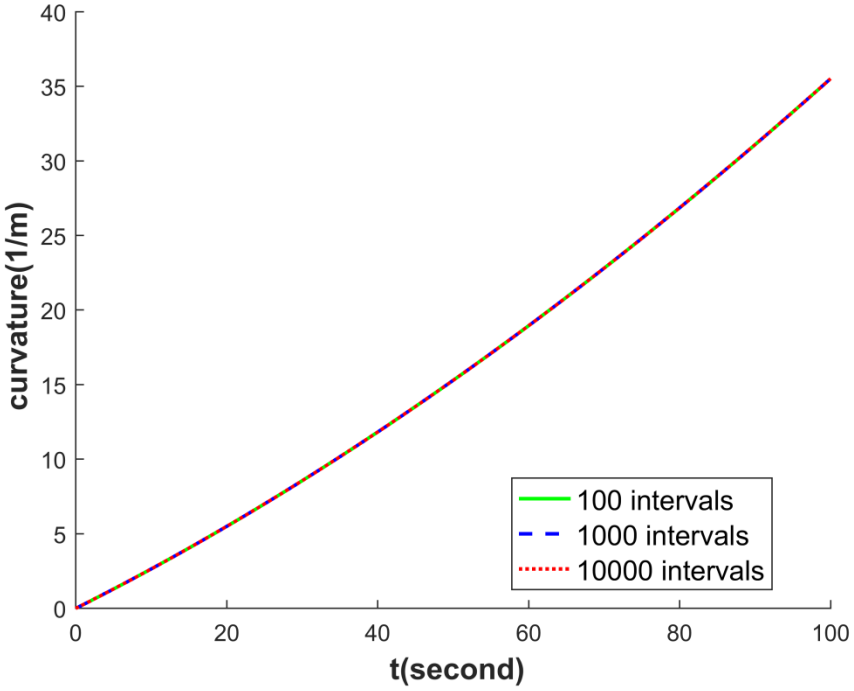

Figure 3.5 Curvature history at $x = L/2$ with different numbers of intervals along y axis

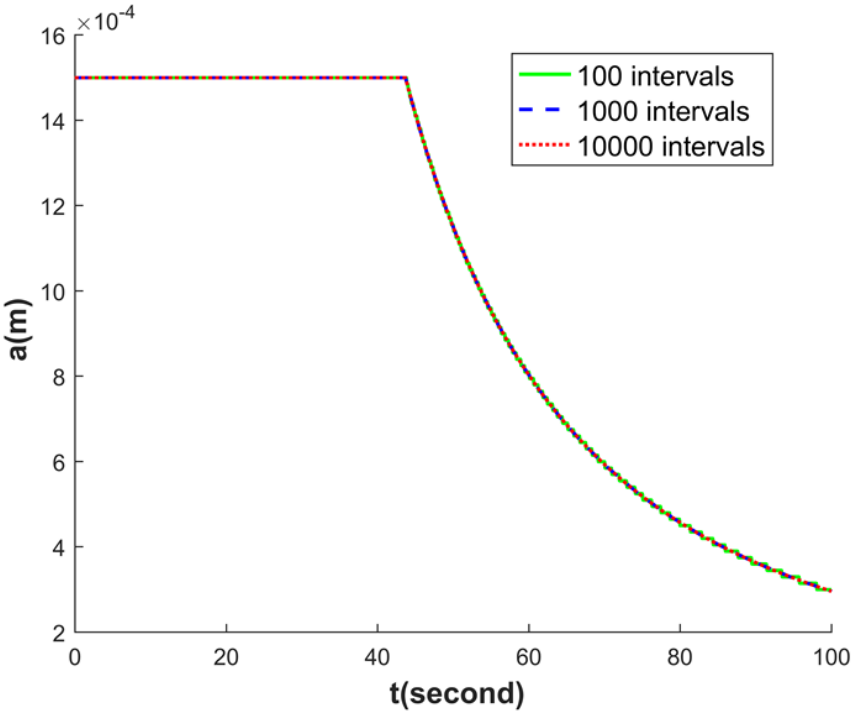

Figure 3.6 a history at $x = L/2$ with different number of intervals along y axis

Chapter 4 Experimental methodology

This chapter details the experiments conducted to compare with the model presented in Chapter 3. In the model, the mechanical behavior of SMP is described by five parameters, E, μ, λ, C and ϵ_L. These parameters for MM7520 were extracted from creep tests using results from Chapter 2. The material behaves differently at different temperatures; therefore, both creep and bending tests were performed at different temperatures.

4.1 Raw materials and filament production

The various manufacturing techniques of SMPs are used by researchers to produce the component. For the work of Tobushi *et al.* [16] [15] [19], the SMP specimens used for experiments were manufactured by Mitsubishi Heavy Industries, Ltd. through injection modeling. In recent years, extrusion based additive manufacturing (EBAM or also known as Fused deposition modeling (FDM)) technique have drawn increasing attention due to its low cost and high efficiency for small scale production. Parts with complex shapes can be produced by adding molten material layer-by-layer which is of particular interest to manufacturers. Raasch *et al.* [28] conducted research on extrusion and 3D printing of SMP (Type MM4520, SMP Technologies Inc.). The extrusion and 3D printing settings that can produce good quality filaments for printing and printed specimens were determined. Mechanical and shape recovery properties of the printed SMPs were outlined. Yang *et al* [29] investigated the influence of different extrusion and 3D printing parameters on the density, tensile strength, dimensional accuracy and surface roughness of the produced specimens (Type MM4520, SMP Technologies Inc.). The design of experiment method was used to investigate the influence of parameters and the specimens with good quality was successfully built.

As mentioned in Chapter 1, this thesis is part of a larger program on the formation and characterization of multifunctional materials based on shape memory composites. As such, use of EBAM is of interest due to its low cost and manufacturing flexibility. The SMP used in this study was purchased from SMP Technologies Inc. (Japan) in pellet form. The manufacturer specified glass transition temperature (T_g) is 75 ℃ (Type MM7520). This SMP is a

polyurethane-based thermoplastic co-polymer. The overall manufacturing process for preparing the filament and specimen used in this work is depicted in Figure 4.1.

4.1.1 Filament preparation

Garces *et al.* [30] studied the extrusion of MM7520, and determined optimal operating parameters. The same procedure and parameters were used in this work for extruding the MM7520 filament. Before extrusion, the pellets were dehumidified in a vacuum oven (Lindberg/Blue M from Thermo Fisher Scientific Inc.) at 80 ℃ for 48 hours.

A single screw extruder (C.W. Brabender Instruments, Inc.) attached to an ATR Plasti-Corder drive system was used to extrude filaments (Figure 4.2 (a)). Figure 4.2 (b) shows the extrusion production line while the corresponding schematic of the extrusion process is illustrated in Figure 4.1 (b). As can be seen from Figure 4.1 (b), the extruder has four continuous heating zones. When the pellets are added into the hopper, they are preheated in zone 1. With the rotation of the screw, the material starts to melt as it is pushed towards the subsequent zones (from zone 1 to zone 3) in the barrel. The screw speed was tuned to 20 rpm to extrude filament with diameter of 2.85 mm that is compatible with the Ultimaker 2 printer. The zone 4 is located in the die of the extruder which molds the shape of the filament. As the extrudate comes out of the extruder, it was collected by a conveyor belt at a constant rate of 28 mm/s. Water spray was used to cool down the filament at the beginning of the conveyer which prevents adhesion of the filament to the conveyor. Then, the filament is cooled down gradually using two fans. As the filament passes through the water bath, it was fully cooled down and its physical properties were fixed. Finally, a take-up mechanism was used to collect the filament. The final product is shown in Figure 4.2 (c). The parameters used are tabulated in Table 4.1. The produced filament was measured every 5 mm. The filaments outside the diameter range from 2.75 mm to 2.95 mm were rejected and not used in the EBAM.

(a)

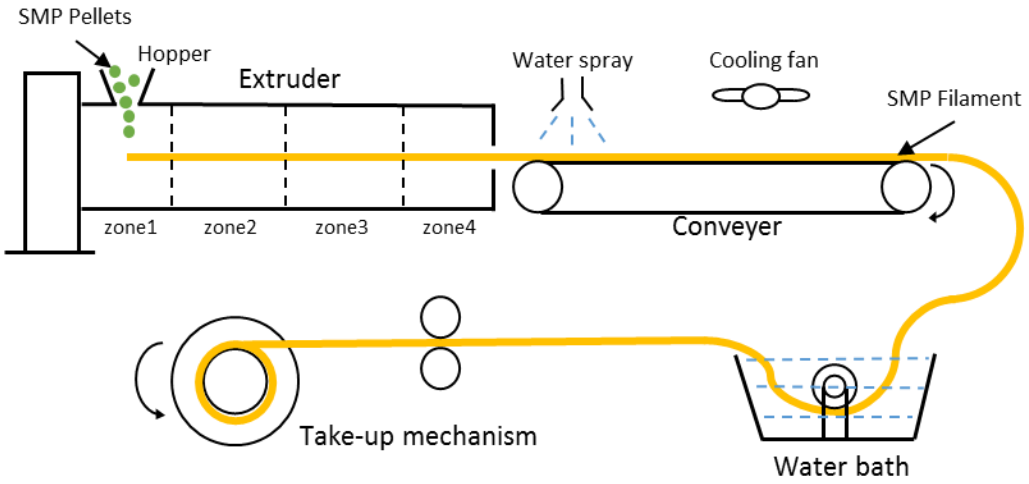

(b)

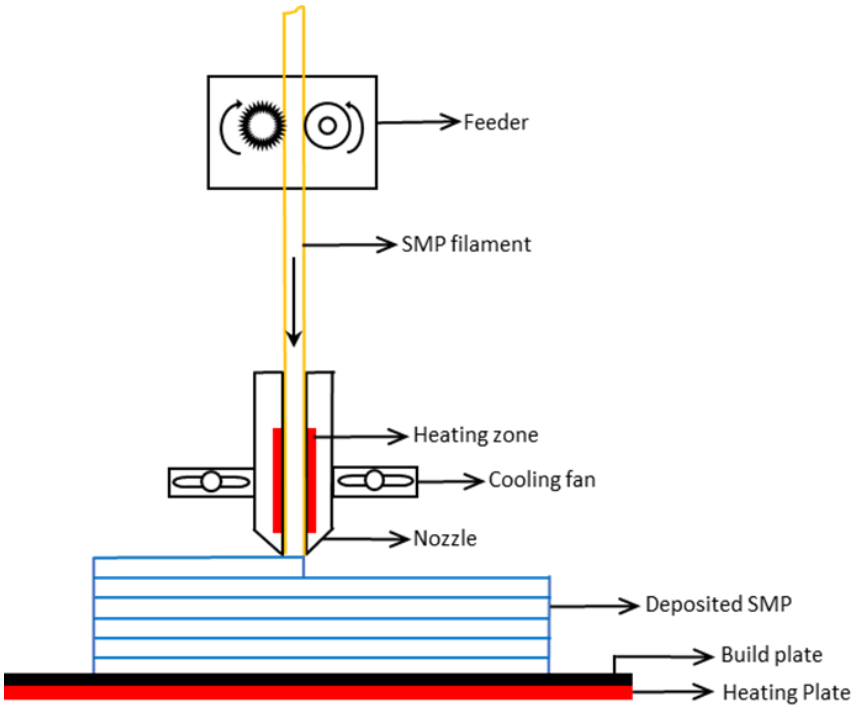

(c)

Figure 4.1 Manufacturing process of SMP specimen. (a) Manufacturing flowchart, (b) Schematic of extrusion process, (c) Schematic of 3D printing (adopted from [29]).

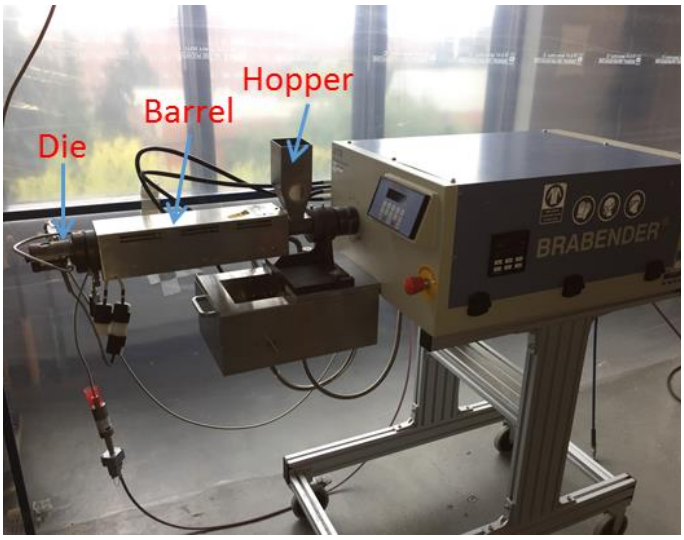

(a)

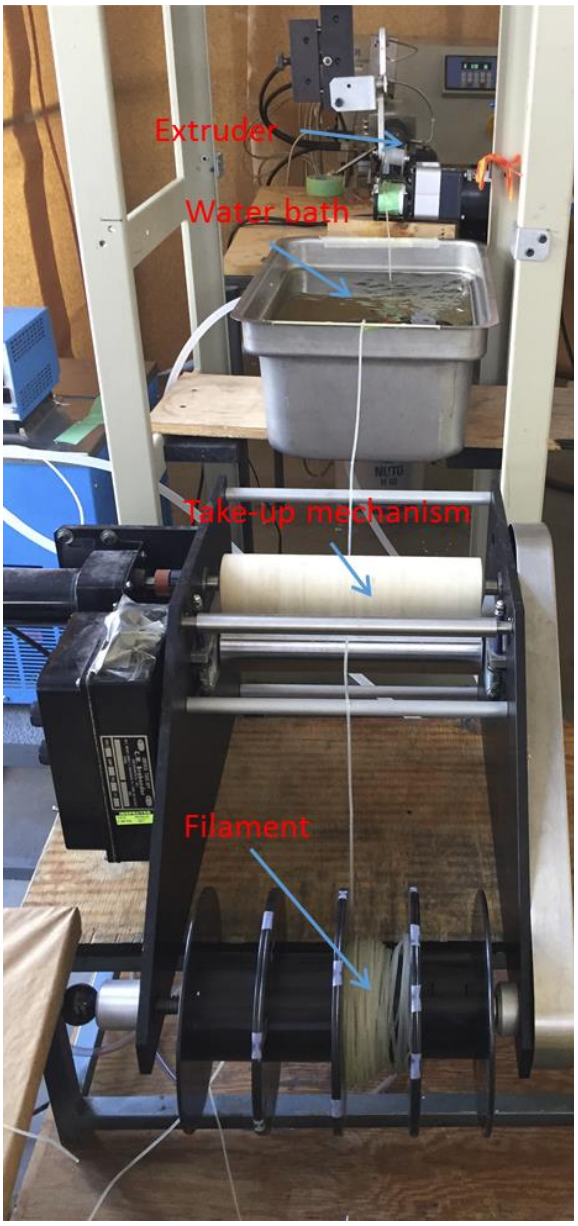

(c)

(b)

Figure 4.2 Actual set-up for the extrusion of SMP filament. (a) Extruder and its drive system, (b) Extrusion production line, (c) extruded SMP filament.

Table 4.1 Extrusion parameters

Parameters	Values
Temperature at zone 1(℃)	175
Temperature at zone 2 (℃)	185
Temperature at zone 3 (℃)	195
Temperature at zone 4 (℃)	205
Screw speed (rpm)	20
Conveyor speed (mm/s)	28

4.1.2 Specimen preparation

Specimens used in this study were prepared using Ultimaker 2 (Netherlands). This EBAM machine was chosen because it is an open source machine that provides users more control compared to some other manufacturers machines. The machine is equipped with a single nozzle, compared to some new dual nozzle machines used for multi-material printing. The machine's working mechanism is shown in the schematic presented in Figure 4.1(c) [29]. The feeder contains one saw-toothed roller and another rounded roller which squeeze the filament slightly and push the filament into the nozzle at a constant feeding rate. As the material passes through the heating zone, the filament is heated up and melted. When the liquid material comes out of the nozzle, it is deposited prior to solidification due to the cooling from the surrounding air. Also, the two fans at the sides of the nozzle can accelerate the cooling speed of the deposited material. With the moving of the nozzle, the material is deposited on the build plate layer by layer until the desired specimen is formed. The printing parameters used in this study is shown in Table 4.2. 230 ℃ was selected as the nozzle temperature because the DSC test indicated that the start of melting point for the material is around 160 ℃ [30]. The reason for the nozzle temperature being higher than the indicated melting point was to ensure complete melting of the filaments prior to being deposited during the print process. The print speed used was 19.5 mm/s for the first layer and 21 mm/s for the rest of layers which was shown to produce high print quality and print efficiency at the same time. Fans were turned off during the printing process to allow the molten material leaving the nozzle more time to fuse and bond, which reduces voids and residual stresses between layers.

The build plate temperature was set at 80 ℃, slightly higher than the glass transition temperature, to minimize the temperature gradient and consequent material property changes in the thickness direction of the specimens. As the build plate temperature is above T_g, soft segment is activated and the thermal motion of molecules increases dramatically [2]. As a result, the molecules in the interface between the layers have more chance to bond with each other which can increase the adhesion between layers. Also, the residual stress between layers can be relieved due to the movement and realignment of molecules [28]. Smaller layer height generates smoother specimen surface morphology but meanwhile takes more time. It was found that 0.2 mm layer height can guarantee the print quality and print efficiency at the same time, which can be generated using 0.4 mm nozzle diameter. Infill density was set to 100% in order to get a solid specimen. The print direction of the machine was set to be $\pm 45°$, alternating at every layer of the print. A previous study [31] suggested that this print angle minimized the differences between longitudinal and transverse direction properties of the printed specimens.

Table 4.2 3D printing parameter settings

Parameter settings for 3D printing	Value
Layer height (mm)	0.2
Nozzle temperature (℃)	230
Build plate temperature (℃)	80
Infill density (%)	100
Print pattern	±45°
Print speed of first layer (mm/s)	19.5
Print speed of other layers (mm/s)	21
Nozzle diameter (mm)	0.4
Fan speed	0

4.2 Experimental testing

4.2.1 Testing machine

The Dynamic Mechanical Analysis (DMA) was conducted using a DMA Q800 (TA Instruments, USA). Remaining tests, creep and bending, were done using a Bose ElectroForce 3200 Series III test instrument (Figure 4.3) equipped with a temperature chamber. Two load cells were used; one

has a maximum load capacity of 450 N with a resolution of 0.01 N and with the other has a maximum load capacity of 10 N with a resolution of 0.001 N. The temperature chamber (Figure 4.3) can control the temperature within ± 1℃ of the target temperature. Figure 4.4 details the elements inside the chamber. Heater elements is put at the back of the chamber and the blower fan blows the hot air through the honeycomb pore in front of the heater elements. A temperature sensor probe is used to record the temperature inside the chamber.

Figure 4.3 Testing machine

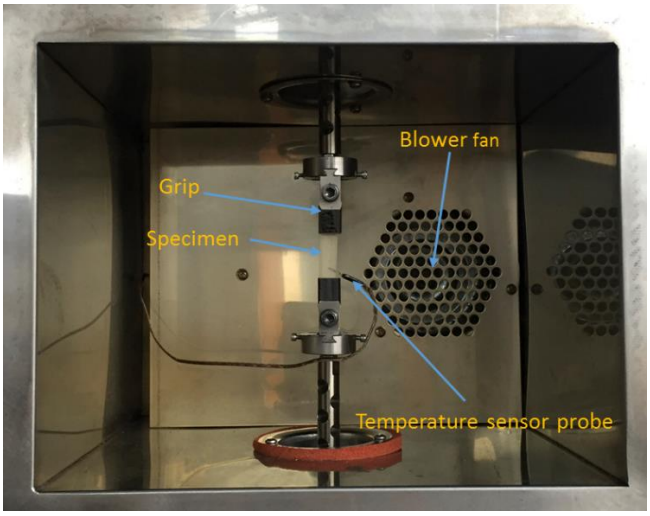

Figure 4.4 Uniaxial test components

4.2.2 Dynamic mechanical analysis test

Dynamic mechanical analysis (DMA) was conducted to investigate the dynamical properties of MM7520. The specimen for DMA test had constant rectangular cross-sections with 12.75 in width, 3.15 mm in thickness and 17.14 mm in length. The sample was clamped at one end as a cantilever beam. A displacement was applied to the free end of the beam in a sinusoidal manner with 30 μm amplitude and 1 Hz frequency. The temperature of the chamber was heated up gradually from -50 ℃ to 150 ℃ at a constant rate of 2 $℃/min$. The loading response was collected and the storage modulus E', loss modulus E'' and tangent delta $tan\delta$ were obtained with respect to temperature.

4.2.3 Creep test

Creep tests were conducted at 55 ℃, 60 ℃, 65 ℃, 70 ℃ and 75 ℃. The rheological model is originally developed with small strain assumption [16]; therefore, the strains for all the creep tests conducted here were limited to 10%.

At each temperature, three independent creep tests were performed, at different stress levels. The reason for performing these tests is as follows. Since the rheological model contains the term ϵ_s as shown in Eqn. (2.11), it is nonlinear in the sense that if the input stress increases from σ to $\alpha\sigma$, the output strain does not necessarily increase proportionally. This can also be seen from the expressions in Eqns. (2.26), (2.28) and (2.30) where the strain response $\epsilon(t)$ is not proportional to the applied stress σ_0. Therefore, in order to capture the creep behavior for a range of stress levels, three different magnitudes of stress were applied on the specimens at each temperature.

The specimens for creep tests have constant rectangular cross-sections. The designed dimensions at 55 ℃, 60 ℃, 65 ℃ and 70 ℃ are 10 mm in width, 1 mm in thickness and 50 mm in length. At 75 ℃, the material is changing into the rubbery state so the thickness of dimension is doubled in order to apply smaller stresses on the specimens due to the limited load level the machine can apply. The real dimensions of the specimens together with their applied loads and resulting stresses are shown in Table 4.3. The standard dog-bone specimens (eg. ASTM D638 V) for creep tests were not used because the gauge length of the specimens changes constantly during the test,

and the strain levels experienced were beyond the capability of the optical extensometer if the gauge length of a dog-bone specimen was to be monitored.

The setup of creep test can be seen in Figure 4.4, where the SMP strip was mounted between two grips. The lower one was fixed and the upper one was attached to a controllable load cell. 15 in·lb (1.7 N·m) torque was applied with a torque wrench to fix the specimen in the grips. The initial length between the two grips was set as 25 mm (the length of specimens is around 50 mm and the length of two grips together is around 25 mm). The temperature sensor probe was placed next to the specimen during the tests. The load, displacement and temperature were recorded at every 0.1 second. The specimens were loaded for 30 minutes and then unloaded for another 30 minutes.

Table 4.3 Dimension of specimens used for creep tests, corresponding load and stress

Temperature (℃)	Specimen number	Applied load (N)	Width (mm)	Thickness (mm)	Length (mm)	Stress (MPa)
55	1	30	10.07	1.06	49.80	2.81
	2	50	10.06	1.11	49.77	4.48
	3	70	10.10	1.08	49.85	6.42
60	1	30	10.02	1.07	49.75	2.80
	2	50	10.07	1.10	49.81	4.51
	3	70	10.07	1.05	49.87	6.62
65	1	10	10.01	1.05	49.77	0.95
	2	15	10.06	1.09	49.76	1.37
	3	20	10.03	1.06	49.77	1.88
70	1	2	10.12	1.29	49.80	0.15
	2	3	10.08	1.20	49.79	0.25
	3	4	10.05	1.20	49.78	0.33
75	1	2	10.20	2.42	50.16	0.08
	2	3	10.17	2.21	50.12	0.13
	3	4	10.22	2.40	50.16	0.16

4.2.4 Bending test

3-point bending test were performed as shown in Figure 4.5 using a 3-point test jig. A force *P* was applied at the mid-span of the upper side of the beam and there were two roller supports on the lower side of the beam. *P* was applied at a constant loading rate (Table 4.4). The temperature sensor probe was put next to the specimen. The load, displacement and temperature were recorded every 0.1 second. Like in the creep tests, bending tests were conducted at 55 ℃, 60 ℃, 65 ℃, 70 ℃ and 75 ℃. At different temperatures, the material behaves differently so different loading rates and loading time were used which are shown in Table 4.4.

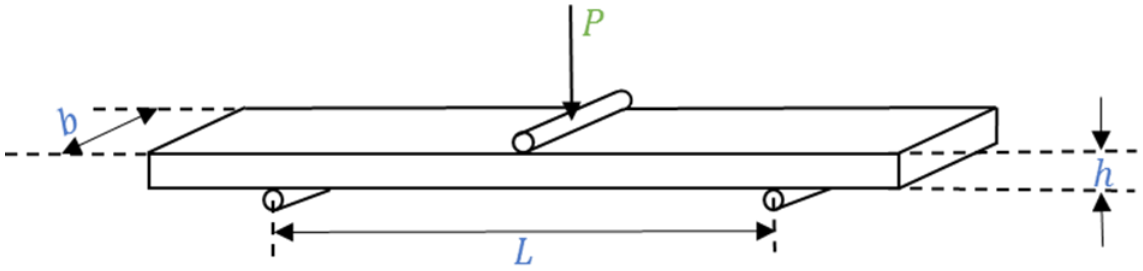

(a)

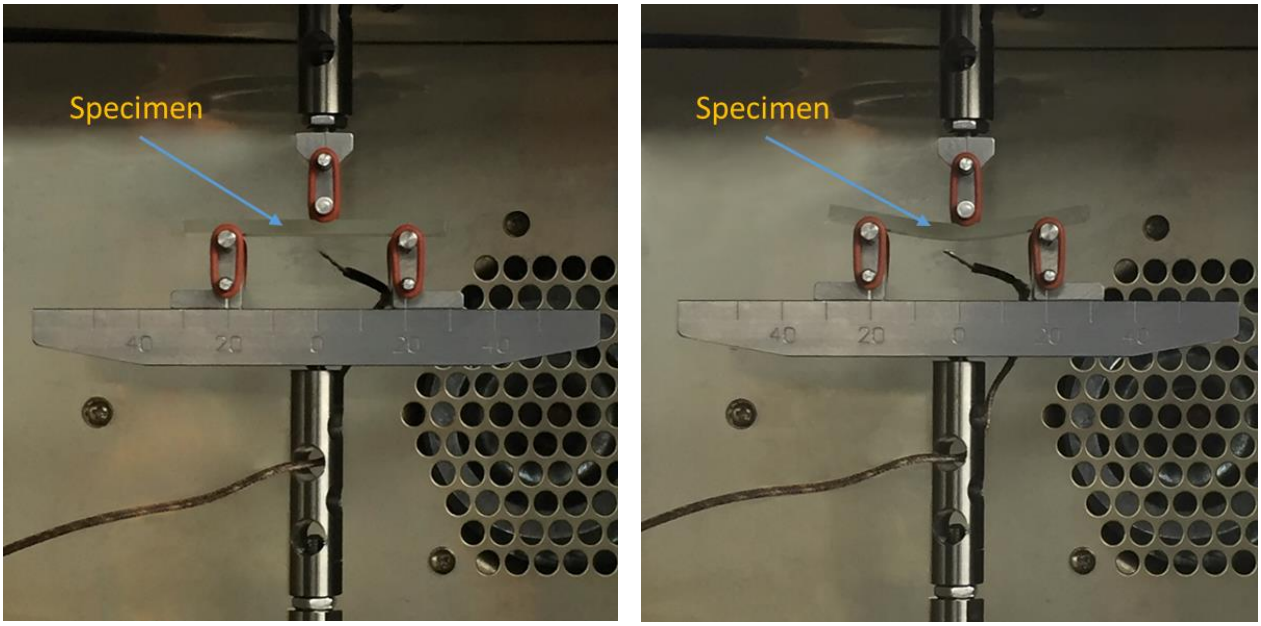

(b) (c)

Figure 4.5. (a) Schematic of 3-point bending, (b) Specimen before loading, (c) Specimen after loading

The specimens for bending tests also have rectangular cross-section. The dimension were 12 mm in width, 3 mm in thickness and 60 mm in length. At each temperature, the bending tests were repeated under the same loading conditions for 3 times, each time with a fresh specimen. The measured dimensions of specimens are shown in Table 4.5. The span between two lower supports were fixed at 40 mm for all bending tests. The deflection at mid span of the beam δ and load P can be obtained from the testing machine.

Table 4.4 Loading rate and loading time at different temperatures

Temperature (°C)	55	60	65	70	75
Loading rate (N/s)	1	1	0.5	0.2	0.185
Loading time (s)	100	100	100	50	15

Table 4.5 Dimension of specimens used for bending tests

Temperature (°C)	Specimen number	Width(mm)	Thickness(mm)	Length(mm)
55	1	12.25	3.32	60.12
	2	12.20	3.34	60.04
	3	12.27	3.41	60.26
60	1	12.25	3.38	60.02
	2	12.18	3.35	60.01
	3	12.18	3.32	60.21
65	1	12.28	3.22	59.97
	2	12.20	3.23	60.01
	3	12.27	3.19	59.73
70	1	12.02	3.19	59.78
	2	11.97	3.16	59.72
	3	11.96	3.20	59.79
75	1	11.99	3.18	59.77
	2	11.98	3.18	59.74
	3	12.07	3.20	59.85

Chapter 5 : Results and Discussion

5.1 Results of dynamic mechanical analysis

In Figure 5.1, the storage modulus, E', loss modulus, E'' and tangent delta, $tan\delta$, are shown with respect to temperature. These three parameters are often used to describe the viscoelastic properties/response of a material that exhibit the characteristics of both elastic solid and viscous fluid [4]. E' is related to the elastic component of the material while E'' is related to the viscous component [2]. $tan\delta$ is the ratio between the loss modulus and the storage modulus [2].

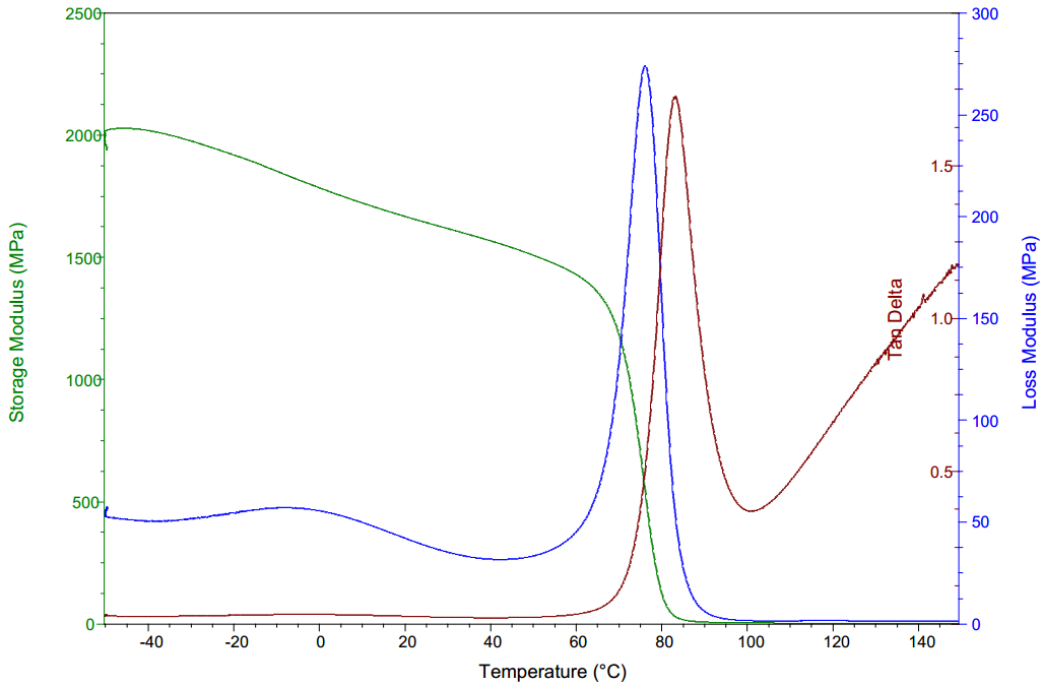

Figure 5.1 Storage modulus E', loss modulus E'' and tangent delta $tan\delta$ of MM7520, measured from dynamic mechanical analysis

It can be seen from Figure 5.1 that the storage modulus maintains a high value (above 1500 MPa) at low temperature and start to decrease quickly at around 60℃. The sharpest drop happens between 70℃ and 80℃. The loss modulus stays at a small value (around 400 MPa) at low temperature but starts to increase drastically from 60℃ to 75℃ at which the loss modulus reaches its peak. After 75℃, the loss modulus drops again. The tangent delta follows the similar pattern as the loss modulus but it peaks at a higher temperature (around 85℃). Overall the most significant change of E' and E'' occurs around 75 ℃ which is consistent with the manufacturer

specified glass transition temperature. It also suggests that the re-process of the SMP (via extrusion based additive manufacturing) did not cause significant changes to its mechanical properties compared with the received material in pellet form.

5.2 Creep test and parameter extraction

5.2.1 Creep test results

At each temperature, three creep tests at different stress levels were performed. Strain history recorded from the creep tests are shown in Figure 5.2 as dashed curves. Ideally, for each creep test, a sudden load should be applied to the specimen. Practically, however, it takes some time (usually less than 0.5 second) for the test machine to increase the load from 0 to the target load. To consistently define the initial strain, the time $t = 0$ is set to be the moment at which the difference between the actual load and the target load is less than 0.1 N. The strain at that time is considered as the initial strain. Qualitatively, the curves in Figure 5.2, across different temperatures, exhibit some similarities. First of all, when the load is first applied at $t = 0$, the material deforms instantaneously. This instantaneous elastic strain is mainly caused by the elongating of the coiled/entangled chain molecules in the amorphous regions in the direction of the applied stress [4]. As discuss in Chapter 1, the chain elongation is enabled by the change of torsional angle of each bond relative to its neighbor. As the specimen is held under the constant load, the chain molecules continue to extend. However, because they are restrained by crosslinks and entanglement with other chains, the flexibility and mobility of the chains has decreased which results in reduced deformation rate, evidenced by the decreasing slope in the strain history (Figure 5.2). Once the load is removed, the material experiences an immediate elastic recovery due to the resilience of the material [4]. The recovery continues but the strain cannot be fully recovered even for a long period of time. Since the extension of the chains during loading can cause slipping and realignment of the chain molecules in the amorphous regions, this result implies that some of the chain slipping and realignment is irreversible.

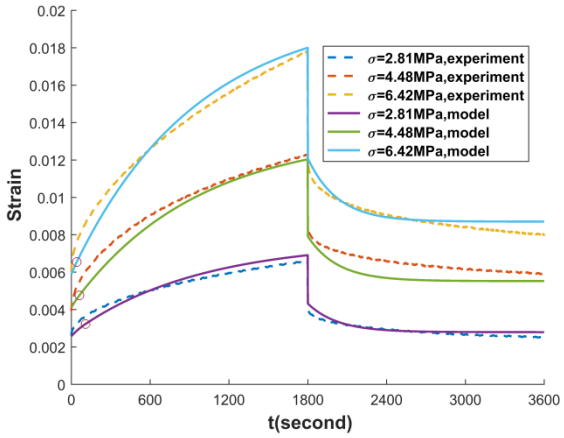

(a)

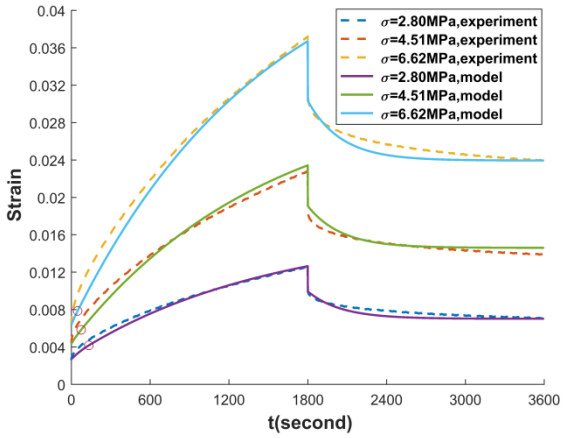

(b)

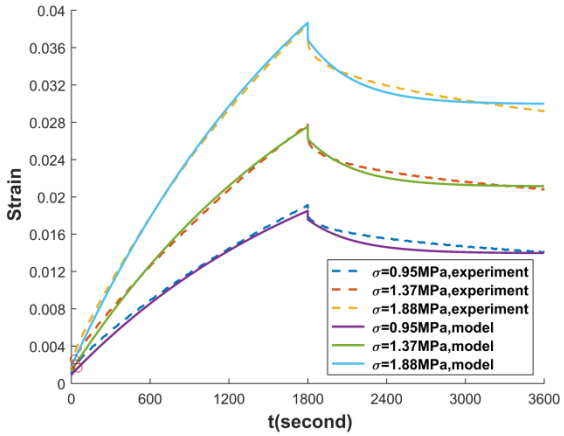

(c)

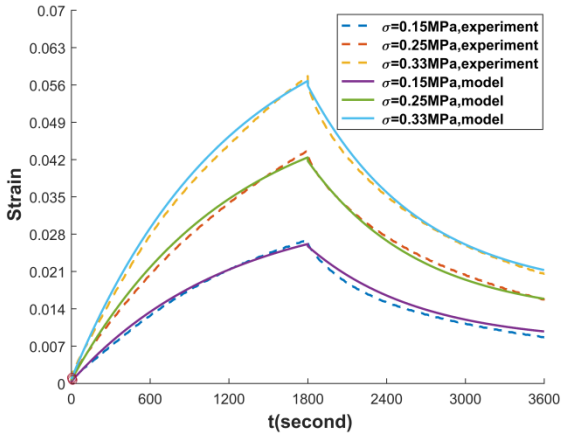

(d)

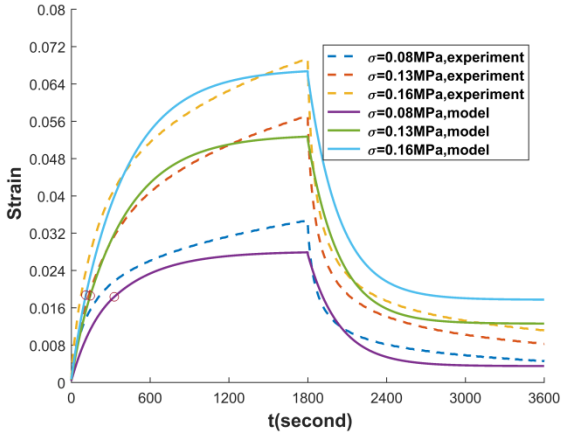

(e)

Figure 5.2 Creep test results and fitting with the rheological model at different temperatures. (a) T=55℃, (b) T=60℃, (c) T=65℃, (d) T=70℃, (e) T=75℃.

Despite the above similarities, the experimental curves also show differences at different temperatures. When the temperature is well below T_g (55 and 60 ℃), the initial elastic deformation $\epsilon(0)$ is significant compared with the maximum deformation $\epsilon(1800^{-}s)$ during loading. For example, at 55℃, the ratio between $\epsilon(0)$ and $\epsilon(1800^{-}s)$ ranges from 0.32 to 0.39 for the three applied stress values. The corresponding ratio at 60℃ ranges from 0.17 to 0.21. In contrast, this ratio drops to 0.044-0.053 at 65℃, 0.013-0.016 at 70℃, and 0.010-0.011 at 75℃. The reason for such a difference is that at relatively low temperatures the thermal motion of molecules in the soft segments is hindered and the material is in the glassy state [7]. The intermolecular forces between the chains and the entangled chain structure inhibit the decoiling of the chain molecules so the material behaves less viscous and more elastic. As the temperature approaches T_g, the thermal motion of molecules in the soft segments is gradually unimpeded and the material begins to enter its rubbery state [7]. At high temperature (around T_g), the higher thermal motion of the molecules in the soft segments makes it easier to overcome the intermolecular forces and the barrier for bond rotation [3]. Therefore, the material behaves more viscous which causes the initial elastic deformation to be less significant. The change of material properties at different temperatures can be illustrated as Figure 5.3. The elastic solid and viscous liquid shows two extremes and the polymer lies between these two extremes. As the temperature increases, the elastic component decreases and the viscous component increases.

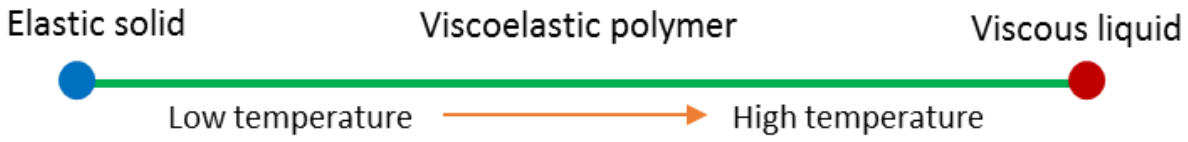

Figure 5.3 Schematic of polymer behavior at different temperature

Another difference among the results at different temperatures is the recoverable strain ratio (Rr). For the creep tests conducted here, Rr is defined as $[\epsilon(1800^{+}) - \epsilon(3600)]/\epsilon(1800^{+})$ which is the ratio of recovered strain (maximum creep strain minus the final residual strain upon unloading) to the maximum creep strain. The recoverable strain ratios are calculated at each temperature and for different stress levels (small, medium and large), shown in Figure 5.4. It is clear that the recovery ratio increases significantly when the temperature is near the T_g. When the

temperature is below T_g (55, 60 and 65℃), larger than 60% of the maximum creep strain cannot be recovered upon unloading. To explain, consider when the material is loaded, the extension of coiled chains is enabled by overcoming the potential energy barrier for bond rotation (Figure 1.2) and the intermolecular forces between the chains. Once the material is unloaded, the elastic restoring force immediately recovers some deformation, driving the chains to partially extended states. However, the partially extended chains can still be separated by energy barriers which need to be surpassed in order for the deformation to be completely recovered. When the material is unloaded at relatively low temperatures, there is insufficient amount of thermal energy to overcome the energy barriers and intermolecular force, [3] which prevents the chains from going back to their original coiled conformation. As the temperature is approaching T_g, the increased thermal energy is able to surpass those energy barriers, leading to more likelihood of returning to the original coiled conformation, and hence higher recovery ratio.

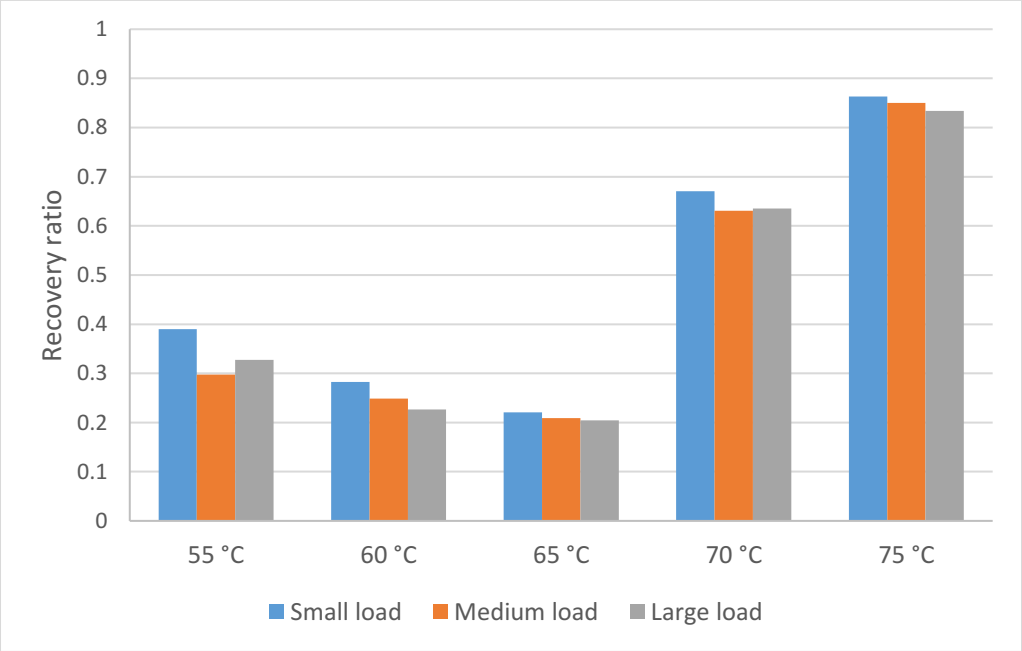

Figure 5.4 Recovery ratio at different temperature and different stress levels for creep tests

5.2.2 Model fitting and parameter extraction

In the rheological model, the material parameters, E, μ, λ, C and ϵ_L are used together to describe the viscoelastic behavior of SMP. For the specific material studied in this work, MM7520, values for these parameters are extracted by performing creep tests and comparing the results with the predictions from the model. At each temperature, three independent creep tests were conducted, as explained in Section 5.2.1, and results from those tests were used together to extract the material parameters. As can be seen from Section 2.3.1, under the rheological model the relationship between the applied constant stress and the initial strain in a creep test can be expressed as $\sigma_0 = E\epsilon(0)$. Therefore, the value of E can be determined by linearly fitting the data σ_0 vs. $\epsilon(0)$ from the three independent creep tests. The fitting details are shown in Appendix A and the values of E are given in Table 5.1.

As for the other four parameters, μ, λ, C and ϵ_L, they are fully coupled (see Eqns. (2.26), (2.28) and (2.30)) and cannot be extracted individually from the creep tests. Therefore, at each temperature, μ, λ, C and ϵ_L are varied together until they provide reasonable fit to all 3 creep tests with different applied stresses. Some guidelines do exist for the initial selection of C and ϵ_L values. Specifically, Eqn. (2.12) predicts the irrecoverable strain at the time of unloading (t_b) as $\epsilon_s(t_b) = C(\epsilon_c(t_b) - \epsilon_L)$. Here, $\epsilon_c(t_b)$ is the creep strain at t_b, which is equal to $\epsilon({t_b}^+)$ and can be obtained from experiments. On the other hand, based on Eqn. (2.30), $\epsilon_s(t_b) = \epsilon(\infty)$. Although the experiments were only performed up to one hour ($3600s$), in Figure 5.2 the strains in most cases have reached plateau after one hour. Therefore we approximate $\epsilon(\infty)$ by ϵ(3600s), which allows us to establish the following relation: $\epsilon(3600s) = C(\epsilon({t_b}^+) - \epsilon_L)$. At each temperature, there are three sets of $\epsilon(3600s)$ and $\epsilon({t_b}^+)$ from the three independent creep tests. By linearly fitting the data of $\epsilon(3600s)$ vs. $\epsilon({t_b}^+)$, C is obtained from the slope and ϵ_L from the intercept. These initial estimates of C and ϵ_L are then tuned, together with μ and λ, to achieve good fitting for all test results. The final fitting values for μ, λ, C and ϵ_L are shown in Table 5.1.

Table 5.1 Parameters values at different temperature

Parameters	E (MPa)	μ (GPa·s)	λ (s)	C	ϵ_L
55 ℃	1088.2	148	226	0.76	0.00065
60 ℃	1038.5	112	253	0.83	0.00149
65 ℃	1028.7	50	352	0.83	0.00076
70 ℃	392.5	5.43	840	0.3	0.00027
75 ℃	218.35	0.79	239	0.37	0.018

Figure 5.2 also shows the predictions from the model (solid curves) in comparison with experiments. The red circle in each curve marks the critical point at which the irrecoverable strain is triggered and the stress-strain relation transitions from regime 1 to regime 2 (definition of different regimes are explained in detail in Section 2.2). R^2 (Table 5.2) is used to examine the quality of fitting and it is calculated separately for different stress levels (small, medium and large). Among the five temperatures R^2 is closest to 1 at 65 ℃ and 70 ℃, while the quality of fitting reduces at lower (55 ℃ and 60 ℃) or higher (75 ℃) temperatures. The worst fitting is found in 75 ℃, which also corresponds to T_g of this polymer.

Table 5.2 Values of R^2 at different temperatures and different stress levels

R^2	Small load	Medium load	Large load
55 ℃	0.9734	0.9242	0.9787
60 ℃	0.9666	0.9723	0.9748
65 ℃	0.9818	0.9951	0.9972
70 ℃	0.9834	0.9932	0.9936
75 ℃	0.9093	0.9692	0.9441

To take a closer look at the comparison, Figure 5.2 (a) shows the fitting at 55 ℃. Comparing the three modelling results with their corresponding experimental data, it can be seen that during loading, the strain measured from experiments increases more sharply at the beginning while grows more slowly than the model prediction after a few hundred seconds. After unloading and during recovery, the strains from experiments decrease faster than the model predicts. In other

words, compared with the model prediction, the actual material is less viscous during short-term loading and unloading, while it is more viscous in long-term loading. Revisiting the schematic of the model shown in Figure 2.6, the dashpot and irrecoverable strain element represent two dissipation mechanisms which contribute to the viscous behavior of the material. The difference between model and experiments seems to indicate that the dashpot is highly viscous, which leads to the underestimation of deformation in short-term loading and slower recovery rate in unloading. The triggering of the irrecoverable strain element introduces another dissipation mechanism and softens the material. Although its triggering occurs quite early in all cases (red circles on the solid curves), its effect is only felt after a certain period of time.

The comparisons between experimental and modeling results at 60 ℃ (Figure 5.2 (b)) are quite similar to what is observed in Figure 5.2 (a). When the temperature is near T_g, at 65 ℃ (Figure 5.2 (c)) and 70 ℃ (Figure 5.2 (d)), the model fits the experimental results very well and the discrepancies between them are insignificant. However, when the temperature increases further to T_g, it was very challenging to find a reasonable fit to the experiments. One of the better fittings is shown in Figure 5.2 (e) which still shows considerable discrepancy. With the present model, it is difficult to capture both the rapid ramping up of the strain during loading and its fast decaying during unloading. One may attempt to increase the strain rate during loading by reducing the stiffness of the two springs (E_1 and E_2), but this would lead to even slower recovery during unloading.

The final values for E, μ, λ, C and ϵ_L are shown in Table 5.1 and plotted in Figure 5.5 against temperature. It can be seen from Figure 5.5 (a) that E is around 1000 MPa from 55 to 65 ℃ and only experiences mild decrease as the temperature increases. When the temperature approaches the glass transition region, E drops sharply from 1028.7 MPa at 65 ℃ to 218.35 MPa at 75 ℃. The trend for E in the temperature range studied here is similar to that of storage modulus E' (Figure 5.1), although their numerical values are quite different. The viscosity μ as shown in Figure 5.5 (b) undergoes continuous decrease from 148 GPa·s at 55℃ to 0.79 GPa·s at 75℃ As for the retardation time λ shown in Figure 5.5 (c), it increases gradually from 226 s at 55 ℃ to 352 s at 65 ℃ and then increases sharply to 840s at 70 ℃. When the temperature reaches T_g, λ decreases drastically to 239 s.

The irrecoverable strain ϵ_s is expressed in Eqn (2.12) in terms of C and ϵ_L. ϵ_L represents the threshold strain above which the irrecoverable strain will appear. C is correlated with the recoverable strain ratio (Rr) which is explained as follows. As mentioned earlier, the final irrecoverable strain can be expressed as $\epsilon(\infty) = C(\epsilon({t_b}^+) - \epsilon_L)$, and is approximately equal to $\epsilon(3600)$. Given the small value of ϵ_L compared with the overall creep strain value (see Figure 5.5 (e)), a further approximation can be made by neglecting ϵ_L in the equation, i.e., $\epsilon(3600) = C\epsilon(1800^+)$ or $C = \frac{\epsilon(3600)}{\epsilon(1800^+)} = 1 - Rr$. Therefore, higher value of C corresponds to lower recoverable strain ratio. In Figure 5.5 (d), the values of C remain stable around 0.8 from 55 to 65 ℃ and then goes down to 0.3 at 70 ℃ and 0.37 at 75 ℃. It suggests that a greater portion of the strain is recovered during unloading at 70 and 75 ℃. This observation is consistent with the calculation of recoverable strain ratio (Figure 5.4). In Figure 5.5 (e) ϵ_L stays at a very small value until the temperature reaches T_g at which ϵ_L reaches 1.8%. Such small values of ϵ_L imply that for temperatures below T_g, even very small deformation (< 0.2%) can trigger the irrecoverable strain in the material. At T_g, the thermal energy is high enough to overcome the energy barriers associated with bond rotation; as such the threshold to trigger irrecoverable strain is raised to 1.8%.

Tobushi *et al.* [16] hypothesized, for the MS5510 SMP, that each parameter (E, μ, λ, C and ϵ_L) can be expressed into a function of normalized temperature (T_g/T) in the exponential form (e.g. $E = E_g exp\left[a_E\left(\frac{T_g}{T} - 1\right)\right]$). For the parameters we obtained for MM7520, numerical fitting was performed, which showed that λ, C and ϵ_L could not be expressed by the exponential functions while E and μ can be approximated by the exponential functions from 65 ℃ to 75 ℃.

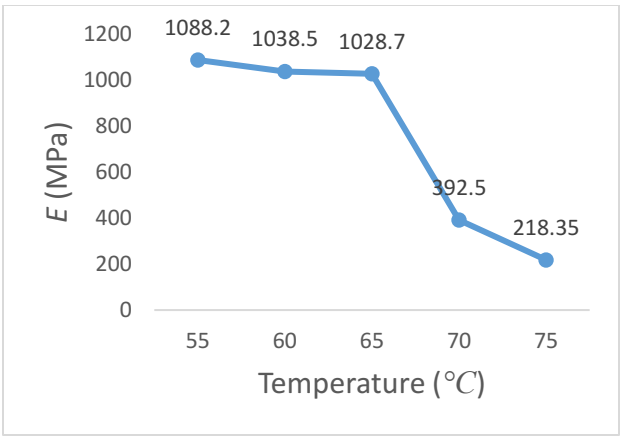

(a)

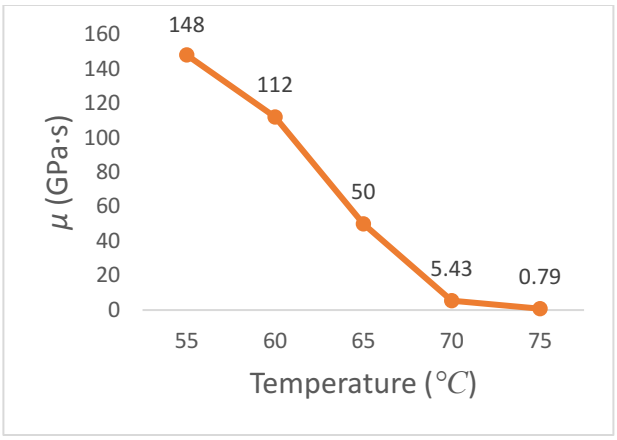

(b)

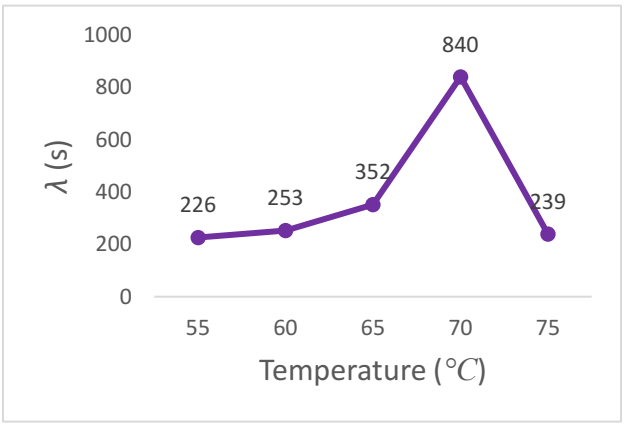

(c)

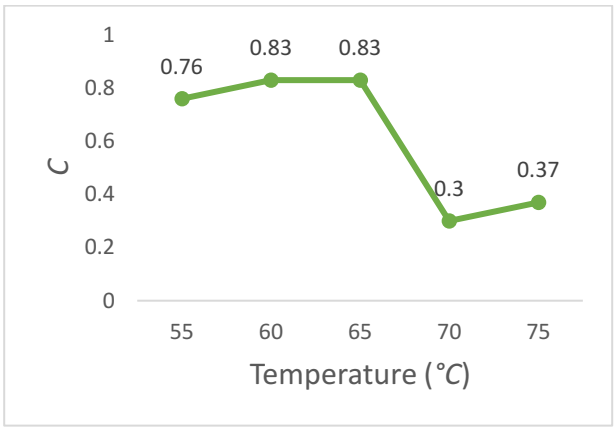

(d)

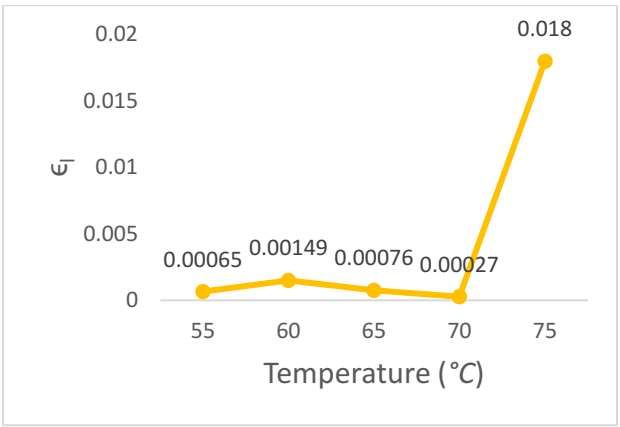

(e)

Figure 5.5 Values of material parameters extracted from fitting creep test data, plotted against temperature. (a) E (b) μ (c) λ (d) C (e) ϵ_L

5.3 Results for three-point bending

At each temperature, 3-point bending tests were repeated 3 times to ensure the repeatability of the experiments. Because of the occurrence of irrecoverable strain, each test used a fresh sample, which did not have exactly the same dimension due to manufacturing tolerances of the machine (Table 4.3). However, the variation is small so the average dimensions at each temperature were used in the model, which are shown in Table 5.3. Values of the material parameters (E, μ, λ, C and ϵ_L) used in model are extracted from the creep tests and given in Table 5.1.

Table 5.3 Average dimension of bending specimens at each temperature used in modeling

Temperature (°C)	Average width (mm)	Average thickness (mm)	Average length (mm)
55	12.24	3.36	60.14
60	12.20	3.35	60.08
65	12.25	3.21	59.90
70	11.98	3.18	59.76
75	12.01	3.19	59.79

5.3.1 Deflection calculation from the model

As discussed in Chapter 3, in order to determine the deflection of the beam from the model, the expression of curvature with respect to x is required. Now that the material parameters and beam dimensions are known at each temperature, the curvature values can be obtained at any time and any cross section given the loading conditions. Technically, once the numerical solution for $\kappa(t,x)$ is known, the deflection at any time and any cross section, $w(t,x)$, can be obtained by numerically integration. When analyzing the results on curvature, $\kappa(t,x)$ is found to be almost linear with respect to x at any time, such that it can be approximated by the following expression

$$\kappa(t,x) = U(t)x \tag{5.1}$$

Details on the linear relation between κ and x is given in Appendix B, and a possible explanation for this linear dependence can be found in Appendix C. Integrating Eqn. (3.8) using Eqns. (3.9) and (5.1), the expression of deflection $w(t,x)$ can be obtained as

$$w(t,x) = \frac{1}{8}L^2U(t)x - \frac{1}{6}U(t)x^3 \quad \left(0 \le x \le \frac{L}{2}\right) \tag{5.2}$$

Finally, the deflection δ at midspan of the beam is given by

$$\delta(t) = w\left(t, x = \frac{L}{2}\right) = \frac{1}{24}U(t)L^3 \tag{5.3}$$

Figure 5.6 shows the calculated deflection along x (from 0 to $L/2$) for several time points separated by equal time intervals. As expected, at any given temperature (i.e. for each subplot) the deflection is increasing with time. However, the increase is progressively faster as t increases, evidenced by the greater distance between neighboring curves at larger t. Since the applied load is a linear function of t (the load was applied at a constant loading rate), the growing deflection rate is caused by the viscoelastic behavior of the material which leads to nonlinear dependence of the deflection on the external force. The increase of deflection rate with respect to time is more significant at higher temperatures as the material exhibits more viscous behaviors.

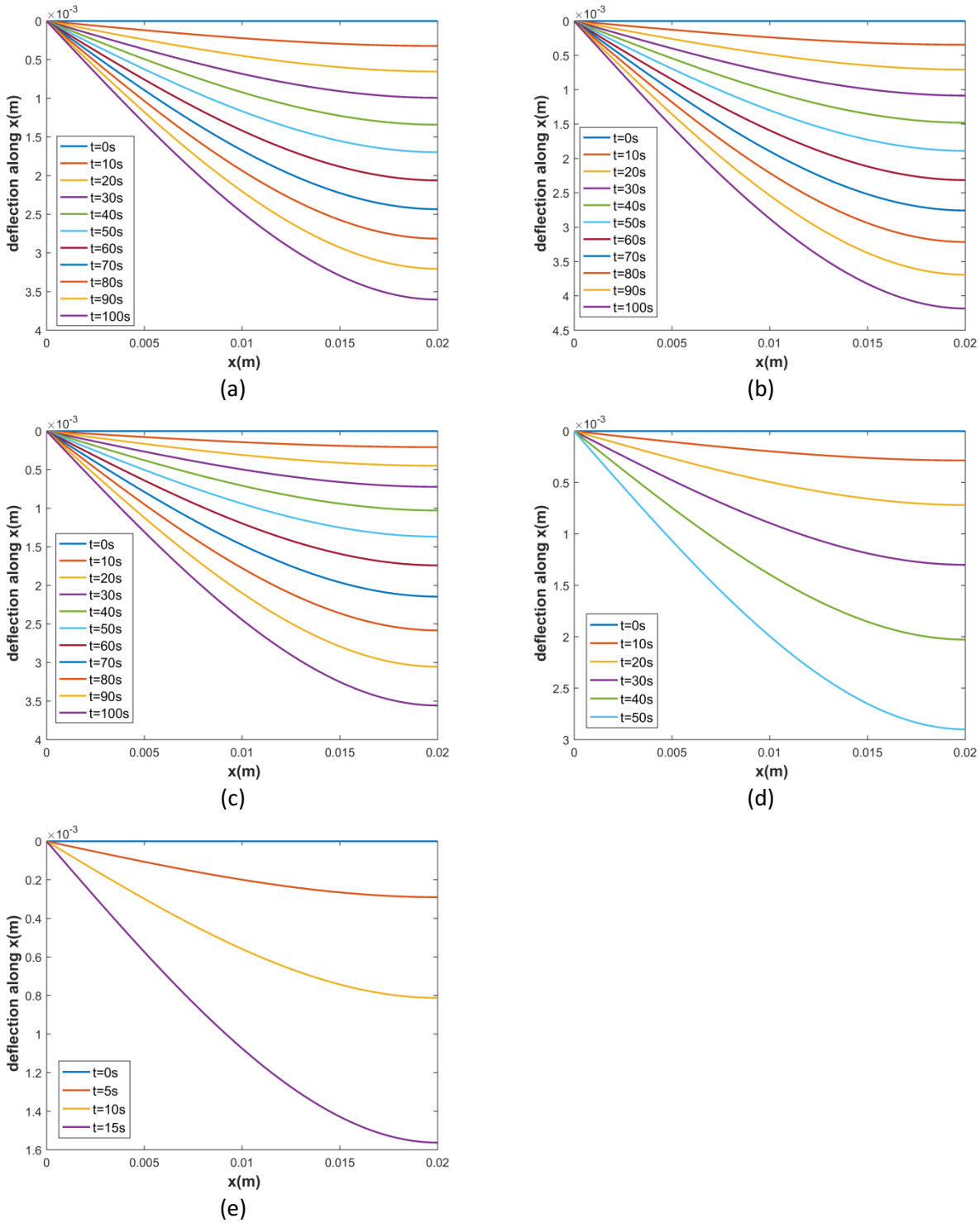

Figure 5.6 Deflection of the beam at different temperature, predicted from the model. (a) T=55℃, (b) T=60℃, (c) T=65℃, (d) T=70℃, (e) T=75℃.

5.3.2 Comparison with experiments

The deflection history, $\delta(t)$, at the mid span of the beam were obtained experimentally. The same quantity can be calculated from the model by Eqn. (5.3). At each temperature independent experiments were conducted for three times, all of which are presented in Figure 5.7 (dashed curves), along with the prediction from the model using the average beam dimension (the single solid curve in each subplot).

Despite some qualitative similarity (e.g., increasing trend in all cases), the discrepancy between the model and experimental results is quite evident. At 55 ℃, the model over-predicts the deformation, by as much as 30%. With the temperature going up to 60 ℃, the modeling result is still larger than experiment, but the discrepancy reduces (largest relative difference = 25%). As the temperature increases further to 65 ℃, the model fits well with the experimental data in the first 50 seconds and only shows discrepancy afterwards. Interestingly, in this case, the model predicts deflections that are smaller than the measured values, different from what is observed at 55 and 60 ℃. At 70 ℃ where the experiments last for a shorter time (50 seconds) due to larger deformation, the model fits very well with the experiment during the entire bending process. However, when the temperature reaches T_g, a large discrepancy is observed again, with the experimental data being almost twice the model prediction.

The SMP exhibits viscoelastic behavior which can be regarded as a combination of elastic solid and viscous liquid [4]. When the temperature is well below T_g, i.e. at 55 or 60 ℃, the material is in its glassy state so the elastic component can play a more important role than the viscous component. The considerable over-prediction of deformation seen in Figure 5.7 (a) and (b) seems to suggest that the material behaves more elastically than the model predicts. In order to verify this speculation, deflections of Euler-Bernoulli elastic beam (using the same E as in Table 5.1) are calculated and added to the comparison with the experimental data at 55 and 60 ℃ (Figure 5.8). The elastic model in fact predicts results closer to the experiments than the viscoelastic rheological model, confirming that that rheological model over-predict the viscous component at low temperature.

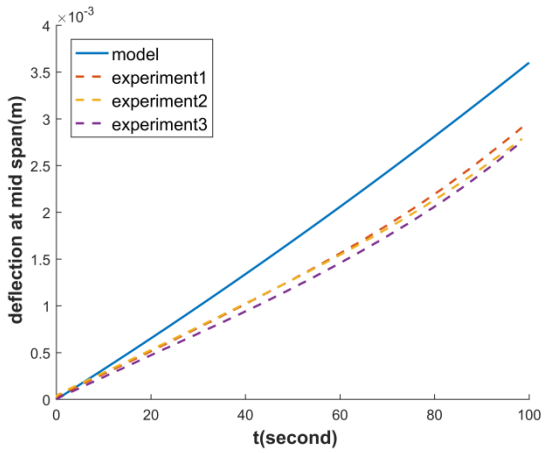

(a)

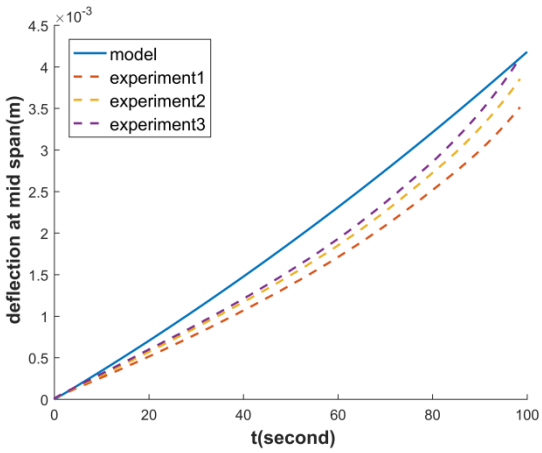

(b)

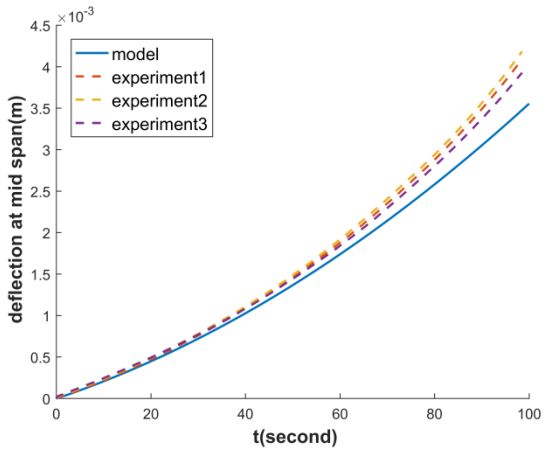

(c)

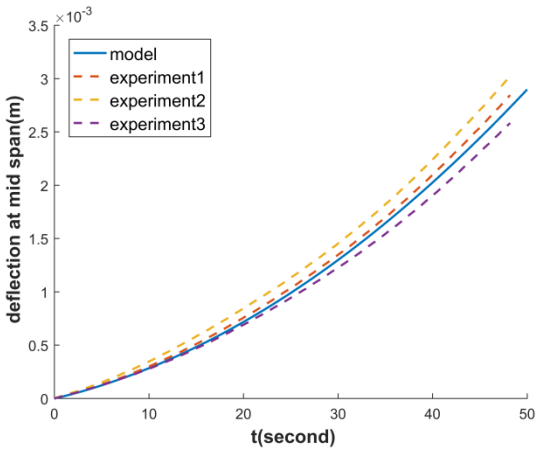

(d)

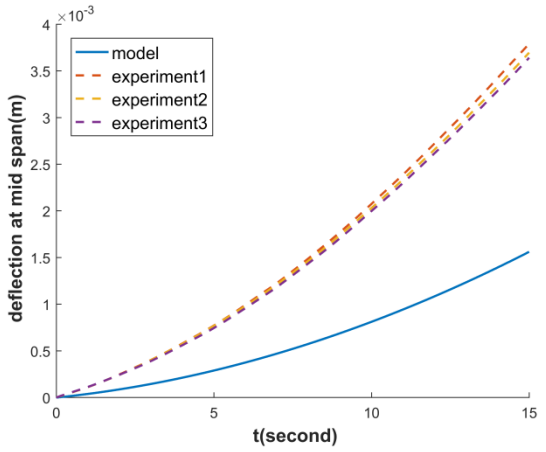

(e)

Figure 5.7 Mid span deflection measured from experiments and compared with model predictions. (a) T=55℃, (b) T=60℃, (c) T=65℃, (d) T=70℃, (e) T=75℃.

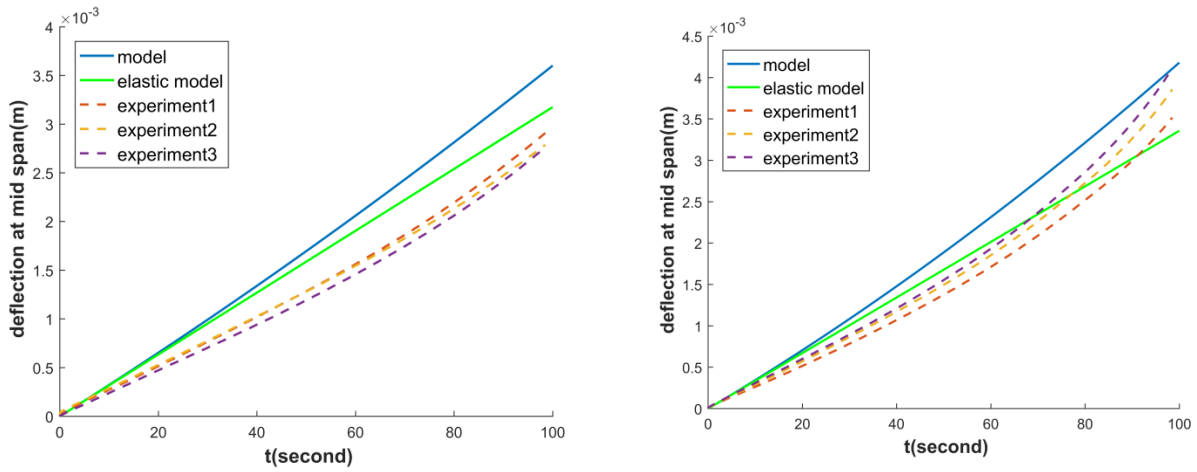

Figure 5.8 Comparison of experimental results with predictions from both elastic beam model and the rheological model. (a) T=55℃, (b) T=60℃.

It is of interest to revisit the creep data in Figure 5.2, where it was found that at low temperatures (55 and 60 ℃) the model underestimate the deformation at the beginning while overestimate the deformation after 15 minutes upon loading. At the same temperatures, the bending deflection is consistently overestimated by the model (Figure 5.7 (a) and (b)), although the maximum strain is only around 5%. While this may appear to be contradictory, several key differences should be noted between creep and bending. First, the behavior of the viscoelastic SMP is history-dependent, and the loading history is different in creep (a sudden application of force) compared with in three-point bending (gradual). Second, the stress and strain in creep are uniform everywhere, while in bending, the materials at different cross sections and at different locations on the same cross section are subjected to different stress and strain (in fact some under tension and some under compression). The mid-span deflection shown in Figure 5.7 is a result of material deformation (non-uniform) of the entire beam, and thus cannot be directly correlated with the uniform deformation in creep.

When the temperature is near T_g, i.e. 65 and 70 ℃, the bending behavior can be described very well by the rheological model. These are also the two temperatures at which best fitting between the model and creep tests was found (Figure 5.2). As the temperature reaches T_g (75 ℃), the material goes into the rubbery state and the viscous component dominates the material behavior. In this case, the model is too “stiff” and significantly underestimates the deformation. This is

also evidenced by the creep fitting at 75 ℃ where the model prediction is stiffer than the actual material for loading under small strain.

The observed discrepancy between the model and bending data could be caused by several reasons. First, the boundary condition used in modeling 3-point bending (simply supported at both end) is slightly different from that in experiment. With the roller boundary condition (Figure 4.5) in the experiments, the contact area between the beam and the rollers are finite, instead of the idealized point contacts in the model. In addition, the beam may slide relative to the rollers, causing the length of the beam between the supports to become longer. Second, one assumption made in the modeling of bending is small deflection so that the geometry of the beam during loading can be always approximated as a cuboid, which may have been violated in the experiments as the deflection increases. Third, in the model, the beam is assumed to be sufficiently thin so that the shear deformation in the cross section can be neglected. In the experiments, the ratio of length between two lower supports to the beam thickness is in the range of 11.73-12.66, which may have violated this assumption. Use of thinner sample was not possible because the test machine had limited resolution which did not permit the application of small load the thinner sample would have required.

Chapter 6 : Conclusions and future work

6.1 Conclusion

In this thesis, a rheological model was introduced and its analytical solutions for several uniaxial loading conditions (creep, stress relaxation and tension) were derived. The model was numerically implemented and the numerical solutions for the uniaxial loading conditions were compared with their corresponding analytical solutions to validate the accuracy of the numerical algorithm. The model was then extended to the bending of a thin beam and numerically implemented to calculate the deflection. Meanwhile, experiments were conducted using a polyurethane based SMP (MM7520), under both creep and three-point bending. Specimens required for the tests were manufactured using an extrusion based additive manufacturing (EBAM) technique. It has the advantage over traditional manufacturing techniques, such as injection modeling, due to its low cost and manufacturing flexibility so it provides an alternative for the production of SMP components.

Creep tests were first conducted at five different temperatures and three different stress levels for each temperature. The values of parameters required for the rheological model were extracted from the creep tests and subsequently applied to model bending. Corresponding bending experiments were conducted and compared with their modeling results at five different temperatures. Results indicate that for simple loading such as creep, the rheological model is able to describe the material behavior well between 55 and 70 ℃ at small deformations (strain less than 10%). However, for the more complex loading condition of bending, the model is only able to properly capture the material behavior for a narrow range of temperatures (from 65 to 70 ℃). The discrepancy between experiment and model becomes significant if the temperature deviates from this range, even if the maximum strain is small (around 5%).

Even though the model is only implemented numerically for 3-point bending in this thesis, it can be extended to other loading conditions. For example, a wing of an airplane is subjected to the distributed aerodynamic forces. The moment history at any cross sections can be calculated if the history of the distributed aerodynamic forces can be estimated. Therefore, the curvature history at any cross sections can be calculated numerically by using the algorithm shown in Figure 3.3. Subsequently, stress, strain and deflection histories can be obtained which is necessary for the design of the wing as a morphing aircraft component.

6.2 Future work

Several future directions can be identified to extend the work presented in this thesis. First, the rheological model here is only implemented to bending at isothermal conditions. It can be extended to loading cycles involving temperature change, for instance, during the thermomechanical bending tests [19] (the process is explained in detail in Chapter 3). As the temperature changes with respect to time, the parameters (E, μ, λ, C and ϵ_L) also changes (see Figure 5.5) and can be expressed as the function of time. This can be implemented numerically to calculate the deformation history of the beam during shape fixity and recovery process, allowing the study of shape memory effect.

Secondly, it has been observed that the model is only able to describe the material behavior well for a limited range of temperatures. It is desirable to modify the components as shown in Figure 2.6 in order to extend the validity of the model to a wider temperature range. For example, as seen in Figure 5.2 (e), the model is not able to capture the fast decay during unloading part of the creep test at 75 ℃. To address this deficiency, a new element may be added in series with the components in Figure 2.6. Upon loading, the new element behaves in the same way as the dashpot so that $\sigma = \eta\dot{\epsilon}$. Upon unloading, the element could be recovered to its original state as according to $\epsilon = -\gamma\dot{\epsilon}$ where γ is a coefficient signifying the rate of recovery. By reducing the value of γ, this modified model has the potential to capture the fast decaying during recovery at 75 ℃.

Due to the low strength and low stiffness of shape memory polymers, shape memory polymer composites (SMPCs) with higher strength and stiffness are developed in order to broaden their application. Since SMPCs exhibit anisotropic material behavior, the anisotropic model could be developed further. Specifically, micromechanical composite mechanics could be used which considers the SMP matrix and fiber as two separate phases. It is reasonable to assume that the matrix and fiber are bonded firmly without slipping so the strain of the matrix and the strain of the fiber are the same along the same direction. Once a force is applied, the matrix and the fiber are undertaking the force together. Considering the volume fraction of the matrix and the fiber in the composite, the stress relation between the matrix and the fiber can be expressed. For the SMP matrix, the stress-strain relation can be expressed by rheological model developed in this thesis. In addition, the stress-strain relation of fiber can be obtained by testing its mechanical behavior.

Therefore, the composite model could be developed. However, it should be noted that due the nature of the rheological model (1D), the proposed composite model is also only applicable to 1D loading conditions.

Finally, the nature of the rheological model is 1D so it is only applicable to one dimensional loading conditions. While it has the advantages of being simple to use and applicable to some common situations (e.g. uniaxial loading and bending), if the multiaxial loading must be taken into consideration, a model that is able to describe 2D or 3D stress-strain relationship must be developed.

Bibliography

[1] M. Behl and A. Lendlein, "Shape-memory polymers," *materialstoday,* vol. 10, 2007.

[2] W. M. Huang, B. Yang and Y. Fu, Polyurethane Shape Memory Polymers, CRC Press, 2011.

[3] A. Rudin and P. Choi, Polymer Science and Engineering, Third Edition, Elsevier, 2013.

[4] W. D. Callister and D. G. Rethwisch, Fundamentals of Material Science and Engineering, 4th Edition, John Wiley & Sons, Inc, 2012.

[5] A. Lendlein and S. Kelch, "Shape-Memory Polymers," *Angew. Chem. Int. Ed,* vol. 41, pp. 2034-2057, 2002.

[6] K. Ngai, W. Graessley, L. Mandelkern, E. Samulski, J. Koenig and G. Wignall, Physical Properties of Polymers, Third Edition, Cambridge University Press, 2004.

[7] M. T. Shaw and W. J. MacKnight, Introduction to Polymer Viscoelasticity, 3rd Edition, John Wiley & Sons, Inc, 2005.

[8] J. Hu, Shape memory polymers and textiles, Cambridge: Woodhead Publishing Limited, 2007.

[9] M. Rubinstein and R. H. Colby, Polymer Physics, New York: Oxford University Press Inc., 2003.

[10] K. Machida, Principles of Molecular Mechanics, Kodansha Ltd. and John Wiley & Sons, Inc., 1999.

[11] J. Leng, X. Lan, Y. Liu and S. Du, "Shape-memory polymers and their composites: Stimulus methods and applications," *Progress in Materials Science,* vol. 56, pp. 1077-1135, 2011.

[12] C. M. Yakacki, R. Shandas, C. Lanning, B. Rech, A. Eckstein and K. Gall, "Unconstrained recovery characterization of shape-memory polymer networks for cardiovascular applications," *Biomaterials,* vol. 28, pp. 2255-2263, 2007.

[13] A. Lendlein and R. Langer, "Biodegradable, Elastic Shape-Memory Polymers for Potential Biomedical Applications," *Science,* vol. 296, pp. 1673-1676, 2002.

[14] P. N. Keller, M. S. Lake, D. Codell, B. Rory, R. Taylor and M. R. Schullz, "Development of Elastic Memory Composite Stiffeners for a Flexible Precision Reflector," in *AIAA/ASME/ASCE/AHS/ASC Structures, Structural Dynamics, and Materials Conference*, 2006.

[15] H. Tobushi, J. Hara, E. Yamada and S. Hayashi, "Thermomechanical properties in a thin film of shape memory polymer of polyurethane series," *Smart Mater. Struct,* vol. 5, pp. 483-491, 1996.

[16] H. Tobushi, T. Hashimoto, S. Hayashi and E. Yamada, "Thermomechanical Constitutive Modeling in Shape Memory Polymer of Polyurethane Series," *Intelligent Material Systems and Structures,* vol. 8, pp. 711-718, 1997.

[17] A. Bhattacharyya and H. Tobushi, "Analysis of the Isothermal Mechanical Response of a Shape Memory Polymer Rheological Model," *Polymer Engineeringand Science,* vol. 40, no. 12, pp. 2498-2510, 2000.

[18] Y. Liu, K. Gall, M. L. Dunn, A. R. Greenberg and J. Diani, "Thermomechanics of shape memory polymers: Uniaxial experiments and constitutive modeling," *Internatinal Journal of Plasticity,* vol. 22, pp. 279-313, 2006.

[19] H. Tobushi, S. Hayashi, K. Hoshio and Y. Ejiri, "Shape recovery and irrecoverable strain control in polyurethane shape-memory polymer," *Science and Technology of Advanced Materials,* vol. 9, 2008.

[20] P. Ghosh, J. N. Reddy and A. Srinivasa, "Development and implementation of a beam theory model for shape memory polymers," *International Journal of Solids and Structures,* pp. 595-608, 2013.

[21] R. Lakes, Viscoelastic Materials, Cambridge University Press, 2009.

[22] R. L. Burden and J. D. Faires, Numerical Analysis, 9th Edition, Boston: Richard Stratton, 2011.

[23] J. Devore and R. Peck, Statistics: The Exploration and Analysis of Data, Fourth Edition, Brooks/Cole, 2001.

[24] Z. Wang, P. Li and Y. Jia, "Predicting shape memory characteristics of polyurethane in three-point bending deformation," *Polym. Adv. Technol.,* vol. 25, pp. 1130-1134, 2014.

[25] M. Baghani, H. Mohammadi and R. Naghdabadi, "An analytical solution for shape-memory-polymer Euler-Bernoulli beams under bending," *International Journal of*

Mechanical Sciences, no. 84, pp. 84-90, 2014.

[26] M. Baghani, R. Naghdabadi, J. Arghavani and S. Sohrabpour, "A thermodynamically-consistent 3 D constitutive model for shape memory polymers," *International Journal of Plasticity,* vol. 35, pp. 13-30, 2012.

[27] R. C. Hibbeler, Mechanics of Materials, Eighth Edition, Pearson, 2011.

[28] J. Raasch, M. Ivey, D. Aldrich, D. S. Nobes and C. Ayranci, "Characterization of polyurethane shape memory polymer porcessed by material extrusion additive manufacturing," *Additive Manufacturing,* vol. 8, pp. 132-141, 2015.

[29] Y. Yang, Y. Chen, Y. Wei and Y. Li, "3D printing of shape memory polymer for functional part fabrication," *Int J Adv Manuf Technol,* 2015.

[30] I. Garces, S. Aslanzadeh, Y. Boluk and C. Ayranci, "Effect of moisture on shape memory polyurethane polymers for extrusion based additive manufacturing-4D Printing," *submitted to Additive Manufacturing on 2017.*

[31] J. F. Villacres, D. S. Nobes and C. Ayranci, "Additive Manufacturing of Shape Memory Polymers: Effects of Print Orientation and Infill Percentage on Mechanical Properties," *Rapid Prototyping,* accepted on 2017.

[32] R. M. Christensen, Theory of Viscoelasticity, An Introduction, Second Edition, Academic Press, 1982.

[33] W. N. Findley, J. S. Lai and K. Onaran, Creep and Relaxation of Nonlinear Viscoelastic Materials, North-Holland Publishing Company, 1976.

Appendices

Appendix A Extracting *E* from fitting initial response in creep test

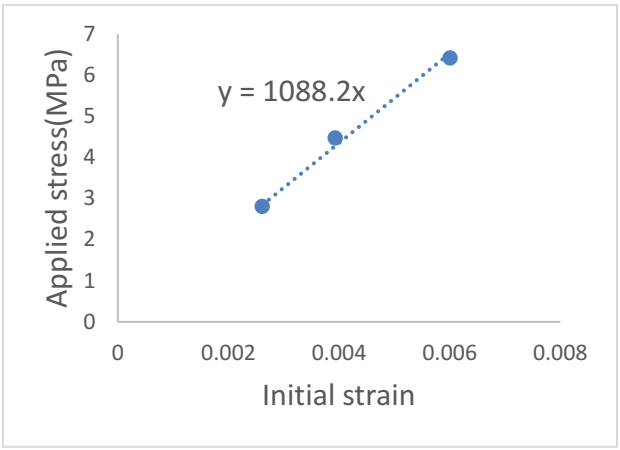

(a)

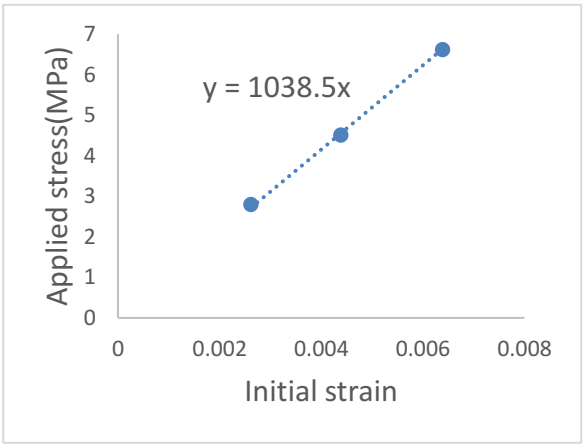

(b)

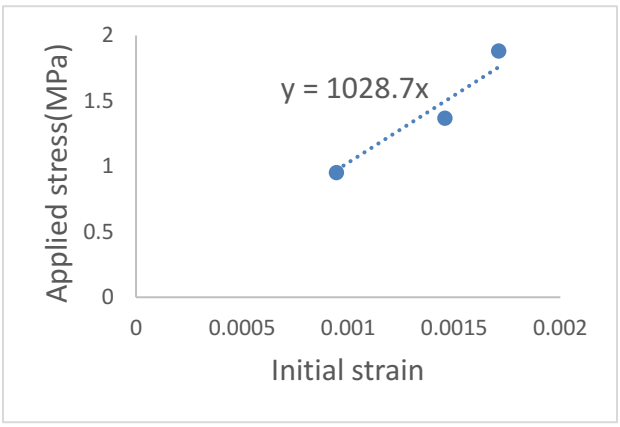

(c)

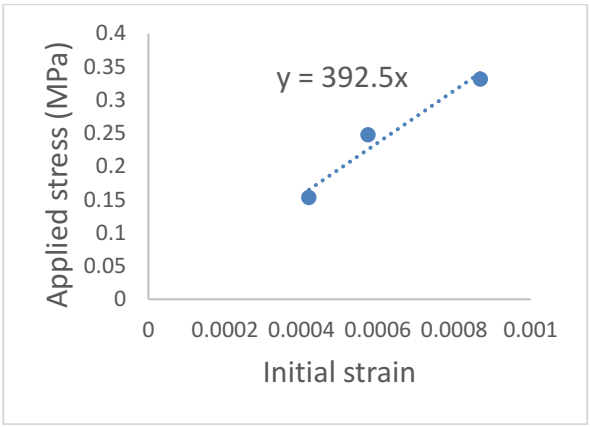

(d)

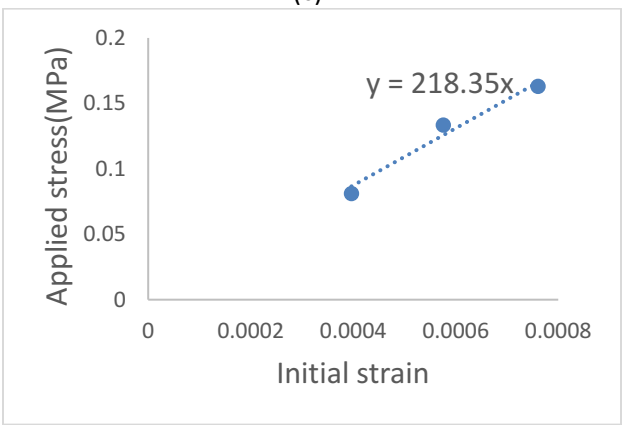

(e)

Figure A.1 Fitting results of E. (a) T=55℃, (b) T=60℃, (c) T=65℃, (d) T=70℃, (e) T=75℃.

Appendix B Verification for the linear fitting of curvature

The domain x from 0 to $L/2$ is discretized into 10 and 100 intervals respectively and the calculated discretized κ values are plotted in Figure B.1 for each temperature. As can be seen, results from the two discretizations almost overlap at all temperatures.

In addition, the discretized $\kappa(t,x)$ values show a linear relation with x at each time. Therefore, $\kappa(t,x)$ can be approximated by a linear function of x at any time and any temperature. The linear fitting is shown in Figure B.2, which proves the accuracy of the approximation.

In the work performed in this thesis at each temperature, the beam (from $x = 0$ to $x = L/2$) was discretized by 100 intervals to evaluate $\kappa(t,x)$. A linear fitting was then performed at each given t (Eqn. 5.1), from which the deflection was determined (Eqn. 5.2).

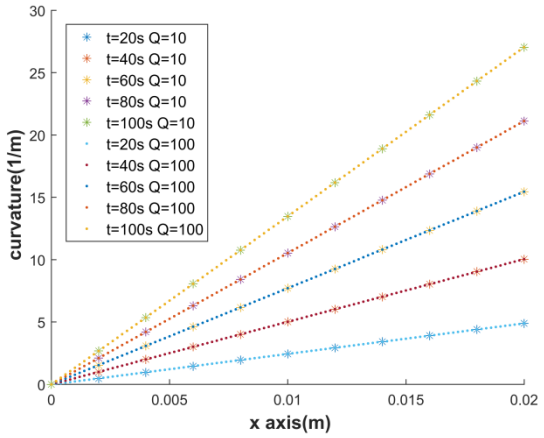

(a)

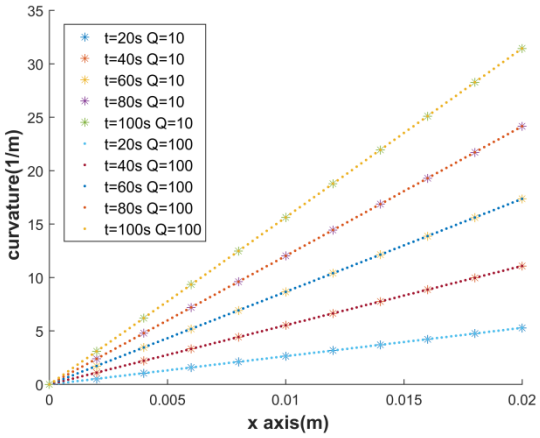

(b)

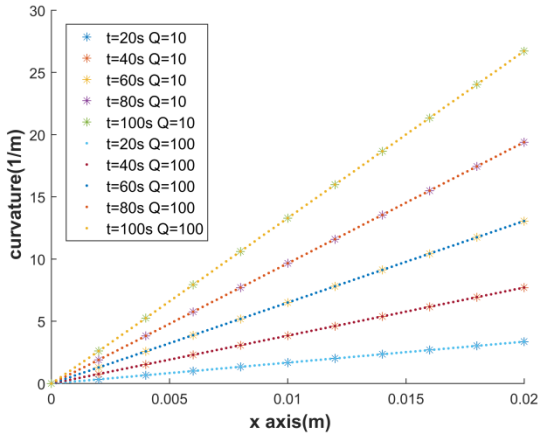

(c)

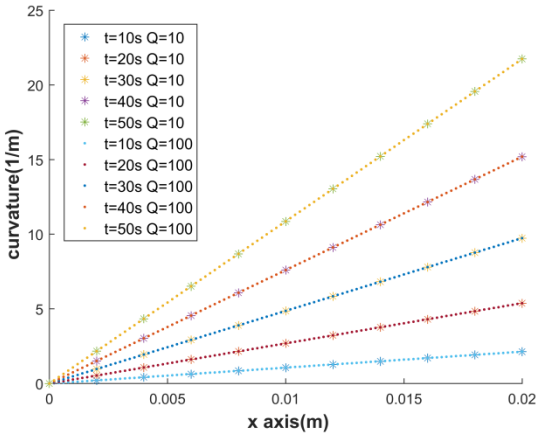

(d)

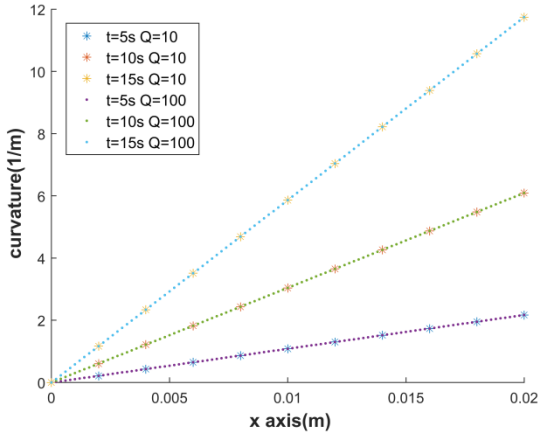

(e)

Figure B.1 $\kappa(t,x)$ obtained by discretizing x with different number (Q) of intervals. (a) T=55℃, (b) T=60℃, (c) T=65℃, (d) T=70℃, (e) T=75℃.

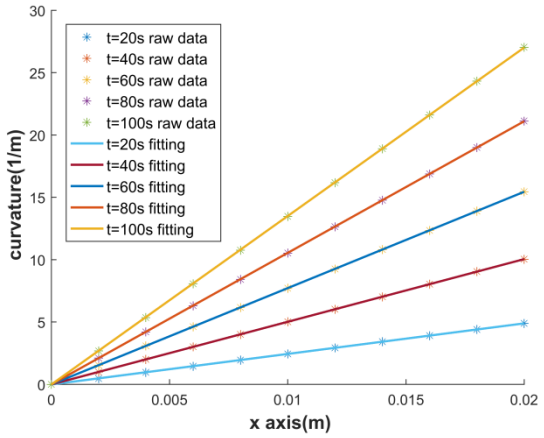

(a)

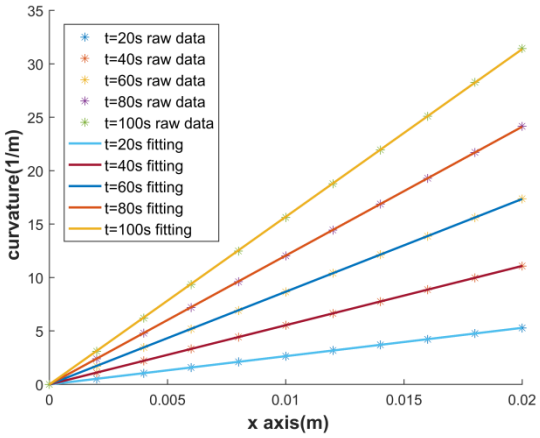

(b)

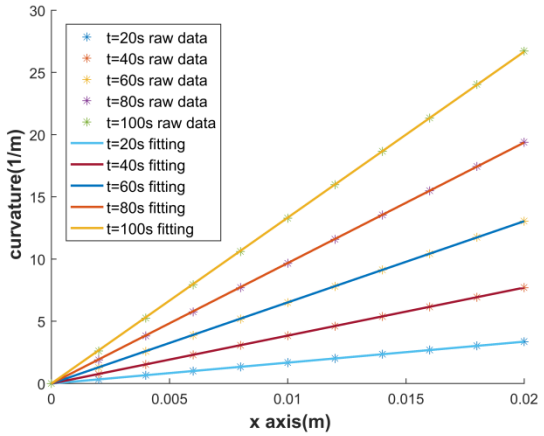

(c)

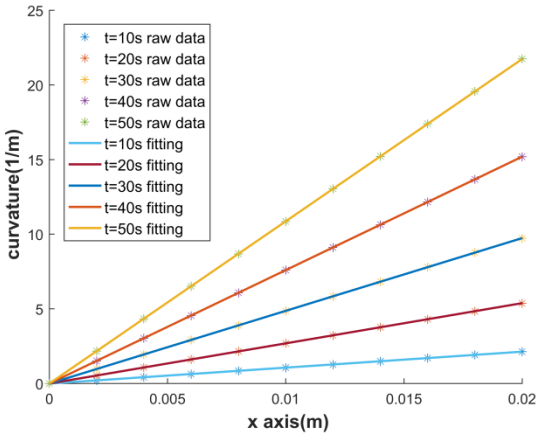

(d)

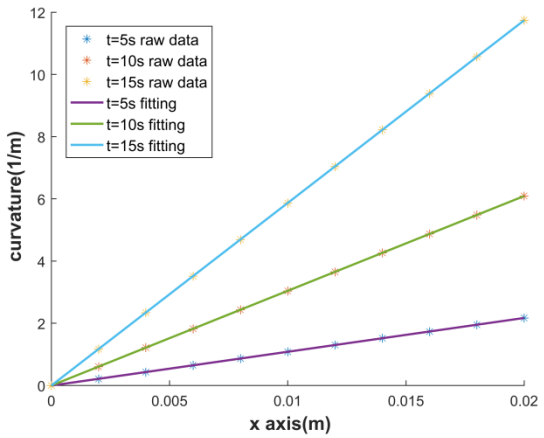

(e)

Figure B.2 $\kappa(t,x)$ fitted by linear lines, x is discretized with 10 intervals. (a) T=55℃, (b) T=60℃, (c) T=65℃, (d) T=70℃, (e) T=75℃.

Appendix C Explanation on the observed linear relation between curvature and x

In the 3-point bending studied in this work, a force $P(t)$ is applied at the mid span of the beam so that the moment can be expression as $M(t) = \frac{P(t)}{2}x, (0 \leq x \leq \frac{L}{2})$. If the beam were linearly elastic, then under the assumptions of Euler-Bernoulli beam, $\sigma = E\epsilon = E\kappa y$ leads to $M = \int y\sigma dA = E\kappa \int y^2 dA = EI\kappa$, where I is the moment of inertia about the neutral axis. Thus, the relation between κ and x is $\kappa(t) = \frac{P(t)}{2EI}x$, that is, for a linearly elastic beam κ is proportional to x at any time.

The viscoelastic model differs from elastic model in terms of the stress-strain relation, i.e. the current value of strain (or stress) is determined not only by the current value of stress (or strain) but also by the history of loading [32]. A viscoelastic model can be further categorized as being either linear, for which Eqn. C.1 holds, or nonlinear. For example, the standard linear solid (SLS) model is linear while the rheological model investigated in this thesis is nonlinear. For a linearly viscoelastic material, the Boltzmann superposition principle is applicable (Eqn. C.2) [33].

$$\epsilon[c\sigma(t)] = c\epsilon[\sigma(t)] \tag{C.1}$$

$$\epsilon[\sigma_1(t) + \sigma_2(t - t_1)] = \epsilon[\sigma_1(t)] + \epsilon[\sigma_2(t - t_1)] \tag{C.2}$$

Applying the two equations to stress relaxation where a constant strain ϵ_0 is applied and its corresponding stress history is obtained as $\sigma(t)$, the relaxation modulus can be determined as $E_r(t) = \sigma(t)/\epsilon_0$ [7]. Similarly, for creep test where a constant stress σ_0 is applied and its corresponding strain history is obtained as $\epsilon(t)$, the compliance modulus is defined as $J(t) = \epsilon(t)/\sigma_0$ [7]. Since the material is linearly viscoelastic, the relaxation modulus is strain independent which means $c \cdot \sigma(t) = E_r(t)(c \cdot \epsilon_0)$. Similarly, the compliance modulus is stress independent in that $c \cdot \epsilon(t) = J(t)(c \cdot \sigma_0)$.

Based on the discussed above, the correspondence principle [32] can be used to derive the response of a linearly viscoelastic beam under bending. Stress can be expressed as Eqn. (C.3) based on Boltzmann superposition principle and the relation can be written in a simple form through Laplace transform as shown in Eqn. (C.4).

$$\sigma(t) = \int_0^t E_r(t-\tau)\frac{d\epsilon}{d\tau}d\tau = y\int_0^\infty E_r(t-\tau)\frac{d\kappa}{d\tau}d\tau \qquad (C.3)$$

$$\bar{\sigma} = y\overline{E_r}s\bar{\kappa} \qquad (C.4)$$

Substituting Eqn. (C.3) and $\epsilon = \kappa y$ into $M = \int y\sigma dA$, the moment at any cross section can be expressed as Eqn. (C.5), and Eqn. (C.6) can be obtained through Laplace transform.

$$M(t) = \int y^2\left[\int_0^t E_r(t-\tau)\frac{d\kappa}{d\tau}d\tau\right]dA = I\int_0^t E_r(t-\tau)\frac{d\kappa}{d\tau}d\tau \qquad (C.5)$$

$$\bar{M} = I\overline{E_r}s\bar{\kappa} \qquad (C.6)$$

Combining Eqns. (C.4) and (C.6) together arrives in $\bar{\sigma} = \frac{\bar{M}}{I}y$. Through inverse Laplace transform, stress can be expressed as

$$\sigma(t) = \frac{M(t)}{I}y = \frac{P(t)}{2I}yx \qquad (C.7)$$

As can be seen from Eqn. (C.7), σ is proportional to x at any time. Again, based on Boltzmann superposition principle, strain can be expressed as $\epsilon(t) = \int_0^t J(t-\tau)\frac{d\sigma}{d\tau}d\tau = \frac{yx}{2I}\int_0^t J(t-\tau)\frac{dP}{d\tau}d\tau$ so that curvature can be expressed as Eqn. (C.8), which is proportional to x at any specific time for a linearly viscoelastic beam.

$$\kappa(t) = \frac{\epsilon(t)}{y} = \frac{x}{2I}\int_0^t J(t-\tau)\frac{dP}{d\tau}d\tau \qquad (C.8)$$

The rheological model investigated in this thesis is a modified SLS model where the term ϵ_s (expressed with respect to C and ϵ_L) is added (Eqn. (2.12)) in order to capture the irrecoverable strain [16]. Only when $C = 0$ or ϵ_l is large (difficult to trigger the irrecoverable strain) will this model reduce to the SLS model. Therefore, the relaxation modulus is strain dependent and the compliance modulus is stress dependent; as a result in principle the above derivations does not apply to the rheological model. However, it can be seen from Table 5.1 that C ranges from [0.3, 0.83] and ϵ_l ranges from [0.00027, 0.018]. By changing C and ϵ_l in the range of [0, 0.9] and [0, 0.1] respectively at each temperature, it was found that the curvature and deflection of the beam

were not sensitive to the variation of C and ϵ_L. The influence of *C* on the mid span deflection is shown in Figure C.1 where C varies and other four parameters maintain their original values at each temperature shown in Table 5.1. The influence of ϵ_L is investigated in Figure C.2 where ϵ_L varies and other four parameters maintain their original values at each temperature shown in Table 5.1. Both figures clearly shows the insensitively of results to C and ϵ_L, which explains why the curvature is approximately proportional to x.

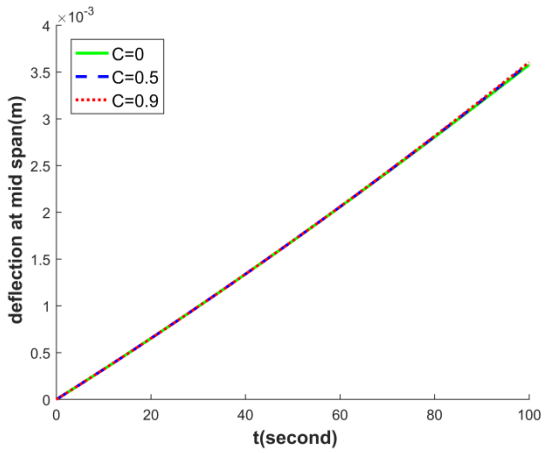

(a)

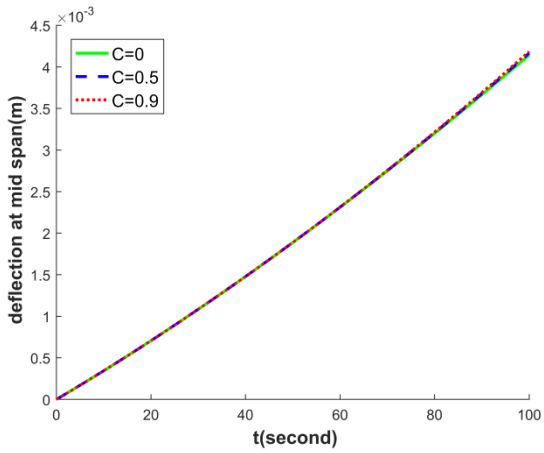

(b)

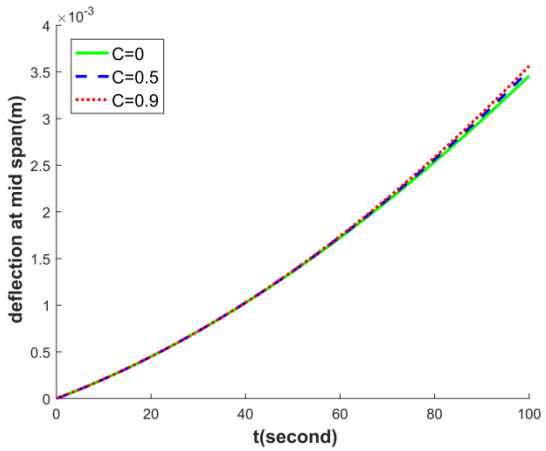

(c)

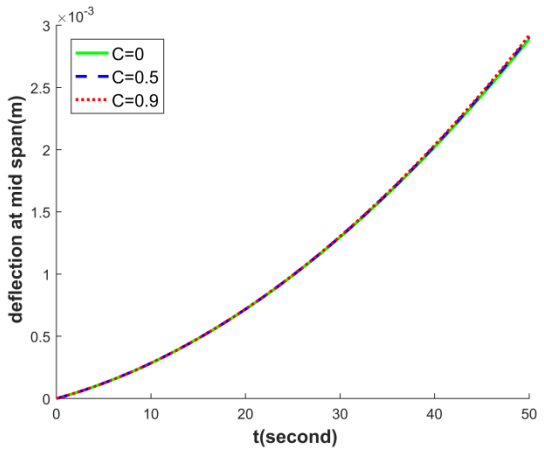

(d)

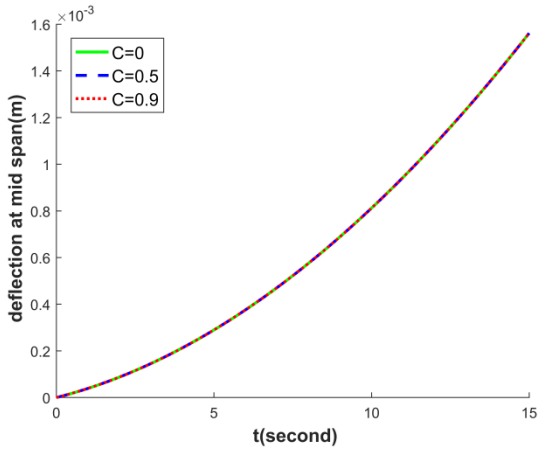

(e)

Figure C.1 Mid span deflection with the variation of C. (a) T=55℃, (b) T=60℃, (c) T=65℃, (d) T=70℃, (e) T=75℃.

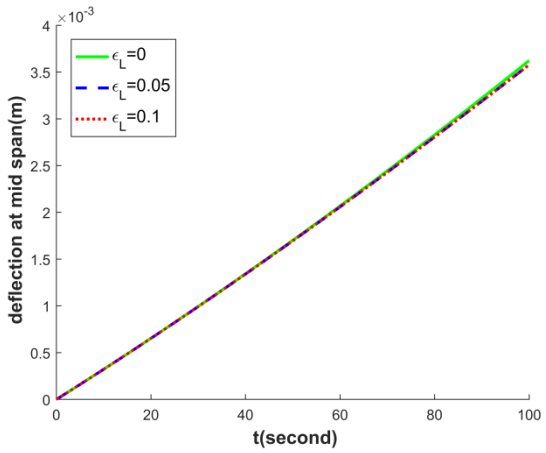

(a)

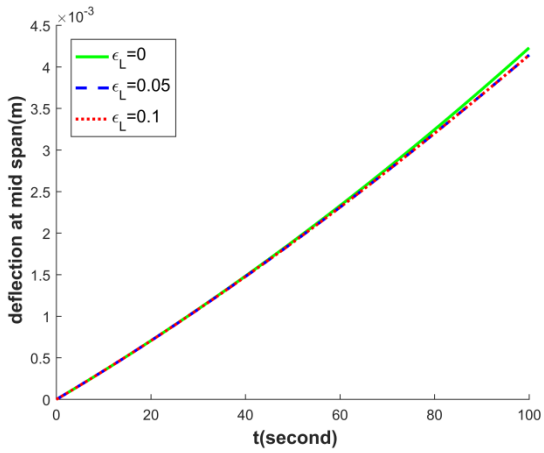

(b)

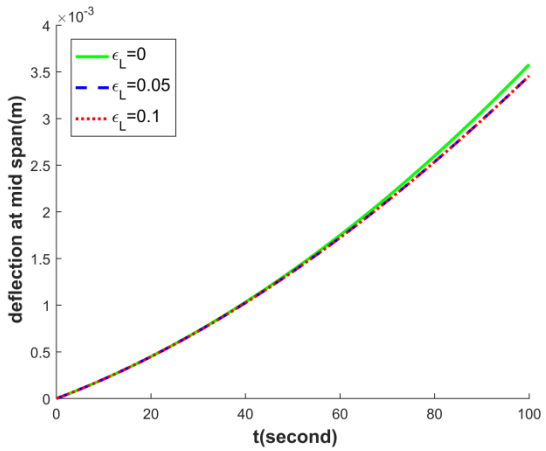

(c)

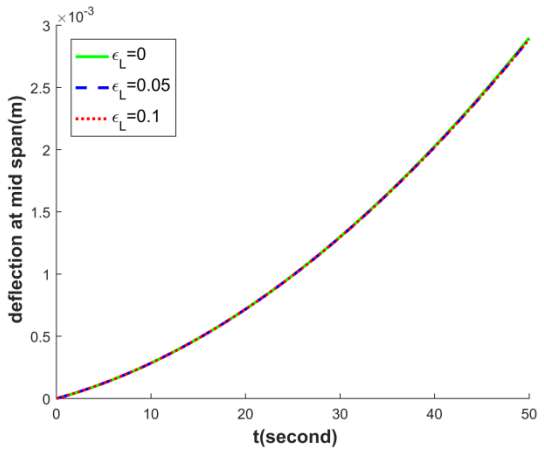

(d)

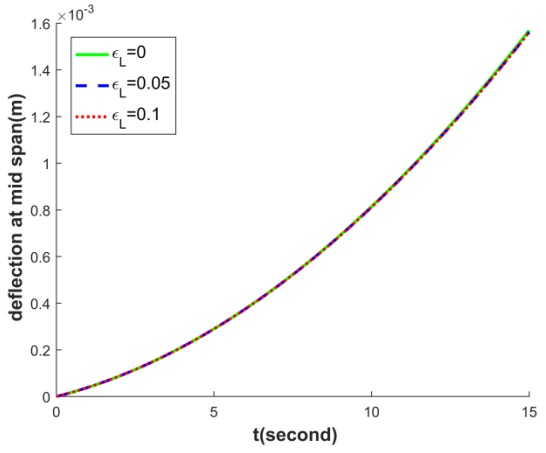

(e)

Figure C.2 Mid span deflection with the variation of ϵ_L. (a) T=55℃, (b) T=60℃, (c) T=65℃, (d) T=70℃, (e) T=75℃.

Appendix D Matlab Code

Creep comparation between Analytical solution and Euler solution

One example when time step = 0.1 for the Euler solution

Input values of parameters which are seleted form Tobushi's paper

```
clear;
E = 146e+6;      % elastic modulus(Pa)
mu = 14e+9;      % viscosity(Pa*s)
lambda = 521;    % retardation time(s)
C = 0.112;       % ratio between epsilons and epsilonc
epsilonl = 0.3/100;   % threshold strain for triggering irrecoverable strain
mu_eff = mu*((1-(mu*C)/(lambda*E))^(-1)); % effective viscosity (Pa*s)
lambda_eff = lambda*((1-C)^(-1));         % effective retardation time(s)
epsilons_eff = -1*(C*epsilonl)/(1-C);     % effective epsilons
% critical stress for creep test that trigger shape memory strain
sigma_critical = epsilonl*((lambda/mu-1/E)^(-1));
```

Euler solution

```
dt = 0.1;   % time step for Euler method
sigma_0 = 2e+6;      % applied stress
tb = 1800;           % loading time
ta_E = 0;       % define the time when the irrecoverable strain is triggered
t_E_1 = 0:dt:tb;     % discretize loading time
num_1 = length(t_E_1);
epsilon_E = zeros(size(t_E_1));  % define strain for Euler solution
epsilon_E(1) = sigma_0/E;        % initial condition
for n = 1:(num_1-1);
    if (epsilon_E(n)-sigma_0/E) <= epsilonl   % regime 1
        mu_EFF = mu;
        lambda_EFF = lambda;
        epsilons_EFF = 0;
        ta_E = ta_E+dt;
    else                                      % regime 2
        mu_EFF = mu_eff;
        lambda_EFF = lambda_eff;
        epsilons_EFF = epsilons_eff;
    end
    epsilon_E(n+1) = (sigma_0/mu_EFF+epsilons_EFF/lambda_EFF)*dt+...
```

```
        epsilon_E(n)*(1-dt/lambda_EFF);
end

epsilonc_E = epsilon_E-sigma_0/E;   % calculate creep strain
epsilons_E_tb = C*(epsilonc_E(num_1)-epsilonl); % the irrecoverable strain at tb

t_E = 0:dt:3600;   % overall time
num = length(t_E);
epsilon_E = [epsilon_E zeros(1,num-num_1)];   % define strain including recovery stage
epsilonc_E = [epsilonc_E zeros(1,num-num_1)]; % define creep strain including
% recovery stage

% calculate strain and creep strain during recovery stage
for n = num_1:(num-1);
    epsilonc_E(n+1) = (epsilons_E_tb/lambda)*dt+epsilonc_E(n)*(1-dt/lambda);
    epsilon_E(n+1) = epsilonc_E(n+1);
end
```

Analytical solution

```
t_A = 0:dt:3600;    % overall time
epsilon_A = zeros(size(t_A)); % define strain for analytical solution
epsilonc_A = zeros(size(t_A)); % define creep strain for analytical solution

% calculate the creep strain first
if  sigma_0 <= sigma_critical;     % if the irrecoverable strain cannot be
    % triggered forever
    regime1 = (0 <= t_A) & (t_A <= tb);
    epsilonc_A(regime1) = sigma_0*(lambda/mu-1/E)*(1-exp(-1*t_A(regime1)/lambda));
    regime3 = (tb <= t_A) & (t_A <= 3600);
    epsilonc_A(regime3) = epsilonc_A(t_A==tb)*exp(-1*(t_A(regime3)-tb)/lambda);
elseif sigma_0 > sigma_critical;   % if the irrecoverable strain can be triggered
    syms x;    % calculate ta when the irrecoverable strain is triggered
    ta_A = solve(sigma_0*(lambda/mu-1/E)*(1-exp(-1*x/lambda)) == epsilonl,x);
    ta_A = double(ta_A);
    if  ta_A >= tb;      % if the irrecoverable strain is not yet triggered before tb
        regime1 = (0 <= t_A) & (t_A <= tb);
        epsilonc_A(regime1) = sigma_0*(lambda/mu-1/E)*(1-exp(-1*t_A(regime1)/lambda));
        regime3 = (tb <= t_A) & (t_A <= 3600);
        epsilonc_A(regime3) = epsilonc_A(t_A==tb)*exp(-1*(t_A(regime3)-tb)/lambda);
    elseif ta_A < tb;        % if the irrecoverable strain is triggered before tb
        regime1 = (0 <= t_A) & (t_A <= ta_A);
        epsilonc_A(regime1) = sigma_0*(lambda/mu-1/E)*(1-exp(-1*t_A(regime1)/lambda));
```

```
        regime2 = (ta_A <= t_A) & (t_A <= tb);
        epsilonc_A(regime2) = epsilonl*exp(-1*(t_A(regime2)-ta_A)/lambda_eff)+...
            sigma_0*(epsilons_eff/sigma_0+lambda_eff/mu_eff-1/E)*...
            (1-exp(-1*(t_A(regime2)-ta_A)/lambda_eff));
        epsilons__A_tb = C*(epsilonc_A(t_A==tb)-epsilonl);
        regime3 = (tb <= t_A) & (t_A <= 3600);
        epsilonc_A(regime3) = epsilons__A_tb+(epsilonc_A(t_A==tb)-epsilons__A_tb)*...
            exp(-1*(t_A(regime3)-tb)/lambda);
    end
end
% calculate strain based on creep strain
epsilon_A(1:(tb/dt+1)) = epsilonc_A(1:(tb/dt+1))+sigma_0/E;
epsilon_A((tb/dt+2):(3600/dt+1)) = epsilonc_A((tb/dt+2):(3600/dt+1));
```

R square between Analytical solution and Euler solution

```
Rsq = 1-sum((epsilon_E-epsilon_A).^2)/sum((epsilon_A-mean(epsilon_A)).^2);
format long  % display R square in a long digit
Rsq
```

Plot figure

```
hold on
plot(t_A,epsilon_A,'b','LineWidth',2)   % plot Analytical solution
plot(t_E,epsilon_E,'--r','LineWidth',2) % plot Euler solution
legend({'\bf Anatical solution','\bf Euler solution'},'FontSize',13)
xlabel('\bf t(second)','FontSize',13)
ylabel('\bf Strain','FontSize',13)
axis([0,3600,0,0.08])
set(gca,'xtick',0:600:3600,'ytick',0:0.01:0.08)
```

Published with MATLAB® R2016a

Stress relaxation comparation between Analytical solution and Euler solution

One example when time step = 0.1 for the Euler solution

Input values of parameters which are seleted form Tobushi's paper

```
clear;
E = 146e+6;      % elastic modulus(Pa)
mu = 14e+9;      % viscosity(Pa*s)
lambda = 521;    % retardation time(s)
C = 0.112;       % ratio between epsilons and epsilonc
epsilonl = 0.3/100;   % threshold strain for triggering irrecoverable strain
mu_eff = mu*((1-(mu*C)/(lambda*E))^(-1)); % effective viscosity (Pa*s)
lambda_eff = lambda*((1-C)^(-1));         % effective retardation time(s)
epsilons_eff = -1*(C*epsilonl)/(1-C);     % effective epsilons
% critical strain for stress relaxation that trigger shape memory strain
epsilon_critical = (epsilonl*lambda/mu)*((lambda/mu-1/E)^(-1));
```

Euler solution

```
dt = 0.1;     % time step for Euler method
epsilon_0 = 0.06;   % applied strain
tb = 1800;          % loading time
ta_E = 0;     % define the time when the irrecoverable strain is triggered
t_E = 0:dt:tb;         % discretize loading time
num_E = length(t_E);
sigma_E = zeros(1,num_E);   % define stress for Euler solution
sigma_E(1) = epsilon_0*E;   % initial condition
for n = 1:(num_E-1);
    if (epsilon_0-sigma_E(n)/E) <= epsilonl    % regime1
        mu_EFF = mu;
        lambda_EFF = lambda;
        epsilons_EFF = 0;
        ta_E = ta_E+dt;
    else                                       % regime2
        mu_EFF = mu_eff;
        lambda_EFF = lambda_eff;
        epsilons_EFF = epsilons_eff;
    end
    sigma_E(n+1) = (epsilon_0-epsilons_EFF)*E*dt/lambda_EFF+sigma_E(n)*...
        (1-E*dt/mu_EFF);
end
```

Analytical solution

```
t_A = 0:dt:tb;      % overall time
sigma_A = zeros(size(t_A));  % define stress for analytical solution
if epsilon_0 <= epsilon_critical;   % if the irrecoverable strain cannot be
    % triggered forever
    regime1 = (0 <= t_A) & (t_A <= tb);
    sigma_A(regime1) = epsilon_0*mu/lambda+epsilon_0*(E-mu/lambda)*...
        exp(-1*E/mu*t_A(regime1));
elseif epsilon_0 > epsilon_critical;    % if the irrecoverable strain can be triggered
    syms x;    % calculate ta when the irrecoverable strain is triggered
    ta_A = solve(epsilon_0-(epsilon_0*mu/lambda+epsilon_0*(E-mu/lambda)*...
        exp(-1*E/mu*x))/E == epsilonl,x);
    ta_A = double(ta_A);
    if ta_A >= tb;   % if the irrecoverable strain is not yet triggered before tb
        regime1 = (0 <= t_A) & (t_A <= tb);
        sigma_A(regime1) = epsilon_0*mu/lambda+epsilon_0*(E-mu/lambda)*...
            exp(-1*E/mu*t_A(regime1));
    elseif ta_A < tb;   % if the irrecoverable strain is triggered before tb
        sigma_A = zeros(size(t_A));
        regime1 = (0 <= t_A) & (t_A <= ta_A);
        sigma_A(regime1) = epsilon_0*mu/lambda+epsilon_0*(E-mu/lambda)*...
            exp(-1*E/mu*t_A(regime1));
        regime2 = (ta_A <= t_A) & (t_A <= tb);
        sigma_A(regime2) = mu_eff/lambda_eff*(epsilon_0-epsilons_eff)+...
            (E*(epsilon_0-epsilonl)-mu_eff/lambda_eff*(epsilon_0-epsilons_eff))*...
            exp(-1*E/mu_eff*(t_A(regime2)-ta_A));
    end
end
```

R square between Analytical solution and Euler solution

```
Rsq = 1-sum((sigma_E-sigma_A).^2)/sum((sigma_A-mean(sigma_A)).^2);
format long  % display R square in a long digit
Rsq
```

Plot figure

```
hold on
plot(t_A,sigma_A,'b','LineWidth',2)    % plot Analytical solution
plot(t_E,sigma_E,'--r','LineWidth',2)  % plot Euler solution
```

```
legend({'\bf Anatical solution','\bf Euler solution'},'FontSize',13)
xlabel('\bf t(second)','FontSize',13)
ylabel('\bf Stress(Pa)','FontSize',13)
axis([0,1800,0,9e+6])
set(gca,'xtick',0:300:1800,'ytick',0:1e6:9e6)
```

Published with MATLAB® R2016a

Tensile comparation between Analytical solution and Euler solution

One example when time step = 0.1 for the Euler solution Tensile test is conducted at a constant stress rate

Input values of parameters which are seleted form Tobushi's paper

```
clear;
E = 146e+6;      % elastic modulus(Pa)
mu = 14e+9;      % viscosity(Pa*s)
lambda = 521;    % retardation time(s)
C = 0.112;       % ratio between epsilons and epsilonc
epsilonl = 0.3/100;   % threshold strain for triggering irrecoverable strain
mu_eff = mu*((1-(mu*C)/(lambda*E))^(-1)); % effective viscosity (Pa*s)
lambda_eff = lambda*((1-C)^(-1));         % effective retardation time(s)
epsilons_eff = -1*(C*epsilonl)/(1-C);     % effective epsilons
```

Euler solution

```
dt = 0.1;  % time step for Euler method
stress_rate = 5e+4;      % stress rate of tensile test
tb = 120;      % overall time
ta_E = 0; % define the time when the irrecoverable strain is triggered
t_E = 0:dt:tb;  % discretize the overall time for Euler method
sigma_E = stress_rate*t_E;  % stress history
num_E = length(t_E);
epsilon_E = zeros(1,num_E);   % define stress for Euler method
epsilon_E(1) = 0;             % Initial condition
for n = 1:(num_E-1);
```

```
    if (epsilon_E(n)-sigma_E(n)/E) <= epsilonl   % regime 1
        mu_EFF = mu;
        lambda_EFF = lambda;
        epsilons_EFF = 0;
        ta_E = ta_E+dt;
    else                                         % regime 2
        mu_EFF = mu_eff;
        lambda_EFF = lambda_eff;
        epsilons_EFF = epsilons_eff;
    end
    epsilon_E(n+1) = (sigma_E(n)/mu_EFF+epsilons_EFF/lambda_EFF+stress_rate/E)*...
        dt+epsilon_E(n)*(1-dt/lambda_EFF);
end
```

Analytical solution

```
t_A = 0:dt:tb;   % discretize the overall time for analytical solution
sigma_A = stress_rate*t_A;  % stress history
syms x;   % calculate ta when the irrecoverable strain is triggered
ta_A = solve(stress_rate*(lambda/mu-1/E)*(x-lambda*(1-exp(-1*x/lambda)))...
    == epsilonl,x);
ta_A = double(ta_A);
epsilon_A = zeros(size(t_A));  % define stress for analytical solution
if ta_A >= tb;   % if the irrecoverable strain is not yet triggered before tb
    regime1 = (0 <= tb) & (t_A <= tb);
    epsilon_A(regime1) = stress_rate*lambda/mu*t_A(regime1)-...
            stress_rate*lambda*(lambda/mu-1/E)*(1-exp(-1*t_A(regime1)/lambda));
elseif ta_A < tb;   % if the irrecoverable strain is triggered before tb
    regime1 = (0 <= t_A) & (t_A <= ta_A);
    epsilon_A(regime1) = stress_rate*lambda/mu*t_A(regime1)-...
        stress_rate*lambda*(lambda/mu-1/E)*(1-exp(-1*t_A(regime1)/lambda));
    regime2 = (ta_A <= t_A) & (t_A <= tb);
    epsilon_A(regime2) = (epsilonl+stress_rate*ta_A/E)*exp(-1*(t_A(regime2)-ta_A)/...
        lambda_eff)+(stress_rate*lambda_eff*(1/E-lambda_eff/mu_eff)+epsilons_eff)*...
        (1-exp(-1*(t_A(regime2)-ta_A)/lambda_eff))+stress_rate*lambda_eff/mu_eff*...
        t_A(regime2)-stress_rate*lambda_eff/mu_eff*ta_A*...
        exp(-1*(t_A(regime2)-ta_A)/lambda_eff);
end
```

R square between Analytical solution and Euler solution

```
Rsq = 1-sum((epsilon_E-epsilon_A).^2)/sum((epsilon_A-mean(epsilon_A)).^2);
format long  % display R square in a long digit
Rsq
```

Plot figure

```
hold on
plot(epsilon_A,sigma_A,'b','LineWidth',2)     % plot Analytical solution
plot(epsilon_E,sigma_E,'--r','LineWidth',2)   % plot Euler solution
legend({'\bf Anatical solution','\bf Euler solution'},'FontSize',13,'Location','best')
xlabel('\bf Strain','FontSize',13)
ylabel('\bf Stress(Pa)','FontSize',13)
axis([0,0.07,0,6e+6])
set(gca,'xtick',0:0.01:0.07,'ytick',0:1e6:6e6)
```

Published with MATLAB® R2016a

Creep test results and fitting with the rheological model

One example when temperauter is 55 C (T = 55 C)

Values of parameters selected for the fitting of experimental results

```
clear;
E = 1088.2e6;    % elastic modulus(Pa)
mu = 148e9;      % viscosity(Pa*s)
lambda = 226;    % retardation time(s)
C = 0.76;        % ratio between epsilons and epsilon
epsilonl = 0.00065;   % threshold strain for triggering irrecoverable strain
mu_eff = mu*((1-(mu*C)/(lambda*E))^(-1));     % effective viscosity (Pa*s)
lambda_eff = lambda*((1-C)^(-1));             % effective retardation time(s)
epsilons_eff = -1*(C*epsilonl)/(1-C);         % effective epsilons
% critical stress for creep test that trigger shape memory strain
```

```
sigma_critical = epsilonl*((lambda/mu-1/E)^(-1));
```

Load experimental data

```
load('Creep_55_different_load.mat')
t_experiment = (0:0.1:3600)';
% plot three experimental results at different stress levels
hold on
plot(t_experiment,strain_55_30,'--','LineWidth',1.5);
plot(t_experiment,strain_55_50,'--','LineWidth',1.5);
plot(t_experiment,strain_55_70,'--','LineWidth',1.5);
strain_experiment = [strain_55_30, strain_55_50, strain_55_70];
```

Analytical solution for three creep tests

```
tb = 1800;     % loading time
t = 0:0.1:3600;  % discretize overall time
% input three different stress level for three different creep test
sigma_real = [2.810515074e+6,4.477638672e+6,6.417308398e+6];
ta_round = [0,0,0];    % define ta when the irrecoverable strain is triggered
epsilon_ta = [0,0,0];  % define the strain at ta
for q = 1:3;  % calculate the strains history at different stress levels respectively
    sigma_0 = sigma_real(q);         % applied stress
    epsilonc = zeros(size(t));       % define creep strain
    epsilon = zeros(size(t));        % define strain
    if  sigma_0 <= sigma_critical;   % if the irrecoverable strain cannot be
        % triggered forever
        case1 = (0 <= t) & (t <= tb);
        epsilonc(case1) = sigma_0*(lambda/mu-1/E)*(1-exp(-1*t(case1)/lambda));
        case3 = (tb <= t) & (t <= 3600);
        epsilonc(case3) = epsilonc(t==tb)*exp(-1*(t(case3)-tb)/lambda);
    elseif sigma_0 > sigma_critical;   % if the irrecoverable strain can be triggered
        syms x;     % calculate ta when the irrecoverable strain is triggered
        ta = solve(sigma_0*(lambda/mu-1/E)*(1-exp(-1*x/lambda)) == epsilonl,x);
        ta = double(ta);
        if  ta >= tb;  % if the irrecoverable strain is not yet triggered before tb
            case1 = (0 <= t) & (t <= tb);
            epsilonc(case1) = sigma_0*(lambda/mu-1/E)*(1-exp(-1*t(case1)/lambda));
            case3 = (tb <= t) & (t <= 3600);
            epsilonc(case3) = epsilonc(t==tb)*exp(-1*(t(case3)-tb)/lambda);
        elseif ta < tb;       % if the irrecoverable strain is triggered before tb
            case1 = (0 <= t) & (t <= ta);
```

```
            epsilonc(case1) = sigma_0*(lambda/mu-1/E)*(1-exp(-1*t(case1)/lambda));
            case2 = (ta <= t) & (t <= tb);
            epsilonc(case2) = epsilonl*exp(-1*(t(case2)-ta)/lambda_eff)+...
                sigma_0*(epsilons_eff/sigma_0+lambda_eff/mu_eff-1/E)*...
                (1-exp(-1*(t(case2)-ta)/lambda_eff));
            epsilons_tb = C*(epsilonc(t==tb)-epsilonl);
            case3 = (tb <= t) & (t <= 3600);
            epsilonc(case3) = epsilons_tb+(epsilonc(t==tb)-epsilons_tb)*...
                exp(-1*(t(case3)-tb)/lambda);
        end
    end

    % calculate strain based on creep strain
    epsilon(1:(tb/0.1)) = epsilonc(1:(tb/0.1))+sigma_0/E;
    epsilon((tb/0.1+1):36001) = epsilonc((tb/0.1+1):36001);

    % obtain time ta and the corresponding strain
    ta_round(q) = round(ta*10)/10;
    epsilon_ta(q) = epsilon(ta_round(q)*10+1);

    % plot strain versus time
    plot(t,epsilon,'LineWidth',1.5)
    xlabel('\bf t(second)','FontSize',13)
    ylabel('\bf Strain','FontSize',13)
    axis([0,3600,0,0.02])
    set(gca,'xtick',0:600:3600,'ytick',0:0.002:0.02)
    strain = (strain_experiment(:,q)');
    % R square between experimental result and modeling result
    Rsq(q) = 1-sum((strain-epsilon).^2)/sum((strain-mean(strain)).^2);
end

% Add legend
legend({'\bf \sigma=2.81MPa,experiment','\bf \sigma=4.48MPa,experiment',...
    '\bf \sigma=6.42MPa,experiment','\bf \sigma=2.81MPa,model',...
    '\bf \sigma=4.48MPa,model','\bf \sigma=6.42MPa,model'},'FontSize',10,...
    'Location','best')
% Plot triggered point at three different stress levels
plot(ta_round,epsilon_ta,'o','LineWidth',1)
```

Published with MATLAB® R2016a

Modeling of bending and experimental comparision

One example when temperature is 55 C (T = 55 C)

Input values of parameters extracted from creep test

```
clear;
E = 1088.2e6;    % elastic modulus(Pa)
mu = 148e9;      % viscosity(Pa*s)
lambda = 226;    % retardation time(s)
C = 0.76;        % ratio between epsilons and epsilonc
epsilonl = 0.00065;   % threshold strain for triggering irrecoverable strain
mu_eff = mu*((1-(mu*C)/(lambda*E))^(-1));     % effective viscosity (Pa*s)
lambda_eff = lambda*((1-C)^(-1));             % effective retardation time(s)
epsilons_eff = -1*(C*epsilonl)/(1-C);         % effective epsilons
```

Defination and discretization

```
%dimension of the beam 40*12*3 mm
L = 40e-3;   % distance between two supports
b = 12.24e-3;    % width of the beam
h = 3.3567e-3;   % height of the beam
I = b*(h^3)/12;  % inertia moment

dx = L/2/100;     % x step
x = 0:dx:(L/2);   % discrete x along beam span direction
x = x';           % for the purpose to calculate moment
num_x = length(x);

dt = 0.1;     % time step
t = 0:dt:100; % discrete time
num_t = length(t);

dy = h/2/1000;   % y step
y = 0:dy:(h/2);  % discrete y along the height of the beam
num_y = length(y);

P_rate = 1;      % loading rate (N/second)
P = P_rate*t;    % load history
M = x*P/2;       % moment (N*m) (x*t dimension)
kappa = zeros(num_x,num_t);  % define curvature, initial condition is zero
sigma = zeros(num_x,num_t,num_y);   % define stress, initial condition is zero
epsilon = zeros(num_x,num_t,num_y); % define strain, initial condition is zero
% define the history of a which shows critical point between regime 1 and regime 2
```

```
a_history = zeros(num_x,num_t);
```

3 dimensional loops for calculating stress, strain, curvature and "a"

```
for q = 1:num_x        % loop for each specific x (cross section)

    for n = 1:(num_t-1)   % loop for each time point

        epsilon_c = epsilon(q,n,:)-sigma(q,n,:)/E;  % calculate creep strain along
% y direction

        if epsilon_c(end) <= epsilonl      % obtain the value of "a"
            a = h/2;
            num_a = num_y;
        else
            [Min_value,num_a] = min(abs(epsilon_c-epsilonl));
            a = (num_a-1)*dy;
        end
        a_history(q,n) = a;     % obtain the history of "a"

        if  a == h/2     % if all creep strains along y direction do not
            % exceed threhold strain
            A_integral = 0;
            B_integral = I*kappa(q,n)*dt/lambda;
            C_integral = M(q,n)*dt/mu;
        elseif a == 0    % if all creep strains along y direction exceed
            % threhold strain
            A_integral = b*dt*epsilons_eff/lambda_eff*(h^2/4);
            B_integral = b*kappa(q,n)*dt*(h^3/12/lambda_eff);
            C_integral = M(q,n)*dt/mu_eff;
        else   % if creep strain exceeds threhold strain at some point of y direction
            A_integral = b*dt*epsilons_eff/lambda_eff*(h^2/4-a^2);
            B_integral = b*kappa(q,n)*dt*(2*a^3/3/lambda+(h^3/12-2*a^3/3)/lambda_eff);
            % below is how to calculate C integral
            sigma_case1_subset = sigma(q,n,1:num_a);
            % remove the singleton dimension
            sigma_case1_subset = squeeze(sigma_case1_subset);
            sigma_case2_subset = sigma(q,n,num_a:num_y);
            % remove the singleton dimension
            sigma_case2_subset = squeeze(sigma_case2_subset);
            y_case1_subset = y(1:num_a);
            % make y_case1_subset a column which is consistent with sigma_case1_subset
            y_case1_subset = y_case1_subset';
```

```
            y_case2_subset = y(num_a:num_y);
            % make y_case2_subset a column which is consistent with sigma_case2_subset
            y_case2_subset = y_case2_subset';
            C_integral = 2*dt*b/mu*trapz...
                (y_case1_subset,sigma_case1_subset.*y_case1_subset)+2*dt*b/mu_eff*...
                trapz(y_case2_subset,sigma_case2_subset.*y_case2_subset);
        end

        kappa(q,n+1) = kappa(q,n)+ M(q,n+1)/E/I-M(q,n)/E/I+A_integral/I-...
            B_integral/I+C_integral/I;

        for m = 1:num_y         %discrete y direction
            % obtain strains along y direction
            epsilon(q,n+1,m) = kappa(q,n+1)*((m-1)*dy);
            if  m <=num_a;
                mu_EFF = mu;
                lambda_EFF = lambda;
                epsilons_EFF = 0;
            else
                mu_EFF = mu_eff;
                lambda_EFF = lambda_eff;
                epsilons_EFF = epsilons_eff;
            end
            % obtain stress along y direction
            sigma(q,n+1,m) = E*epsilon(q,n+1,m)+sigma(q,n,m)*(1-E*dt/mu_EFF)+...
                epsilon(q,n,m)*(E*dt/lambda_EFF-E)-epsilons_EFF*dt*E/lambda_EFF;
        end

    end

    %calculate value of "a" at the last time point
    epsilon_c = epsilon(q,num_t,:)-sigma(q,num_t,:)/E;
    if epsilon_c(end) <= epsilonl      % obtain "a"
        a = h/2;
        num_a = num_y;
    else
        [Min_value,num_a] = min(abs(epsilon_c-epsilonl));
        a = (num_a-1)*dy;
    end
    a_history(q,num_t) = a;
end
```

Plot curvature versus t

```
% extract curvature at each L/2/10 along x direction
kappa_extract_x = zeros(11,num_t);
for i = 1:11
    kappa_extract_x(i,:)= kappa((10*i-9),:);
end
figure(1)
plot(t,kappa_extract_x)
legend('x=0','x=0.05L','x=0.1L','x=0.15L','x=0.2L','x=0.25L','x=0.3L',...
    'x=0.35L','x=0.4L','x=0.45L','x=0.5L')
xlabel('time (s)')
ylabel('curvature (1/m)')
title('curvature versus time')
grid on
```

Plot “a” versus t

```
% extract history of “a” at each L/2/10 along x direction
a_history_x = zeros(11,num_t);
for i = 1:11
    a_history_x(i,:)= a_history((10*i-9),:);
end
figure(2)
plot(t,a_history_x)
axis([0,max(t),0,h/2])
legend('x=0','x=0.05L','x=0.1L','x=0.15L','x=0.2L','x=0.25L','x=0.3L',...
    'x=0.35L','x=0.4L','x=0.45L','x=0.5L')
title('a with respect time')
xlabel('time (s)')
ylabel('value of a (m)')
grid on
```

Plot curvature versus x

```
% extract curvature at each 10 seconds
kappa_extract_time = zeros(num_x,11);
for j = 1:11
    kappa_extract_time(:,j)= kappa(:,(100*j-99));
```

```
end
figure(3)
plot(x,kappa_extract_time,'.')
legend('t=0s','t=10s','t=20s','t=30s','t=40s','t=50s','t=60s','t=70s',...
    't=80s','t=90s','t=100s')
xlabel('x along beam span direction (m)')
ylabel('curvature (1/m)')
title('curvature versus x')
```

Obtain deflection

```
% least square fitting of kappa = c1*x
c1 = zeros(1,num_t);
for u = 1:num_t
    c1(u) = x\kappa(:,u);
end
% get deflection w along x and deflection at mid-span delta
w = zeros(num_x,num_t);
delta = zeros(1,num_t);
% obtain delta
for v = 1:num_t
    w(:,v) = L^2*c1(v)*x/8-c1(v)*x.^3/6;
    delta(1,v) = c1(v)*L^3/24;
end
% obtain w at each 10 seconds
w_extract = zeros(num_x,11);
for j = 1:11
    w_extract(:,j)= w(:,(100*j-99));
    delta_extract(j) = delta(100*j-99); % do not plot this
end
```

Plot deflection with respect to x

```
figure(4)
plot(x,w_extract,'-','LineWidth',1.5)
set(gca,'Ydir','reverse')
xlabel('\bf x(m)','FontSize',13)
ylabel('\bf deflection along x(m)','FontSize',13)
legend({'t=0s','t=10s','t=20s','t=30s','t=40s','t=50s','t=60s','t=70s',...
    't=80s','t=90s','t=100s'},...
    'FontSize',11,'Location','best')
```

Plot deflection at mid span of the beam and experimental results

```
figure(5)
hold on
plot(t,delta,'-','LineWidth',1.5)
% load experimental data
load('bending_55.mat')
plot(t_bending,bending_55_1,'--','LineWidth',1.5)
plot(t_bending,bending_55_2,'--','LineWidth',1.5)
plot(t_bending,bending_55_3,'--','LineWidth',1.5)
xlabel('\bf t(second)','FontSize',13)
ylabel('\bf deflection at mid span(m)','FontSize',13)
legend({'model','experiment1','experiment2','experiment3'},'FontSize',12,...
    'Location','northwest');
```

Published with MATLAB® R2016a